AD-A207 508 THEORETICAL ANALYSIS OF MICROWAVE AND MILLIMETER WAVE INTEGRATED CIRCUITS (U) MASSACHUSETTS INST OF TECH CAMBRIDGE RESEARCH LAB OF ELECTRON... J A KONG

1/1

UNCLASSIFIED 31 MAR 89 N00014-89-J-1019 F/G 9/1 NL

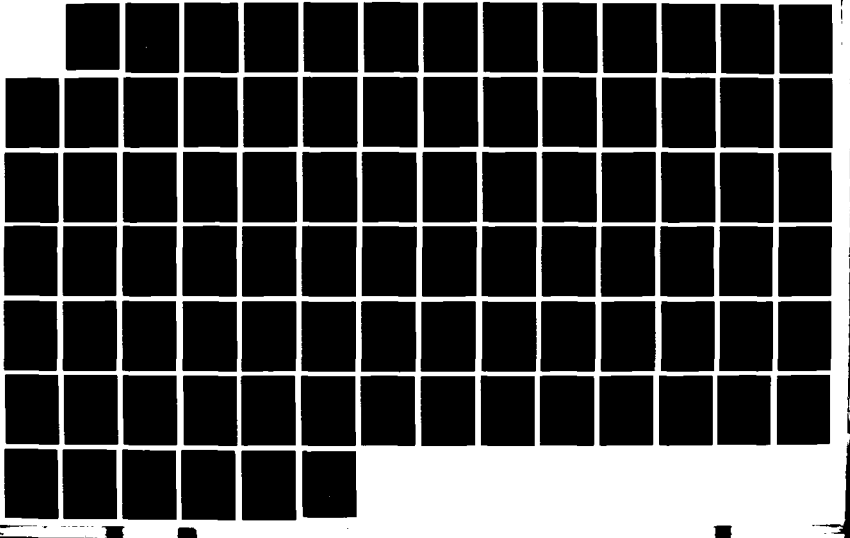

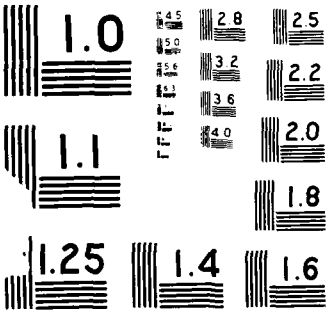
1.0
1.1
1.25
1.4
1.6
1.8
2.0
2.2
2.5
2.8
3.2
3.6
4.0
4.5
5.0
5.6
6.3

(4)

THEORETICAL ANALYSIS OF MICROWAVE AND MILLIMETER WAVE INTEGRATED CIRCUITS BASED ON MAGNETIC FILMS

Department of the Navy
Office of Naval Research
Contract N00014-89-J-1019
OSP 71387

SEMI-ANNUAL REPORT

covering the period

October 1, 1988 – March 31, 1989

prepared by

J. A. Kong

Principal Investigator

Massachusetts Institute of Technology
Research Laboratory of Electronics
Cambridge, Massachusetts 02139

89

REPORT DOCUMENTATION PAGE

Form Approved OMB No. 0704-0188

1a. REPORT SECURITY CLASSIFICATION UNCLASSIFIED	1b. RESTRICTIVE MARKINGS
2a. SECURITY CLASSIFICATION AUTHORITY	3. DISTRIBUTION / AVAILABILITY OF REPORT Approved for public release; distribution unlimited
2b. DECLASSIFICATION / DOWNGRADING SCHEDULE	
4. PERFORMING ORGANIZATION REPORT NUMBER(S)	5. MONITORING ORGANIZATION REPORT NUMBER(S)
6a. NAME OF PERFORMING ORGANIZATION Research Laboratory of Electronics Massachusetts Institute of Technology 6b. OFFICE SYMBOL (If applicable)	7a. NAME OF MONITORING ORGANIZATION Office of Naval Research
6c. ADDRESS (City, State, and ZIP Code) 77 Massachusetts Avenue Cambridge, MA 02139	7b. ADDRESS (City, State, and ZIP Code) 800 North Quincy Street Arlington, VA 22217-5000
8a. NAME OF FUNDING / SPONSORING ORGANIZATION Office of Naval Research 8b. OFFICE SYMBOL (If applicable)	9. PROCUREMENT INSTRUMENT IDENTIFICATION NUMBER N00014-89-J-1019
8c. ADDRESS (City, State, and ZIP Code) 800 North Quincy Street Arlington, VA 22217-5000	10. SOURCE OF FUNDING NUMBERS PROGRAM ELEMENT NO. / PROJECT NO. / TASK NO. / WORK UNIT ACCESSION NO.

11. TITLE (Include Security Classification)
Theoretical Analysis of Microwave and Millimeter Wave Integrated Circuits Based on Magnetic Films

12. PERSONAL AUTHOR(S)
J.A. Kong

13a. TYPE OF REPORT	13b. TIME COVERED	14. DATE OF REPORT (Year, Month, Day)	15. PAGE COUNT
Semi-Annual	FROM 10/1/88 TO 3/31/89	March 29, 1989	198 pp.

16. SUPPLEMENTARY NOTATION

17. COSATI CODES			18. SUBJECT TERMS (Continue on reverse if necessary and identify by block number)
FIELD	GROUP	SUB-GROUP	

19. ABSTRACT (Continue on reverse if necessary and identify by block number)

Work by J.A. Kong and his collaborators is summarized here.

20. DISTRIBUTION / AVAILABILITY OF ABSTRACT ☒ UNCLASSIFIED/UNLIMITED ☐ SAME AS RPT. ☐ DTIC USERS	21. ABSTRACT SECURITY CLASSIFICATION UNCLASSIFIED
22a. NAME OF RESPONSIBLE INDIVIDUAL Elisabeth Colford - RLE Contract Reports	22b. TELEPHONE (Include Area Code) (617) 258-5871 22c. OFFICE SYMBOL

THEORETICAL ANALYSIS OF MICROWAVE AND MILLIMETER WAVE INTEGRATED CIRCUITS BASED ON MAGNETIC FILMS

Principal Investigator: Jin Au Kong

Program Manager: A. K. Jordan

SEMI-ANNUAL REPORT

Under the sponsorship of the ONR Contract Contract N00014–89–J-1019 we have published 3 referenced journal and conference papers.

The complex resonant frequencies of the open structure of a microstrip antenna consisting of two circular microstrip disks in a three layer stacked configuration have been rigorously calculated as a function of the layered parameters and the ratio of the radii of the two disks. Using a dyadic Green's function formulation for horizontally stratified media and the vector Hankel transform, the mixed boundary value problem is reduced to a set of coupled vector integral equations. Employing Galerkin's method in the spectral domain, the complex resonant frequencies are calculated and convergence of the results is demonstrated. It is shown that for each mode, the stacked circular microstrip structure has dual resonant frequencies which are associated with the two coupled constitutive resonators of the structure and which are a function of the mutual coupling between them. This mutal coupling depends on the geometrical configuration of the stacked structure, the layered parameters, and the disk radii. The maximum coupling effect occurs where the real parts of the resonant frequencies of the constitutive resonators are approximately equal, where the behavior of the resonances in this region is a function of the coupling. The dual frequency behavior of the stacked microstrip structure, easily controlled by varying the

parameters of layer 2 and disk radii ratio, given fixed parameters for layer 1 and layer 3, may be used to broaden the bandwidth or provide for dual frequency use of the antenna.

A rigorous dyadic Green's function formulation in the spectral domain is used to study the dispersion characteristics of signal strip lines in the presence of metallic crossing strips. A set of coupled vector integral equations for the current distribution on the conductors is derived. Galerkin's method is then applied to derive the matrix eigenvalue equation for the propagation constant. The dispersion properties of the signal lines are studied for both cases of finite and infinite length crossing strips. The effects of the structure dimensions on the passband and stopband characteristics are investigated. For crossing strips of finite length, the stopband is mainly affected by the period, the crossing strip length, and the separation between the signal and the crossing strips. For crossing strips of infinite length carrying travelling waves, attenuation along the signal line exists over the whole frequency range of operation.

A new method for analyzing frequency-dependent transmission line systems with nonlinear terminations is presented. The generalized scattering matrix formulation is used as the foundation for the time domain iteration scheme. Compared to the admittance matrix approach proposed in a previous paper, it has the advantage of shorter impulse response which leads to smaller computer memory requirement and faster computation time. Examples of a microstrip line loaded with nonlinear elements are given to illustrate the efficiency of this method.

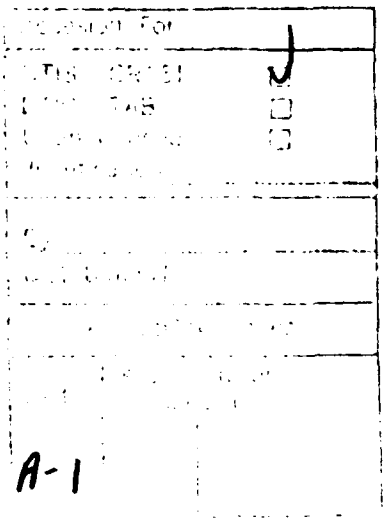

A-1

PUBLICATIONS SUPPORTED BY ONR CONTRACT N00014-89-J-1019 SINCE 1988

Resonant frequencies of stacked circular microstrip antennas (A. N. Tulintseff, S. M. Ali, and J. A. Kong), *IEEE Transactions on Antennas and Propagation,* submitted for publication.

Propagation properties of strip lines periodically loaded with crossing strips (J. F. Kiang, S. M. Ali, and J. A. Kong), *IEEE Transactions on Microwave Theory and Techniques,* accepted for publication.

Transient Analysis of frequency-dependent transmission line systems terminated with nonlinear loads, (Q. Gu, Y. E. Yang, and J. A. Kong), *J. of Electromagnetic Waves and Applications,* Vol. 3, No. 3, 183–197, 1989.

RESONANT FREQUENCIES OF STACKED CIRCULAR MICROSTRIP ANTENNAS

A. N. Tulintseff, S. M. Ali, and J. A. Kong

Department of Electrical Engineering and Computer Science

Massachusetts Institute of Technology

Cambridge, Massachusetts 02139

Abstract– The complex resonant frequencies of a microstrip antenna consisting of two circular microstrip disks in a stacked configuration are investigated. Using a dyadic Green's function formulation, a rigorous analysis of the two stacked circular disks in a layered medium is performed. The mixed boundary value problem is reduced to a set of coupled vector integral equations using the vector Hankel transform. Employing Galerkin's method in the spectral domain, the complex resonant frequencies are calculated as a function of the layered parameters and the ratio of the radii of the two disks. It is shown that for each mode the stacked circular microstrip structure has dual resonant frequencies which may provide for dual frequency or wide bandwidth use.

1. INTRODUCTION

Conventional microstrip antennas, consisting of a single perfectly conducting patch on a grounded dielectric slab, have received much attention in recent years [1]-[2] due to their many advantanges, including low profile and light weight. However, due to their resonant behavior, their use is severely limited in that they radiate efficiently only over a narrow band of frequencies, with bandwidths typically only a few percent [1]. Techniques for increasing the bandwidth have included stacking a number of microstrip patches in multilayer configurations, introducing additional resonances in the frequency range of interest and achieving bandwidths up to approximately 10-20 percent.

The first multilayered microstrip element was described by Oltman [3],[4] as an electromagnetically coupled microstrip dipole where a printed dipole was excited by an open ended microstrip transmission line in the same plane as the dipole or in the layer below the dipole. Hall et al. [5] stacked rectangular microstrip patches in two- and three-layer configurations, achieving bandwidths in excess of 16 times that of alumina substrate microstrip antennas, and noted that the stacked configurations allowed for simple antenna/circuit integration. Experimental work by Sabban [6] and Chen et al. [7] with two-layer stacked circular microstrip patches produced wider bandwidths and higher efficiencies than those obtained with conventional single patch configurations. Stacking microstrip patches for dual frequency use was investigated experimentally for circular disks by Long et al. [8] and for annular rings by Dahele et al. [9].

Rigorous analyses employing Galerkin's method have been applied to conventional single-layer microstrip antennas of circular, rectangular, annular ring, and elliptic geometries [10]-[14]. The coupling between two microstrip antennas on a single substrate has also been rigorously treated [15]-[17]. However, theoretical analyses of stacked microstrip patches is limited. Printed microstrip dipoles in stacked configurations coupled to an open ended microstrip transmission line have been studied by Katehi et al. [18]. Tulintseff et al. [19] used the method of moments with triangular basis functions to analyze the open structure of a two-layer circular microstrip antenna excited by an incident plane wave. Kastner et al. [20] described a spectral domain iterative anlaysis of single- and double-layered microstrip antennas algorithm to compute radiation patterns.

Considered here is a microstrip antenna consisting of two circular microstrip disks in a stacked configuration. The two stacked configurations shown in Figures 1(a) and 1(b),

denoted configurations A and B, respectively, are investigated. A rigorous analysis of the two stacked circular disks in a layered medium is performed using a dyadic Green's function formulation. Using the Vector Hankel transform, the mixed boundary value problem is reduced to a set of coupled vector integral equations and solved by employing Galerkin's method in the spectral domain. The current distribution on each disk is expanded in terms of a complete set of transverse magnetic (TM) and transverse electric (TE) modes of a cylindrical resonant cavity with magnetic side walls. Complex resonant frequencies are calculated for different configurations versus substrate height h_2. The convergence of the results is investigated and ensured by using a proper number of basis functions. It is shown that there are dual resonant frequencies of the stacked structure for each mode which are related to the constitutive resonators of the structure and a function of the mutual coupling between them. Throughout the analysis, the $\exp(-i\omega t)$ time dependence is used and suppressed.

2. DYADIC GREEN'S FUNCTION FORMULATION

Consider the horizontally stratified medium shown in the Figure 2 where each layer l is of thickness h_l and characterized by permittivity ϵ_l and permeability μ_l. The two coaxial, circular conducting disks are carrying electric current distributions $\overline{J}_1(\overline{r}')$ and $\overline{J}_2(\overline{r}')$ and located in medium 1 and medium 2, respectively. Configurations A and B are obtained, respectively, by placing $\overline{J}_1(\overline{r}')$ at $z_1' = d_0$ and $z_1' = d_1$.

The electric fields in regions 1 and 2 due to the current distributions $\overline{J}_1(\overline{r}')$ and $\overline{J}_2(\overline{r}')$ may be expressed as

$$\overline{E}_1(\overline{r}) = i\omega\mu_1 \iiint_{V'} dV' \overline{\overline{G}}_{1,1}(\overline{r},\overline{r}') \cdot \overline{J}_1(\overline{r}') + i\omega\mu_2 \iiint_{V'} dV' \overline{\overline{G}}_{1,2}(\overline{r},\overline{r}') \cdot \overline{J}_2(\overline{r}') \qquad (1a)$$

$$\overline{E}_2(\overline{r}) = i\omega\mu_1 \iiint_{V'} dV' \overline{\overline{G}}_{2,1}(\overline{r},\overline{r}') \cdot \overline{J}_1(\overline{r}') + i\omega\mu_2 \iiint_{V'} dV' \overline{\overline{G}}_{2,2}(\overline{r},\overline{r}') \cdot \overline{J}_2(\overline{r}') \qquad (1b)$$

where $\overline{\overline{G}}_{l,p}(\overline{r},\overline{r}')$ is the dyadic Green's function relating the electric field in region l to an impressed current source in region p.

For the stacked microstrip antenna structure, the current distributions are surface currents at $z' = z_1'$ and $z' = z_2'$

$$\overline{J}_1(\overline{r}') = \overline{K}^{(1)}(\overline{\rho}')\delta(z' - z_1') \qquad (2a)$$

$$\overline{J}_2(\overline{r}') = \overline{K}^{(2)}(\overline{\rho}')\delta(z'-z_2') \tag{2b}$$

Using a dyadic Green's function formulation for horizontally stratified media [21]-[23], we may write the spectral domain dyadic Green's function $\overline{\overline{G}}_{l,p}(\overline{r},\overline{r}')$ in cylindrical coordinates as

$$\overline{\overline{G}}_{l,p}(\overline{r},\overline{r}') = -\hat{z}\hat{z}\frac{\delta(\overline{r}-\overline{r}')}{k_l^2} + \frac{i}{4\pi}\sum_{m=-\infty}^{\infty} e^{im(\phi-\phi')}\int_0^\infty dk_\rho k_\rho \overline{\overline{g}}_{l,p}^{(m)}(\overline{\rho},z;\overline{\rho}',z') \tag{3}$$

where $\overline{\overline{g}}_{l,p}^{(m)}(\overline{\rho},z;\overline{\rho}',z')$ is given in the following for the four cases of source and observer positions. When both observation and source positions are in region l with $z > z'$, we have

$$\begin{aligned}\overline{\overline{g}}_{l+,l}^{(m)}(\overline{\rho},z;\overline{\rho}',z') = {} & \frac{1}{k_{lz}}\frac{1}{1-R_{\cup l}^{\mathrm{TE}}R_{\cap l}^{\mathrm{TE}}e^{i2k_{lz}h_l}}\left[\hat{h}_m(\rho,k_{lz})e^{ik_{lz}z} + R_{\cup l}^{\mathrm{TE}}e^{i2k_{lz}d_{l-1}}\hat{h}_m(\rho,-k_{lz})e^{-ik_{lz}z}\right] \\ & \left[\hat{h}'_m(\rho',k_{lz})e^{-ik_{lz}z'} + R_{\cap l}^{\mathrm{TE}}e^{-i2k_{lz}d_l}\hat{h}'_m(\rho',-k_{lz})e^{ik_{lz}z'}\right] \\ & + \frac{1}{k_{lz}}\frac{1}{1-R_{\cup l}^{\mathrm{TM}}R_{\cap l}^{\mathrm{TM}}e^{i2k_{lz}h_l}}\left[\hat{v}_m(\rho,k_{lz})e^{ik_{lz}z} + R_{\cup l}^{\mathrm{TM}}e^{i2k_{lz}d_{l-1}}\hat{v}_m(\rho,-k_{lz})e^{-ik_{lz}z}\right] \\ & \left[\hat{v}'_m(\rho',k_{lz})e^{-ik_{lz}z'} + R_{\cap l}^{\mathrm{TM}}e^{-i2k_{lz}d_l}\hat{v}'_m(\rho',-k_{lz})e^{ik_{lz}z'}\right]\end{aligned} \tag{4}$$

where k_{lz} satisfies $k_{lz}^2 = k_l^2 - k_\rho^2$. When both observation and source positions are in region l with $z < z'$, we have

$$\begin{aligned}\overline{\overline{g}}_{l-,l}^{(m)}(\overline{\rho},z;\overline{\rho}',z') = {} & \frac{1}{k_{lz}}\frac{1}{1-R_{\cup l}^{\mathrm{TE}}R_{\cap l}^{\mathrm{TE}}e^{i2k_{lz}h_l}}\left[R_{\cap l}^{\mathrm{TE}}e^{-i2k_{lz}d_l}\hat{h}_m(\rho,k_{lz})e^{ik_{lz}z} + \hat{h}_m(\rho,-k_{lz})e^{-ik_{lz}z}\right] \\ & \left[R_{\cup l}^{\mathrm{TE}}e^{i2k_{lz}d_{l-1}}\hat{h}'_m(\rho',k_{lz})e^{-ik_{lz}z'} + \hat{h}'_m(\rho',-k_{lz})e^{ik_{lz}z'}\right] \\ & + \frac{1}{k_{lz}}\frac{1}{1-R_{\cup l}^{\mathrm{TM}}R_{\cap l}^{\mathrm{TM}}e^{i2k_{lz}h_l}}\left[R_{\cap l}^{\mathrm{TM}}e^{-i2k_{lz}d_l}\hat{v}_m(\rho,k_{lz})e^{ik_{lz}z} + \hat{v}_m(\rho,-k_{lz})e^{-ik_{lz}z}\right] \\ & \left[R_{\cup l}^{\mathrm{TM}}e^{i2k_{lz}d_{l-1}}\hat{v}'_m(\rho',k_{lz})e^{-ik_{lz}z'} + \hat{v}'_m(\rho',-k_{lz})e^{ik_{lz}z'}\right]\end{aligned} \tag{5}$$

When the observation point in region l is above the source point in region p, we have

$$\begin{aligned}\overline{\overline{g}}_{l,p}^{(m)}(\overline{\rho},z;\overline{\rho}',z') = {} & \frac{1}{k_{pz}}\frac{X_{\cup l}^{\mathrm{TE}}}{1-R_{\cup p}^{\mathrm{TE}}R_{\cap p}^{\mathrm{TE}}e^{i2k_{pz}h_p}}\left[\hat{h}_m(\rho,k_{lz})e^{ik_{lz}z} + R_{\cup l}^{\mathrm{TE}}e^{i2k_{lz}d_{l-1}}\hat{h}_m(\rho,-k_{lz})e^{-ik_{lz}z}\right] \\ & \left[\hat{h}'_m(\rho',k_{pz})e^{-ik_{lz}z'} + R_{\cap p}^{\mathrm{TE}}e^{-i2k_{pz}d_p}\hat{h}'_m(\rho',-k_{pz})e^{ik_{lz}z'}\right] \\ & + \frac{1}{k_{pz}}\frac{X_{\cup l}^{\mathrm{TM}}}{1-R_{\cup p}^{\mathrm{TM}}R_{\cap p}^{\mathrm{TM}}e^{i2k_{pz}h_p}}\left[\hat{v}_m(\rho',k_{lz})e^{ik_{lz}z} + R_{\cup l}^{\mathrm{TM}}e^{i2k_{lz}d_{l-1}}\hat{v}_m(\rho,-k_{lz})e^{-ik_{lz}z}\right] \\ & \left[\hat{v}'_m(\rho',k_{pz})e^{-ik_{lz}z'} + R_{\cap p}^{\mathrm{TM}}e^{-i2k_{pz}d_p}\hat{v}'_m(\rho',-k_{pz})e^{ik_{lz}z'}\right]\end{aligned} \tag{6}$$

When the observation point in region l is above the source point in region p, we have

$$\begin{aligned}\overline{\overline{g}}_{l,p}^{(m)}(\overline{\rho},z;\overline{\rho}',z') = \frac{1}{k_{pz}}\frac{X_{\cap l}^{\mathrm{TE}}}{1-R_{\cup p}^{\mathrm{TE}}R_{\cap p}^{\mathrm{TE}}e^{i2k_{pz}h_p}}\left[R_{\cap l}^{\mathrm{TE}}e^{-i2k_{lz}d_l}\hat{h}_m(\rho,k_{lz})e^{ik_{lz}z}+\hat{h}_m(\rho,-k_{lz})e^{-ik_{lz}z}\right]\\ \left[R_{\cup p}^{\mathrm{TE}}e^{i2k_{pz}d_{p-1}}\hat{h}'_m(\rho',k_{pz})e^{-ik_{lz}z'}+\hat{h}'_m(\rho',-k_{pz})e^{ik_{lz}z'}\right]\\ +\frac{1}{k_{pz}}\frac{X_{\cap l}^{\mathrm{TM}}}{1-R_{\cap p}^{\mathrm{TM}}R_{\cap p}^{\mathrm{TM}}e^{i2k_{pz}h_p}}\left[R_{\cap l}^{\mathrm{TM}}e^{-i2k_{lz}d_l}\hat{v}_m(\rho,k_{lz})e^{ik_{lz}z}+\hat{v}_m(\rho,-k_{lz})e^{-ik_{lz}z}\right]\\ \left[R_{\cup p}^{\mathrm{TM}}e^{i2k_{pz}d_{p-1}}\hat{v}'_m(\rho',k_{pz})e^{-ik_{lz}z'}+\hat{v}'_m(\rho',-k_{pz})e^{ik_{lz}z'}\right]\end{aligned} \tag{7}$$

In the previous equations (4)-(7), the dyadic Green's function is decomposed with TE and TM wave components with the following unit vectors

$$\hat{h}_m(\rho,\pm k_{lz}) = \left[\hat{\rho}\frac{im}{k_\rho\rho}J_m(k_\rho\rho)-\hat{\phi}J'_m(k_\rho\rho)\right] \tag{8a}$$

$$\hat{h}'_m(\rho',\pm k_{lz}) = \left[\hat{\rho}'\frac{-im}{k_\rho\rho'}J_m(k_\rho\rho')-\hat{\phi}'J'_m(k_\rho\rho')\right] \tag{8b}$$

$$\hat{v}_m(\rho,\pm k_{lz}) = \left[\mp\hat{\rho}\frac{k_{lz}}{k_l}J'_m(k_\rho\rho)\mp\hat{\phi}\frac{k_{lz}}{k_l}\frac{im}{k_\rho\rho}J_m(k_\rho\rho)+\hat{z}\frac{ik_\rho}{k_l}J_m(k_\rho\rho)\right] \tag{9a}$$

$$\hat{v}'_m(\rho',\pm k_{lz}) = \left[\mp\hat{\rho}'\frac{k_{lz}}{k_l}J'_m(k_\rho\rho')\pm\hat{\phi}'\frac{k_{lz}}{k_l}\frac{im}{k_\rho\rho'}J_m(k_\rho\rho')-\hat{z}\frac{ik_\rho}{k_l}J_m(k_\rho\rho')\right] \tag{9b}$$

It may be noted that the unit vector $\hat{h}_m(\rho,\pm k_{lz})$ is in the direction of the electric field for a horizontally polarized TE wave and that the unit vector $\hat{v}_m(\rho,\pm k_{lz})$ is in the direction of the electric field for a vertically polarized TM wave.

The reflection coefficients, $R_{\cup l}^a$ and $R_{\cap l}^a$, at the upper and lower boundaries, respectively, of layer l, and are given by the following recursion relations

$$R_{\cup l}^a = \frac{R_{l(l-1)}^a + R_{\cup(l-1)}^a e^{i2k_{(l-1)z}h_{l-1}}}{1+R_{l(l-1)}^a R_{\cup(l-1)}^a e^{i2k_{(l-1)z}h_{l-1}}} \tag{10a}$$

$$R_{\cap l}^a = \frac{R_{l(l+1)}^a + R_{\cap(l+1)}^a e^{i2k_{(l+1)z}h_{l+1}}}{1+R_{l(l+1)}^a R_{\cap(l+1)}^a e^{i2k_{(l+1)z}h_{l+1}}} \tag{10b}$$

where $R_{\cup 0}^{\mathrm{TE}} = R_{\cup 0}^{\mathrm{TM}} = 0$ and $R_{\cap 3}^{\mathrm{TE}} = -1$ and $R_{\cap 3}^{\mathrm{TM}} = 1$. The Fresnel reflection coefficients $R_{l(l\pm1)}^{\mathrm{TE}}$ and $R_{l(l\pm1)}^{\mathrm{TM}}$ are defined by

$$R_{l(l\pm1)}^{\mathrm{TE}} = \frac{\mu_{(l\pm1)}k_{lz} - \mu_l k_{(l\pm1)z}}{\mu_{(l\pm1)}k_{lz} + \mu_l k_{(l\pm1)z}} \tag{11a}$$

$$R_{l(l\pm1)}^{\mathrm{TM}} = \frac{\epsilon_{(l\pm1)}k_{lz} - \epsilon_l k_{(l\pm1)z}}{\epsilon_{(l\pm1)}k_{lz} + \epsilon_l k_{(l\pm1)z}} \tag{11b}$$

The transmission coefficients, $X_{\cup l}^{\mathrm{TE}}$ and $X_{\cup l}^{\mathrm{TM}}$, for observation positions above the source points are given by the following recursion relations

$$X_{\cup l}^{\mathrm{TE}} = \frac{e^{ik_{(l+1)z}d_l}}{e^{ik_l\ d_l}} \frac{\left[1 + R_{\cup(l+1)}^{\mathrm{TE}}\right]}{\left[1 + R_{\cup l}^{\mathrm{TE}} e^{i2k_{lz}h_l}\right]} X_{\cup(l+1)}^{\mathrm{TE}} \tag{12a}$$

$$X_{\cup l}^{\mathrm{TM}} = \frac{k_l}{k_{(l+1)}} \frac{k_{(l+1)z}}{k_{lz}} \frac{e^{ik_{(l+1)z}d_l}}{e^{ik_{lz}d_l}} \frac{\left[1 - R_{\cup(l+1)}^{\mathrm{TM}}\right]}{\left[1 - R_{\cup l}^{\mathrm{TM}} e^{i2k_{lz}h_l}\right]} X_{\cup(l+1)}^{\mathrm{TM}} \tag{12b}$$

for $l = 0, 1, \ldots, p-1$ where $X_{\cup p}^{\mathrm{TE}} = X_{\cup p}^{\mathrm{TM}} = 1$ and those for observation positions below the source points, $X_{\cap l}^{\mathrm{TE}}$ and $X_{\cap l}^{\mathrm{TM}}$, are given by the following recursion relations

$$X_{\cap(l+1)}^{\mathrm{TE}} = \frac{e^{-ik_{lz}d_l}}{e^{-ik_{(l+1)z}d_l}} \frac{\left[1 + R_{\cap l}^{\mathrm{TE}}\right]}{\left[1 + R_{\cap(l+1)}^{\mathrm{TE}} e^{i2k_{(l+1)z}h_{(l+1)}}\right]} X_{\cap l}^{\mathrm{TE}} \tag{13a}$$

$$X_{\cap(l+1)}^{\mathrm{TM}} = \frac{k_{(l+1)}}{k_l} \frac{k_{lz}}{k_{(l+1)z}} \frac{e^{-ik_{lz}d_l}}{e^{-ik_{(l+1)z}d_l}} \frac{\left[1 - R_{\cap l}^{\mathrm{TM}}\right]}{\left[1 - R_{\cap(l+1)}^{\mathrm{TM}} e^{i2k_{(l+1)z}h_{(l+1)}}\right]} X_{\cap l}^{\mathrm{TM}} \tag{13b}$$

for $l = p+1, p+2, \ldots, 3$ where $X_{\cap p}^{\mathrm{TE}} = X_{\cap p}^{\mathrm{TM}} = 1$.

The transverse (to z) components of the spectral domain dyadic Green's function $\left[\overline{\overline{G}}_{l,p}(\overline{r}, \overline{r}')\right]_T$ may be written in the following form

$$\left[\overline{\overline{G}}_{l,p}(\overline{r}, \overline{r}')\right]_T = \frac{i}{4\pi} \sum_{m=-\infty}^{\infty} e^{im(\phi-\phi')} \int_0^{\infty} dk_\rho k_\rho \overline{\overline{J}}_m(k_\rho\rho) \cdot \overline{\overline{\zeta}}_{l,p}(k_\rho, z, z') \cdot \overline{\overline{J}}_m^{\dagger}(k_\rho\rho') \tag{14}$$

where $\overline{\overline{J}}_m^{\dagger}(k_\rho\rho)$ is the complex conjugate transpose of the kernel of the vector Hankel transform (VHT) [24] given by

$$\overline{\overline{J}}_m(k_\rho\rho) = \begin{bmatrix} J_m'(k_\rho\rho) & \frac{-im}{k_\rho\rho} J_m(k_\rho\rho) \\ \frac{im}{k_\rho\rho} J_m(k_\rho\rho) & J_m'(k_\rho\rho) \end{bmatrix} \tag{15}$$

and

$$\bar{\bar{\zeta}}_{l,p}(k_\rho, z, z') = \begin{bmatrix} \zeta_{l,p}^{\mathrm{TM}} & 0 \\ 0 & \zeta_{l,p}^{\mathrm{TE}} \end{bmatrix} \tag{16}$$

For source and observer in region 1 (assuming $z > z'$), we have

$$\zeta_{1,1}^{\mathrm{TM}} = \frac{k_{1z}}{k_1^2} \frac{\left[1 - R_{\cup 1}^{\mathrm{TM}} e^{i2k_{1z}(d_0 - z)}\right]\left[1 - R_{\cap 1}^{\mathrm{TM}} e^{i2k_{1z}(z' - d_1)}\right]}{1 - R_{\cup 1}^{\mathrm{TM}} R_{\cap 1}^{\mathrm{TM}} e^{i2k_{1z}h_1}} e^{ik_{1z}(z - z')} \tag{17a}$$

$$\zeta_{1,1}^{\mathrm{TE}} = \frac{1}{k_{1z}} \frac{\left[1 + R_{\cup 1}^{\mathrm{TE}} e^{i2k_{1z}(d_0 - z)}\right]\left[1 + R_{\cap 1}^{\mathrm{TE}} e^{i2k_{1z}(z' - d_1)}\right]}{1 - R_{\cup 1}^{\mathrm{TE}} R_{\cap 1}^{\mathrm{TE}} e^{i2k_{1z}h_1}} e^{ik_{1z}(z - z')} \tag{17b}$$

where k_{lz} satisfies the dispersion relation $k_{lz}^2 + k_\rho^2 = k^2 = \omega^2 \mu_l \epsilon_l$. For an observer in region 2 and source in region 1, we have

$$\zeta_{2,1}^{\mathrm{TM}} = \frac{k_{1z}}{k_1^2} \frac{\left[1 - R_{\cap 1}^{\mathrm{TM}}\right]\left[1 - R_{\cap 2}^{\mathrm{TM}} e^{i2k_{2z}(z - d_2)}\right]\left[1 - R_{\cup 1}^{\mathrm{TM}} e^{i2k_{1z}(d_0 - z')}\right]}{\left[1 - R_{\cup 1}^{\mathrm{TM}} R_{\cap 1}^{\mathrm{TM}} e^{i2k_{1z}h_1}\right]\left[1 - R_{\cap 2}^{\mathrm{TM}} e^{i2k_{2z}h_2}\right]} e^{ik_{1z}(z' - d_1)} e^{ik_{2z}(d_1 - z)} \tag{18a}$$

$$\zeta_{2,1}^{\mathrm{TE}} = \frac{1}{k_{1z}} \frac{\left[1 + R_{\cap 1}^{\mathrm{TE}}\right]\left[1 + R_{\cap 2}^{\mathrm{TE}} e^{i2k_{2z}(z - d_2)}\right]\left[1 + R_{\cup 1}^{\mathrm{TE}} e^{i2k_{1z}(d_0 - z')}\right]}{\left[1 - R_{\cup 1}^{\mathrm{TE}} R_{\cap 1}^{\mathrm{TE}} e^{i2k_{1z}h_1}\right]\left[1 + R_{\cap 2}^{\mathrm{TE}} e^{i2k_{2z}h_2}\right]} e^{ik_{1z}(z' - d_1)} e^{ik_{2z}(d_1 - z)} \tag{18b}$$

For source and observer in region 2 (assuming $z > z'$), we have

$$\zeta_{2,2}^{\mathrm{TM}} = \frac{k_{2z}}{k_2^2} \frac{\left[1 - R_{\cup 2}^{\mathrm{TM}} e^{i2k_{2z}(d_1 - z)}\right]\left[1 - R_{\cap 2}^{\mathrm{TM}} e^{i2k_{2z}(z' - d_2)}\right]}{1 - R_{\cup 2}^{\mathrm{TM}} R_{\cap 2}^{\mathrm{TM}} e^{i2k_{2z}h_2}} e^{ik_{2z}(z - z')} \tag{19a}$$

$$\zeta_{2,2}^{\mathrm{TE}} = \frac{1}{k_{2z}} \frac{\left[1 + R_{\cup 2}^{\mathrm{TE}} e^{i2k_{2z}(d_1 - z)}\right]\left[1 + R_{\cap 2}^{\mathrm{TE}} e^{i2k_{2z}(z' - d_2)}\right]}{1 - R_{\cup 2}^{\mathrm{TE}} R_{\cap 2}^{\mathrm{TE}} e^{i2k_{2z}h_2}} e^{ik_{2z}(z - z')} \tag{19b}$$

For an observer in region 1 and source in region 2, we have

$$\zeta_{1,2}^{\mathrm{TM}} = \frac{k_{2z}}{k_2^2} \frac{\left[1 - R_{\cup 2}^{\mathrm{TM}}\right]\left[1 - R_{\cup 1}^{\mathrm{TM}} e^{i2k_{1z}(d_0 - z)}\right]\left[1 - R_{\cap 2}^{\mathrm{TM}} e^{i2k_{2z}(z' - d_2)}\right]}{\left[1 - R_{\cup 2}^{\mathrm{TM}} R_{\cap 2}^{\mathrm{TM}} e^{i2k_{2z}h_2}\right]\left[1 - R_{\cup 1}^{\mathrm{TM}} e^{i2k_{1z}h_1}\right]} e^{ik_{1z}(z - d_1)} e^{ik_{2z}(d_1 - z')} \tag{20a}$$

$$\zeta_{1,2}^{\mathrm{TE}} = \frac{1}{k_{2z}} \frac{\left[1 + R_{\cup 2}^{\mathrm{TE}}\right]\left[1 + R_{\cup 1}^{\mathrm{TE}} e^{i2k_{1z}(d_0 - z)}\right]\left[1 + R_{\cap 2}^{\mathrm{TE}} e^{i2k_{2z}(z' - d_2)}\right]}{\left[1 - R_{\cup 2}^{\mathrm{TE}} R_{\cap 2}^{\mathrm{TE}} e^{i2k_{2z}h_2}\right]\left[1 + R_{\cup 1}^{\mathrm{TE}} e^{i2k_{1z}h_1}\right]} e^{ik_{1z}(z - d_1)} e^{ik_{2z}(d_1 - z')} \tag{20b}$$

Due to reciprocity, $\mu_1\zeta^{\alpha}_{2,1}(k_\rho, z, z') = \mu_2\zeta^{\alpha}_{1,2}(k_\rho, z', z)$ where $\alpha = \mathrm{TE}, \mathrm{TM}$.

The transverse components of the electric fields for the mth mode at $z = z_1'$ and $z = z_2'$ vanish on the conducting disks and may be expressed as

$$\begin{aligned}\left[\overline{E}_{1,m}(\overline{\rho}, z = z_1')\right]_T &= -\frac{\omega\mu_1}{2}\int_0^\infty dk_\rho k_\rho \overline{\overline{J}}_m(k_\rho\rho)\cdot\overline{\overline{\zeta}}_{1,1}\Big|_{z'=z_1', z=z_1'}\cdot\overline{K}_m^{(1)}(k_\rho) \\ &\quad -\frac{\omega\mu_2}{2}\int_0^\infty dk_\rho k_\rho \overline{\overline{J}}_m(k_\rho\rho)\cdot\overline{\overline{\zeta}}_{1,2}\Big|_{z'=z_2', z=z_1'}\cdot\overline{K}_m^{(2)}(k_\rho) \\ &= 0, \qquad \rho < a_1 \end{aligned} \tag{21a}$$

$$\begin{aligned}\left[\overline{E}_{2,m}(\overline{\rho}, z = z_2')\right]_T &= -\frac{\omega\mu_1}{2}\int_0^\infty dk_\rho k_\rho \overline{\overline{J}}_m(k_\rho\rho)\cdot\overline{\overline{\zeta}}_{2,1}\Big|_{z'=z_1', z=z_2'}\cdot\overline{K}_m^{(1)}(k_\rho) \\ &\quad -\frac{\omega\mu_2}{2}\int_0^\infty dk_\rho k_\rho \overline{\overline{J}}_m(k_\rho\rho)\cdot\overline{\overline{\zeta}}_{2,2}\Big|_{z'=z_2', z=z_2'}\cdot\overline{K}_m^{(2)}(k_\rho) \\ &= 0, \qquad \rho < a_2 \end{aligned} \tag{21b}$$

where $\overline{K}_m^{(j)}(k_\rho)$ $(j = 1, 2)$ is defined by

$$\overline{K}_m^{(j)}(k_\rho) = \int_0^\infty d\rho\rho\overline{\overline{J}}_m^{\dagger}(k_\rho\rho)\cdot\overline{K}_m^{(j)}(\rho) \tag{22}$$

and where $\overline{K}_m^{(j)}(\rho)$ is the Fourier coefficient

$$\overline{K}_m^{(j)}(\rho) = \frac{1}{2\pi}\int_0^{2\pi} d\phi e^{-im\phi}\overline{K}^{(j)}(\overline{\rho}) \tag{23}$$

With the use of the vector Hankel transform, we obtain

$$\overline{K}_m^{(1)}(\rho) = \int_0^\infty d\rho\,\rho\,\overline{\overline{J}}_m(k_\rho\rho)\cdot\overline{K}_m^{(1)}(k_\rho) = 0, \qquad \rho > a_1 \tag{24a}$$

$$\overline{K}_m^{(2)}(\rho) = \int_0^\infty d\rho\,\rho\,\overline{\overline{J}}_m(k_\rho\rho)\cdot\overline{K}_m^{(2)}(k_\rho) = 0, \qquad \rho > a_2 \tag{24b}$$

Equations (21) and (24) constitute a set of coupled vector integral equations for the currents $\overline{K}_m^{(1)}(k_\rho)$ and $\overline{K}_m^{(2)}(k_\rho)$. For configuration A, $z_1' = d_1 = -h_1$ and $z_2' = d_2 = -(h_1 + h_2)$, and for configuration B, $z_1' = d_0 = 0$ and $z_2' = d_2 = -(h_1 + h_2)$.

3. GALERKIN'S METHOD

Galerkin's method is now employed to solve the coupled vector integral equations of (21) and (24). The currents on the circular disks are expanded in terms of the complete orthogonal set of TE and TM modes of the corresponding cylindrical cavities with magnetic side walls

$$\overline{K}_m^{(1)}(\rho) = \sum_{n=1}^{N} a_{mn}^{(1)} \overline{\psi}_{mn}^{(1)}(\rho) + \sum_{p=1}^{P} b_{mp}^{(1)} \overline{\phi}_{mp}^{(1)}(\rho) \tag{25a}$$

$$\overline{K}_m^{(2)}(\rho) = \sum_{r=1}^{R} a_{mr}^{(2)} \overline{\psi}_{mr}^{(2)}(\rho) + \sum_{s=1}^{S} b_{ms}^{(2)} \overline{\phi}_{ms}^{(2)}(\rho) \tag{25b}$$

where $j = 1, 2$ and

$$\overline{\psi}_{mn}^{(j)}(\rho) = \begin{cases} \begin{bmatrix} J_m'(\beta_{mn}\rho/a_j) \\ \frac{ima_j}{\beta_{mn}\rho} J_m(\beta_{mn}\rho/a_j) \end{bmatrix}, & \text{for } \rho < a_j \\ 0, & \text{for } \rho > a_j \end{cases} \tag{26a}$$

$$\overline{\phi}_{mp}^{(j)}(\rho) = \begin{cases} \begin{bmatrix} \frac{-ima_j}{\alpha_{mp}\rho} J_m(\alpha_{mp}\rho/a_j) \\ J_m'(\alpha_{mp}\rho/a_j) \end{bmatrix}, & \text{for } \rho < a_j \\ 0, & \text{for } \rho > a_j \end{cases} \tag{26b}$$

β_{mn} and α_{mp} are the nth and pth zeros of $J_m'(\beta_{mn}) = 0$ and $J_m(\alpha_{mp}) = 0$, respectively. In the above, N and P correspond to the number of TM and TE basis functions, respectively, taken for the upper disk and R and S correspond to those taken for the lower disk.

The corresponding vector Hankel transform of the currents $\overline{K}_m^{(j)}(k_\rho)$ $(j = 1, 2)$ are given by the following

$$\overline{K}_m^{(1)}(k_\rho) = \sum_{n=1}^{N} a_{mn}^{(1)} \overline{\psi}_{mn}^{(1)}(k_\rho) + \sum_{p=1}^{P} b_{mp}^{(1)} \overline{\phi}_{mp}^{(1)}(k_\rho) \tag{27a}$$

$$\overline{K}_m^{(2)}(k_\rho) = \sum_{r=1}^{R} a_{mr}^{(2)} \overline{\psi}_{mr}^{(2)}(k_\rho) + \sum_{s=1}^{S} b_{ms}^{(2)} \overline{\phi}_{ms}^{(2)}(k_\rho) \tag{27b}$$

where

$$\overline{\psi}_{mn}^{(j)}(k_\rho) = \beta_{mn} J_m(\beta_{mn}) \begin{bmatrix} \frac{1}{(\beta_{mn}/a_j)^2 - k_\rho^2} J_m'(k_\rho a_j) \\ \frac{ima_j}{\beta_{mn}^2 k_\rho} J_m(k_\rho a_j) \end{bmatrix} \tag{28a}$$

$$\overline{\phi}_{mp}^{(j)}(k_\rho) = \frac{k_\rho a_j J_m'(\alpha_{mp})}{k_\rho^2 - (\alpha_{mp}/a_j)^2} \begin{bmatrix} 0 \\ J_m(k_\rho a_j) \end{bmatrix} \tag{28b}$$

Substituting these expressions into equation (21), we obtain for the mth mode

$$\begin{aligned}
\left[\overline{E}_{1,m}(\overline{\rho}, z = z_1')\right]_T &= \sum_{n=1}^{N} a_{mn}^{(1)} \int_0^\infty dk_\rho k_\rho \overline{\overline{J}}_m(k_\rho\rho) \cdot \overline{\overline{\xi}}_{1,1}\Big|_{x'=x_1', z=z_1'} \cdot \overline{\psi}_{mn}^{(1)}(k_\rho) \\
&+ \sum_{p=1}^{P} b_{mp}^{(1)} \int_0^\infty dk_\rho k_\rho \overline{\overline{J}}_m(k_\rho\rho) \cdot \overline{\overline{\xi}}_{1,1}\Big|_{x'=x_1', z=z_1'} \cdot \overline{\phi}_{mp}^{(1)}(k_\rho) \\
&+ \sum_{r=1}^{R} a_{mr}^{(2)} \int_0^\infty dk_\rho k_\rho \overline{\overline{J}}_m(k_\rho\rho) \cdot \overline{\overline{\xi}}_{1,2}\Big|_{x'=x_2', z=z_1'} \cdot \overline{\psi}_{mr}^{(2)}(k_\rho) \\
&+ \sum_{s=1}^{S} b_{ms}^{(2)} \int_0^\infty dk_\rho k_\rho \overline{\overline{J}}_m(k_\rho\rho) \cdot \overline{\overline{\xi}}_{1,2}\Big|_{x'=x_2', z=z_1'} \cdot \overline{\phi}_{ms}^{(2)}(k_\rho) \\
&= 0, \qquad \rho < a_1
\end{aligned} \tag{29a}$$

$$\begin{aligned}
\left[\overline{E}_{2,m}(\overline{\rho}, z = z_2')\right]_T &= \sum_{n=1}^{N} a_{mn}^{(1)} \int_0^\infty dk_\rho k_\rho \overline{\overline{J}}_m(k_\rho\rho) \cdot \overline{\overline{\xi}}_{2,1}\Big|_{x'=x_1', z=z_2'} \cdot \overline{\psi}_{mn}^{(1)}(k_\rho) \\
&+ \sum_{p=1}^{P} b_{mp}^{(1)} \int_0^\infty dk_\rho k_\rho \overline{\overline{J}}_m(k_\rho\rho) \cdot \overline{\overline{\xi}}_{2,1}\Big|_{x'=x_1', z=z_2'} \cdot \overline{\phi}_{mp}^{(1)}(k_\rho) \\
&+ \sum_{r=1}^{R} a_{mr}^{(2)} \int_0^\infty dk_\rho k_\rho \overline{\overline{J}}_m(k_\rho\rho) \cdot \overline{\overline{\xi}}_{2,2}\Big|_{x'=x_2', z=z_2'} \cdot \overline{\psi}_{mr}^{(2)}(k_\rho) \\
&+ \sum_{s=1}^{S} b_{ms}^{(2)} \int_0^\infty dk_\rho k_\rho \overline{\overline{J}}_m(k_\rho\rho) \cdot \overline{\overline{\xi}}_{2,2}\Big|_{x'=x_2', z=z_2'} \cdot \overline{\phi}_{ms}^{(2)}(k_\rho) \\
&= 0, \qquad \rho < a_2
\end{aligned} \tag{29b}$$

where we have defined $\overline{\overline{\xi}}_{l,p}(k_\rho, z, z') = -\frac{\omega\mu_p}{2}\overline{\overline{\zeta}}_{l,p}(k_\rho, z, z')$.

Multiplying (29a) by $\rho\overline{\psi}_{mh}^{(1)\dagger}(\rho)$ and $\rho\overline{\phi}_{mi}^{(1)\dagger}(\rho)$ and integrating from zero to infinity for $h = 1, 2, \ldots, N$ and $i = 1, 2, \ldots, P$, and applying Parseval's relation for the vector Hankel transform [24], we obtain

$$\begin{aligned}
&\sum_{n=1}^{N} a_{mn}^{(1)} \int_0^\infty dk_\rho k_\rho \overline{\psi}_{mh}^{(1)\dagger}(k_\rho) \cdot \overline{\overline{\xi}}_{1,1}\Big|_{x'=x_1', z=z_1'} \cdot \overline{\psi}_{mn}^{(1)}(k_\rho) \\
&+ \sum_{p=1}^{P} b_{mp}^{(1)} \int_0^\infty dk_\rho k_\rho \overline{\psi}_{mh}^{(1)\dagger}(k_\rho) \cdot \overline{\overline{\xi}}_{1,1}\Big|_{x'=x_1', z=z_1'} \cdot \overline{\phi}_{mp}^{(1)}(k_\rho) \\
&+ \sum_{r=1}^{R} a_{mr}^{(2)} \int_0^\infty dk_\rho k_\rho \overline{\psi}_{mh}^{(1)\dagger}(k_\rho) \cdot \overline{\overline{\xi}}_{1,2}\Big|_{x'=x_2', z=z_1'} \cdot \overline{\psi}_{mr}^{(2)}(k_\rho) \\
&+ \sum_{s=1}^{S} b_{ms}^{(2)} \int_0^\infty dk_\rho k_\rho \overline{\psi}_{mh}^{(1)\dagger}(k_\rho) \cdot \overline{\overline{\xi}}_{1,2}\Big|_{x'=x_2', z=z_1'} \cdot \overline{\phi}_{ms}^{(2)}(k_\rho) \\
&= 0, \qquad h = 1, 2, \ldots, N
\end{aligned} \tag{30a}$$

$$\sum_{n=1}^{N} a_{mn}^{(1)} \int_0^\infty dk_\rho k_\rho \overline{\phi}_{mi}^{(1)\dagger}(k_\rho) \cdot \overline{\overline{\xi}}_{1,1}\Big|_{x'=x_1',x=x_1'} \cdot \overline{\psi}_{mn}^{(1)}(k_\rho)$$
$$+ \sum_{p=1}^{P} b_{mp}^{(1)} \int_0^\infty dk_\rho k_\rho \overline{\phi}_{mi}^{(1)\dagger}(k_\rho) \cdot \overline{\overline{\xi}}_{1,1}\Big|_{x'=x_1',x=x_1'} \cdot \overline{\phi}_{mp}^{(1)}(k_\rho)$$
$$+ \sum_{r=1}^{R} a_{mr}^{(2)} \int_0^\infty dk_\rho k_\rho \overline{\phi}_{mi}^{(1)\dagger}(k_\rho) \cdot \overline{\overline{\xi}}_{1,2}\Big|_{x'=x_2',x=x_1'} \cdot \overline{\psi}_{mr}^{(2)}(k_\rho)$$
$$+ \sum_{s=1}^{S} b_{ms}^{(2)} \int_0^\infty dk_\rho k_\rho \overline{\phi}_{mi}^{(1)\dagger}(k_\rho) \cdot \overline{\overline{\xi}}_{1,2}\Big|_{x'=x_2',x=x_1'} \cdot \overline{\phi}_{ms}^{(2)}(k_\rho)$$
$$= 0, \qquad i = 1, 2, \ldots, P \tag{30b}$$

Similarly, multiplying (29b) by $\rho\overline{\psi}_{mj}^{(2)\dagger}(\rho)$ and $\rho\overline{\phi}_{mk}^{(2)\dagger}(\rho)$ and integrating from zero to infinity for $j = 1, 2, \ldots, R$ and $k = 1, 2, \ldots, S$, and applying Parseval's relation, we obtain

$$\sum_{n=1}^{N} a_{mn}^{(1)} \int_0^\infty dk_\rho k_\rho \overline{\psi}_{mj}^{(2)\dagger}(k_\rho) \cdot \overline{\overline{\xi}}_{2,1}\Big|_{x'=x_1',x=x_2'} \cdot \overline{\psi}_{mn}^{(1)}(k_\rho)$$
$$+ \sum_{p=1}^{P} b_{mp}^{(1)} \int_0^\infty dk_\rho k_\rho \overline{\psi}_{mj}^{(2)\dagger}(k_\rho) \cdot \overline{\overline{\xi}}_{2,1}\Big|_{x'=x_1',x=x_2'} \cdot \overline{\phi}_{mp}^{(1)}(k_\rho)$$
$$+ \sum_{r=1}^{R} a_{mr}^{(2)} \int_0^\infty dk_\rho k_\rho \overline{\psi}_{mj}^{(2)\dagger}(k_\rho) \cdot \overline{\overline{\xi}}_{2,2}\Big|_{x'=x_2',x=x_2'} \cdot \overline{\psi}_{mr}^{(2)}(k_\rho)$$
$$+ \sum_{s=1}^{S} b_{ms}^{(2)} \int_0^\infty dk_\rho k_\rho \overline{\psi}_{mj}^{(2)\dagger}(k_\rho) \cdot \overline{\overline{\xi}}_{2,2}\Big|_{x'=x_2',x=x_2'} \cdot \overline{\phi}_{ms}^{(2)}(k_\rho)$$
$$= 0, \qquad j = 1, 2, \ldots, R \tag{30c}$$

$$0 = \sum_{n=1}^{N} a_{mn}^{(1)} \int_0^\infty dk_\rho k_\rho \overline{\phi}_{mk}^{(2)\dagger}(k_\rho) \cdot \overline{\overline{\xi}}_{2,1}\Big|_{x'=x_1',x=x_2'} \cdot \overline{\psi}_{mn}^{(1)}(k_\rho)$$
$$+ \sum_{p=1}^{P} b_{mp}^{(1)} \int_0^\infty dk_\rho k_\rho \overline{\phi}_{mk}^{(2)\dagger}(k_\rho) \cdot \overline{\overline{\xi}}_{2,1}\Big|_{x'=x_1',x=x_2'} \cdot \overline{\phi}_{mp}^{(1)}(k_\rho)$$
$$+ \sum_{r=1}^{R} a_{mr}^{(2)} \int_0^\infty dk_\rho k_\rho \overline{\phi}_{mk}^{(2)\dagger}(k_\rho) \cdot \overline{\overline{\xi}}_{2,2}\Big|_{x'=x_2',x=x_2'} \cdot \overline{\psi}_{mr}^{(2)}(k_\rho)$$
$$+ \sum_{s=1}^{S} b_{ms}^{(2)} \int_0^\infty dk_\rho k_\rho \overline{\phi}_{mk}^{(2)\dagger}(k_\rho) \cdot \overline{\overline{\xi}}_{2,2}\Big|_{x'=x_2',x=x_2'} \cdot \overline{\phi}_{ms}^{(2)}(k_\rho)$$
$$= 0, \qquad j = 1, 2, \ldots, S \tag{30d}$$

These four equations (30a)-(30d) constitute a system of $N + P + R + S$ linear algebraic equations which may be written in matrix form

$$\overline{\overline{A}} \cdot \overline{c} = 0 \tag{31}$$

where

$$\overline{\overline{A}} = \begin{bmatrix} [A]^{\psi^{(1)}\psi^{(1)}}_{N\times N} & [A]^{\psi^{(1)}\phi^{(1)}}_{N\times P} & [A]^{\psi^{(1)}\psi^{(2)}}_{N\times R} & [A]^{\psi^{(1)}\phi^{(2)}}_{N\times S} \\ [A]^{\phi^{(1)}\psi^{(1)}}_{P\times N} & [A]^{\phi^{(1)}\phi^{(1)}}_{P\times P} & [A]^{\phi^{(1)}\psi^{(2)}}_{P\times R} & [A]^{\phi^{(1)}\phi^{(2)}}_{P\times S} \\ [A]^{\psi^{(2)}\psi^{(1)}}_{R\times N} & [A]^{\psi^{(2)}\phi^{(1)}}_{R\times P} & [A]^{\psi^{(2)}\psi^{(2)}}_{R\times R} & [A]^{\psi^{(2)}\phi^{(2)}}_{R\times S} \\ [A]^{\phi^{(2)}\psi^{(1)}}_{S\times N} & [A]^{\phi^{(2)}\phi^{(1)}}_{S\times P} & [A]^{\phi^{(2)}\psi^{(2)}}_{S\times R} & [A]^{\phi^{(2)}\phi^{(2)}}_{S\times S} \end{bmatrix} \tag{32}$$

and

$$\overline{c} = \begin{bmatrix} [a_m^{(1)}]_{N\times 1} \\ [b_m^{(1)}]_{P\times 1} \\ [a_m^{(2)}]_{R\times 1} \\ [b_m^{(2)}]_{S\times 1} \end{bmatrix} \tag{33}$$

Each element of the submatrices of $\overline{\overline{A}}$ is given by

$$A^{\gamma^{(i)}\chi^{(p)}}_{jk} = \int_0^\infty dk_\rho k_\rho \overline{\gamma}^{(i)\dagger}_{mj}(k_\rho) \cdot \overline{\overline{\xi}}_{l,p}(k_\rho) \cdot \overline{\chi}^{(p)}_{mk}(k_\rho) \tag{34}$$

where $\overline{\gamma}^{(i)}_{mn}(k_\rho)$ and $\overline{\chi}^{(i)}_{mn}(k_\rho)$ represent either $\overline{\psi}^{(i)}_{mn}(k_\rho)$ or $\overline{\phi}^{(i)}_{mn}(k_\rho)$. More explicitly, the integrals of (34) may be written as

$$\begin{aligned} A^{\psi^{(i)}\psi^{(p)}}_{jk} &= \beta_{mj} J_m(\beta_{mj}) \beta_{mk} J_m(\beta_{mk}) \int_0^\infty dk_\rho k_\rho \frac{J'_m(k_\rho a_l) J'_m(k_\rho a_p)}{\left[(\beta_{mj}/a_l)^2 - k_\rho^2\right]\left[(\beta_{mk}/a_p)^2 - k_\rho^2\right]} \xi^{\mathrm{TM}}_{l,p}(k_\rho) \\ &\quad + J_m(\beta_{mj}) J_m(\beta_{mk}) \frac{m^2 a_l a_p}{\beta_{mj}\beta_{mk}} \int_0^\infty dk_\rho \frac{J_m(k_\rho a_l) J_m(k_\rho a_p)}{k_\rho} \xi^{\mathrm{TE}}_{l,p}(k_\rho) \end{aligned} \tag{35a}$$

$$A^{\psi^{(i)}\phi^{(p)}}_{jk} = -A^{\phi^{(p)}\psi^{(i)}}_{kj} = im a_l a_p \frac{J_m(\beta_{mj})}{\beta_{mj}} J'_m(\alpha_{mk}) \int_0^\infty dk_\rho k_\rho \frac{J_m(k_\rho a_l) J_m(k_\rho a_p)}{(\alpha_{mk}/a_p)^2 - k_\rho^2} \xi^{\mathrm{TE}}_{l,p}(k_\rho) \tag{35b}$$

$$A^{\phi^{(i)}\phi^{(p)}}_{jk} = a_l a_p J'_m(\alpha_{mj}) J'_m(\alpha_{mk}) \int_0^\infty dk_\rho k_\rho^3 \frac{J_m(k_\rho a_l) J_m(k_\rho a_p)}{\left[(\alpha_{mj}/a_l)^2 - k_\rho^2\right]\left[(\alpha_{mk}/a_p)^2 - k_\rho^2\right]} \xi^{\mathrm{TE}}_{l,p}(k_\rho) \tag{35c}$$

As the resonant frequencies are complex due to radiation loss, the branch point and the surface wave pole singularities of the functions $\xi^{\alpha}_{l,p}(k_\rho)$ ($\alpha = \mathrm{TE}, \mathrm{TM}$) are also complex. Therefore, the path of integration in the complex k_ρ-plane is deformed below the real axis to avoid these singularities. The integrals of equations (35) are evaluated numerically along the integration path shown in Figure 3.

For nontrivial solutions of the system of equations (31), it is required that

$$\det |\overline{\overline{A}}(\omega)| = 0 \tag{36}$$

This is the eigenvalue equation for the stacked circular microstrip antenna. Since the basis functions (25) form a complete set, the eigenvalues of (36) correspond to the exact resonant frequencies of the stacked microstrip antenna structure as N, P, R, and $S \rightarrow \infty$. With a judicious choice of basis functions, usually only several basis functions are needed to obtain accurate results.

4. NUMERICAL RESULTS AND DISCUSSION

The complex resonant frequencies in the following results are calculated versus the parameter h_2/a_2, which from a practical viewpoint, is the parameter most easily varied if the substrates of medium 1 and medium 3, on which the microstrip disks are printed, are fixed. Attention is given to the lowest order mode with $m = 1$. This mode is the lowest order mode which radiates maximally in the broadside direction and is widely used in microstrip antenna applications. For the lowest $m = 1$ mode, convergence of the solution for the different configurations presented is confirmed by varying the number of current basis functions on the upper and lower disks, which are taken to be $\left[(N = 2, P = 0), (R = 1, S = 0)\right]$, $\left[(N = 2, P = 1), (R = 2, S = 1)\right]$, $\left[(N = 3, P = 2), (R = 2, S = 2)\right]$, and $\left[(N = 4, P = 3), (R = 3, S = 2)\right]$. It is found that the solutions converge and that the resonance curves using basis functions with $\left[(N = 4, P = 3), (R = 3, S = 2)\right]$ follow closely those using basis functions with $\left[(N = 3, P = 2), (R = 2, S = 2)\right]$ for the cases presented, where the maximum relative difference between the two curves is less than one percent. The convergence of the solution for the lowest $m = 1$ mode is illustrated in Figure 4 for configuration A with $a_1/a_2 = 1$, $h_1 = h_3 = 0.1a_2$, $\epsilon_1 = \epsilon_3 = 2.65\epsilon_0$, and $\epsilon_2 = 1.01\epsilon_0$. From Figure 4, it is shown that the stacked circular microstrip structure has dual resonant frequencies associated with the two disks. As illustrated in the figure, the number of basis functions must be sufficient so that the correct resonant behavior near $h_2/a_2 \cong 0.8$ is obtained, or, so that the coupling interaction between the two disks may be adequately accounted for.

To explain physically the resonant behavior of the stacked microstrip structure, it will be shown that the dual resonant frequencies may be related to the resonant frequencies of two constitutive resonators of the structure which are electromagnetically coupled through their fringing fields. For thin substrates, the constitutive resonators have resonant frequencies close to those of cavities with electric top and bottom walls and lossy magnetic side walls. Considering configuration A, one resonance of the stacked structure is associated with the cavity formed by the lower disk and the ground plane illustrated in Figure 5(a). The second resonance is considered in two limits of the substrate height h_2. In the small h_2 limit when the ratio a_1/a_2 is not too large, the second resonance may be associated with the cavity formed by the two disks as shown in Figure 5(b). For large h_2, the second resonance may be associated with the cavity formed by the upper disk and the ground plane as shown in Figure 5(c). In comparing the resonances of the stacked microstrip structure to those associated with the constitutive cavity resonators, the resonances associated with the cavities of Figures 5(a) and 5(c) are calculated using the configurations of Figures 6(a) and 6(c), respectively. The resonant frequency associated with the cavity of Figure 5(b) formed by the two disks is calculated approximately using the configuration of Figure 6(b). Configuration B may be considered in a similar manner.

To illustrate the relation between the resonances of the stacked microstrip structure to those of its constitutive resonators, shown in Figure 7 are the resonant frequencies for the lowest $m = 1$ mode of configuration A, compared with the resonances associated with the configurations of Figure 6. The open circles and squares on the solid curves are used to help distinguish the two pairs of resonant frequencies. For small h_2, the two resonances correspond to $k_3 a_2 \cong \beta_{11}$ and $k_2 a_1 \cong \beta_{11}$ where $\beta_{11} \cong 1.84$. It is seen that, for comparable disk radii, the ratio $a_1\sqrt{\mu_2\epsilon_2}/a_2\sqrt{\mu_3\epsilon_3}$ approximately determines the separation of the two resonant frequencies for small h_2. It is shown that in both the small and large h_2 limits, the resonant frequencies approach those associated with the constitutive resonators. Thus, the coupling interaction between the two constitutive resonators in these two limits is small. For intermediate values of h_2, the resonant frequencies associated with the constitutive resonators are affected by the electromagnetic coupling between them. As in Figure 7, the two resonance curves essentially follow those of the constitutive resonators with the most deviation occuring where the real parts of the resonant frequencies of the constitutive resonators are approximately equal. The presence of the upper disk increases that radiation

loss associated with the cavity formed by the lower disk and the ground plane.

To illustrate the effect of different disk radii on the resonance frequencies, shown in Figures 8 and 9 are the resonant frequencies for configuration A with $a_1/a_2 = 0.9$ and $a_1/a_2 = 1.1$, respectively. The constitutive resonators with $a_1/a_2 = 0.9$ are less coupled than those with $a_1/a_2 = 1$. This is consistent with the resonance curves in that the resonant frequencies with $a_1/a_2 = 0.9$ follow more closely the constitutive resonances than those of Figure 7 where $a_1/a_2 = 1$. Conversely, the resonators with $a_1/a_2 = 1.1$ are more tightly coupled than those with $a_1/a_2 = 1$, and therefore, the resonance curves deviate significantly from the constitutive resonances in the region of maximum coupling interaction. In fact, in the case $a_1/a_2 = 1.1$, the coupling is such that in the region where the constitutive resonances are approximately equal, the resonances of the coupled structure split such that the resonant curves follow opposite constitutive resonances in the small and large h_2 limits.

The effect of increasing the substrate heights is illustrated in Figure 10 where the resonance curves for configuration A with $a_1/a_2 = 1$ and $h_1 = h_3 = 0.2a_2$ are plotted. The coupling between the resonators is tighter in this case relative to that of Figure 7 where $h_1 = h_3 = 0.1a_2$ due to the increase in fringing fields.

The resonant frequencies for configuration B with $a_1/a_2 = 1$, $h_1 = h_3 = 0.1a_2$, $\epsilon_1 = \epsilon_3 = 2.65\epsilon_0$, and $\epsilon_2 = 1.01\epsilon_0$ are shown in Figure 11. In this case, as h_2 approaches zero, both resonant frequencies approach the same value. However, due to the presence of the air gap, when h_2 is small, the resonant frequency associated with the cavity fromed by the two disks is a rapidly varying function of h_2, making this configuration undesirable in some practical cases where height tolerances cannot be maintained.

The advantage of the stacked structure over conventional microstrip antennas is the introduction of the second resonance which, when close to the first resonance may provide for wide bandwidth operation, or, when separated from the first resonance, may provide for dual frequency operation. In addition, the radiation loss associated with the cavity formed by lower disk and the ground plane may be enhanced by the presence of the upper disk, making the stacked microstrip antenna a better radiator than conventional microstrip antennas.

5. CONCLUSION

The complex resonant frequencies of the open structure of a microstrip antenna consisting of two circular microstrip disks in a stacked configuration have been rigorously calculated as a function of the layered parameters and the ratio of the radii of the two disks. Using a dyadic Green's function formulation for horizontally stratified media and the vector Hankel transform, the mixed boundary value problem is reduced to a set of coupled vector integral equations. Employing Galerkin's method in the spectral domain, the complex resonant frequencies are calculated and convergence of the results is demonstrated. It is shown that for each mode, the stacked circular microstrip structure has dual resonant frequencies which are associated with the two coupled constitutive resonators of the structure and which are a function of the mutual coupling between them. This mutal coupling depends on the geometrical configuration of the stacked structure, the layered parameters, and the disk radii. In the large and small h_2 limits, the resonant frequencies of the stacked microstrip structure approach those of the constitutive resonators. The maximum coupling effect occurs where the real parts of the resonant frequencies of the constitutive resonators are approximately equal, where the behavior of the resonances in this region is a function of the coupling. The dual frequency behavior of the stacked microstrip structure, easily controlled by varying the parameters of medium 2 and disk radii ratio, given fixed parameters for medium 1 and medium 3, may be used to broaden the bandwidth or provide for dual frequency use of the antenna.

Acknowledgments

This work was supported by the RADC Contract F19628-88-K-0013, the ARO Contract DAAL03-88-j-0057, the ONR Contract N00014-89-J-1019, the Joint Services Electronics Program under the Contract DAAL03-86-K-0002, and the NSF Grant 8620029-ECS.

6. REFERENCES

[1] K. R. Carver and J. W. Mink, "Microstrip Antenna Technology," *IEEE Trans. Antennas Propagat.*, Vol. AP-29, No. 1, pp. 2-23, Jan. 1981.

[2] R. J. Mailloux, J. F. McIlvenna, and N. P. Kernweis, "Microstrip Array Technology," *IEEE Trans. Antennas Propagat.*, Vol. AP-29, No. 1, pp. 25-37, Jan. 1981.

[3] H. G. Oltman, "Electromagnetically coupled microstrip dipole antenna elements," *Proceedings of the 8th European Microwave Conference*, Paris, pp. 281-285, 1977.

[4] H. G. Oltman and D. A. Huebner, "Electromagnetically coupled microstrip dipoles," *IEEE Trans. Antennas Propagat.*, Vol. AP-29, No. 1, pp. 151-157, Jan. 1981.

[5] P. S. Hall, C. Wood, and C. Garrett, "Wide bandwidth microstrip antennas for circuit integration," *Electron. Lett.*, Vol. 15, No. 15, pp. 458-460, 19 July 1979.

[6] A. Sabban, "A new broadband stacked two-layer microstrip antenna," *1983 IEEE AP-S International Symposium Digest*, pp. 63-66, June 1983.

[7] C. H. Chen, A. Tulintseff, and R. M. Sorbello, "Broadband two-layer microstrip antenna," *1984 IEEE AP-S International Symposium Digest*, pp. 251-254, June 1984.

[8] S. A. Long, and M. D. Walton, "A dual-frequency stacked circular-disc antenna," *IEEE Trans. Antennas Propagat.*, Vol. AP-27, No. 2, pp. 270-273, March 1979.

[9] J. S. Dahele, K.-F. Lee, and D. P. Wong, "Dual-frequency stacked annular-ring microstrip antenna," *IEEE Trans. Antennas Propagat.*, Vol. AP-35, No. 11, pp. 1281-1285, Nov. 1987.

[10] W. C. Chew and J. A. Kong, "Resonance of the axial-symmetric modes in microstrip disk resonators," *J. Math. Phys.*, Vol. 21, No. 3, pp. 582-591, March 1980.

[11] W. C. Chew and J. A. Kong, "Resonance of the nonaxial symmetric modes in circular microstrip disk antenna," *J. Math. Phys.*, Vol. 21, No. 10, pp. 2590-2598, Oct. 1980.

[12] S. Y. Poh, "Resonant frequencies and input impedance of a rectangular microstrip disk," S.M. thesis, Massachusetts Institute of Technology; Cambridge, MA, Sep. 1981.

[13] S. M. Ali, W. C. Chew and J. A. Kong, "Vector Hankel transform analysis of annular-ring microstrip antenna," *IEEE Trans. Antennas Propagat.*, Vol. AP-30, No. 4, pp. 637-644, July 1982.

[14] T. M. Habashy, J. A. Kong, and W. C. Chew, "Resonance and radiation of the elliptic disk microstrip structure, part I: Formulation," *IEEE Trans. Antennas Propagat.*, Vol. AP-35, No. 8, pp. 877-886, Aug. 1987.

[15] D. M. Pozar, "Input impedance and mutual coupling of rectangular microstrip antennas," *IEEE Trans. Antennas Propagat.*, Vol. AP-23, No. 6, pp. 1191-1196, Nov. 1982.

[16] S. M. Ali, T. M. Habashy, and J. A. Kong, "Resonance in two coupled circular microstrip disk resonators," *J. Math. Phys.*, Vol. 53, No. 9, pp. 6418-6429, Sep. 1982.

[17] T. M. Habashy, S. M. Ali, and J. A. Kong, "Impedance paramters and radiation pattern of two coupled circular microstrip disk antennas," *J. Math. Phys.*, Vol. 54, No. 2, pp. 493-506, Feb. 1983.

[18] P. B. Katehi, N. G. Alexopoulos, and I. Y. Hsia, "Bandwidth enhancement method for microstrip antennas," *IEEE Trans. Antennas Propagat.*, Vol. AP-35, No. 1, pp. 5-12, Jan. 1987.

[19] A. N. Tulintseff, and R. M. Sorbello, "Current and radiation fields of electromagnetically coupled microstrip antennas," *1987 IEEE AP-S International Symposium Digest*, Vol. 2, pp. 928-931, June 1987.

[20] R. Kastner, E. Heyman, and A. Sabban, "Spectral domain iterative analysis of single- and double-layered microstrip antennas using the conjugate gradient algorithm," *IEEE Trans. Antennas Propagat.*, Vol. AP-36, No. 9, pp. 1204-1212, Sep. 1988.

[21] J. A. Kong, *Electromagnetic Wave Theory*, John Wiley & Sons, Inc., 1986.

[22] S. M. Ali, T. M. Habashy, and J. A. Kong, "Dyadic Green's functions for multilayered anisotropic media," to be submitted for publication.

[23] T. M. Habashy, S. M. Ali, and J. A. Kong, "Dyadic Green's function representations in cylindrical and elliptical coordinates in uniaxially anisotropic media," to be submitted for publication.

[24] W. C. Chew and T. M. Habashy, "The use of vector transforms in solving some electromagnetic scattering problems," *IEEE Trans. Antennas Propagat.*, Vol. AP-34, No. 7, pp. 871-879, July 1986.

LIST OF FIGURES

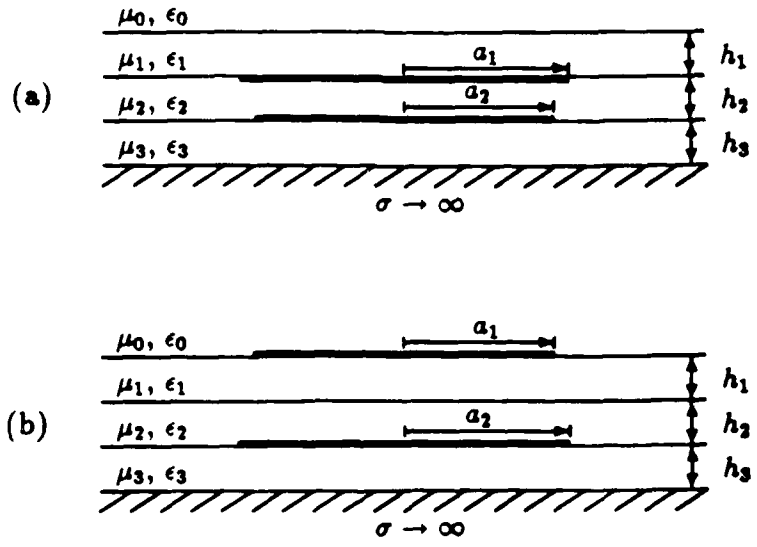
(a)
μ_0, ϵ_0
μ_1, ϵ_1
μ_2, ϵ_2
μ_3, ϵ_3
a_1
a_2
h_1
h_2
h_3
$\sigma \to \infty$
(b)
μ_0, ϵ_0
μ_1, ϵ_1
μ_2, ϵ_2
μ_3, ϵ_3
a_1
a_2
h_1
h_2
h_3
$\sigma \to \infty$

FIGURE 1

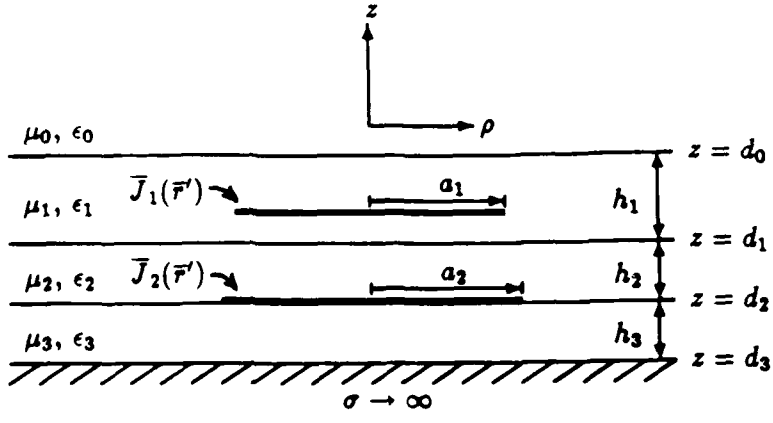

FIGURE 2

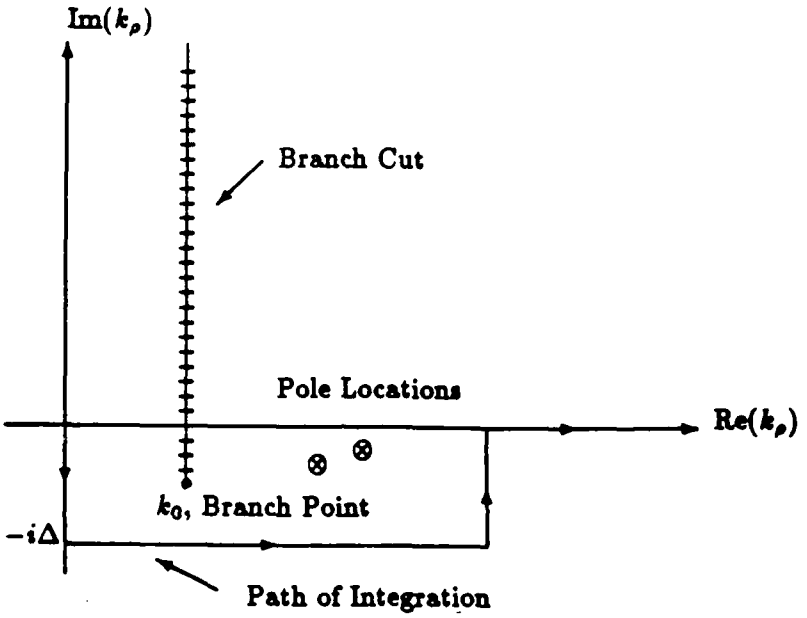
Im(k_ρ)
Branch Cut
Pole Locations
Re(k_ρ)
k_0, Branch Point
$-i\Delta$
Path of Integration

FIGURE 3

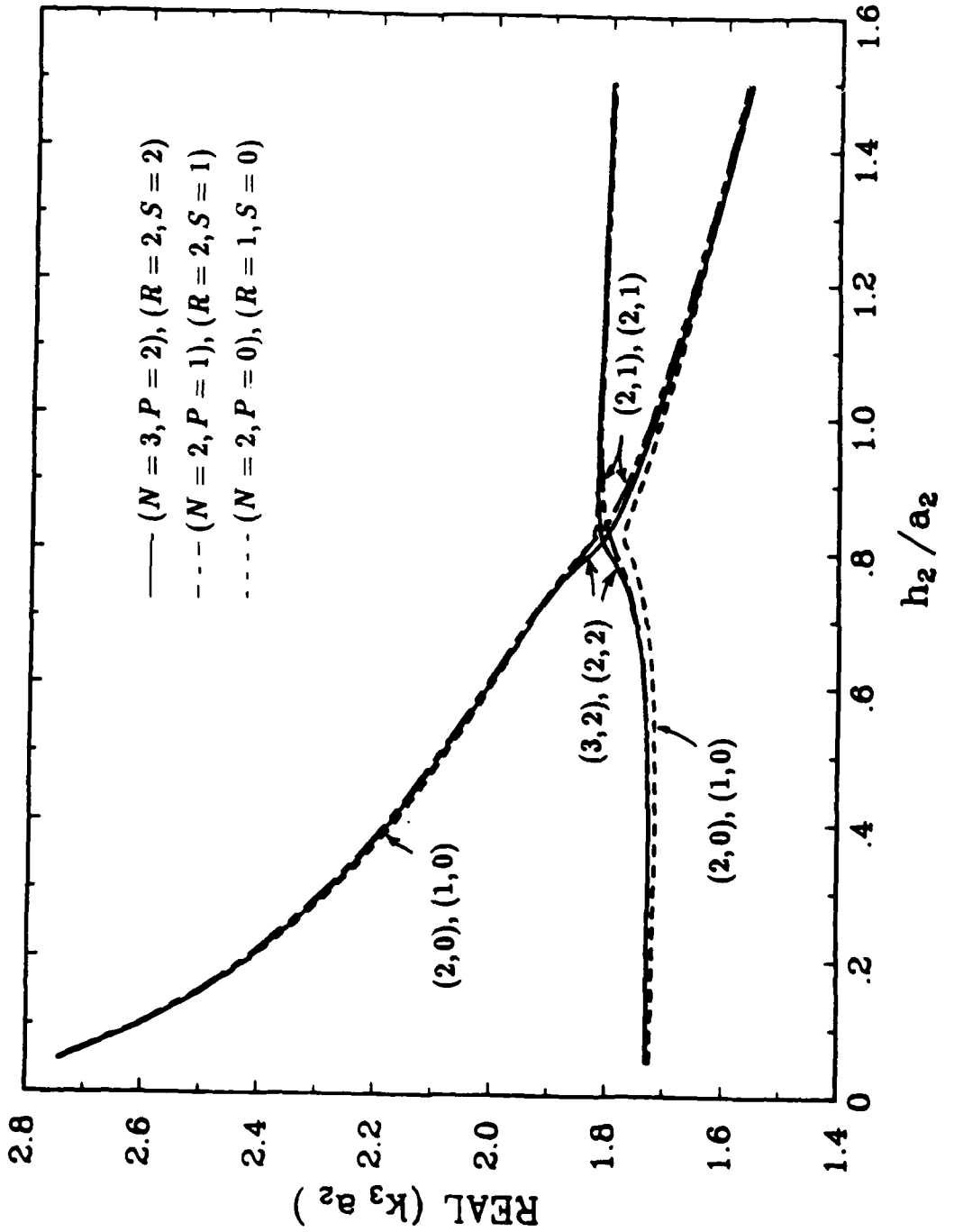
REAL (k_3 a_2)
h_2 / a_2
$(N = 3, P = 2), (R = 2, S = 2)$
$(N = 2, P = 1), (R = 2, S = 1)$
$(N = 2, P = 0), (R = 1, S = 0)$
(2,0), (1,0)
(3,2), (2,2)
(2,1), (2,1)
(2,0), (1,0)
2.8
2.6
2.4
2.2
2.0
1.8
1.6
1.4
0
.2
.4
.6
.8
1.0
1.2
1.4
1.6

FIGURE 4(a)

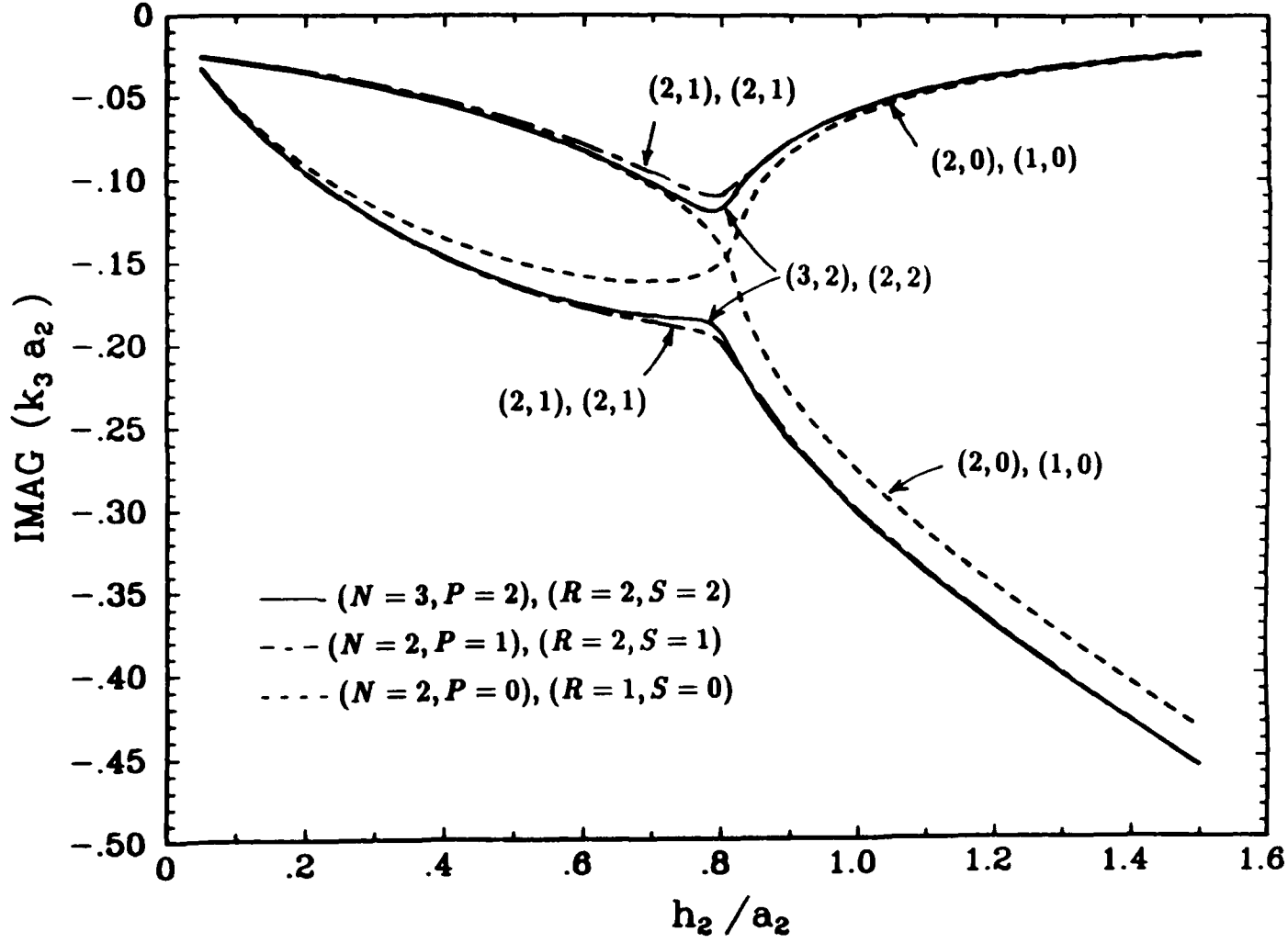
0
-.05
-.10
-.15
-.20
-.25
-.30
-.35
-.40
-.45
-.50
IMAG (k_3 a_2)
0
.2
.4
.6
.8
1.0
1.2
1.4
1.6
h_2 / a_2
(2,1), (2,1)
(2,0), (1,0)
(3,2), (2,2)
(2,1), (2,1)
(2,0), (1,0)
—— ($N = 3, P = 2$), ($R = 2, S = 2$)
- - - ($N = 2, P = 1$), ($R = 2, S = 1$)
- - - - ($N = 2, P = 0$), ($R = 1, S = 0$)

Figure 4(b)

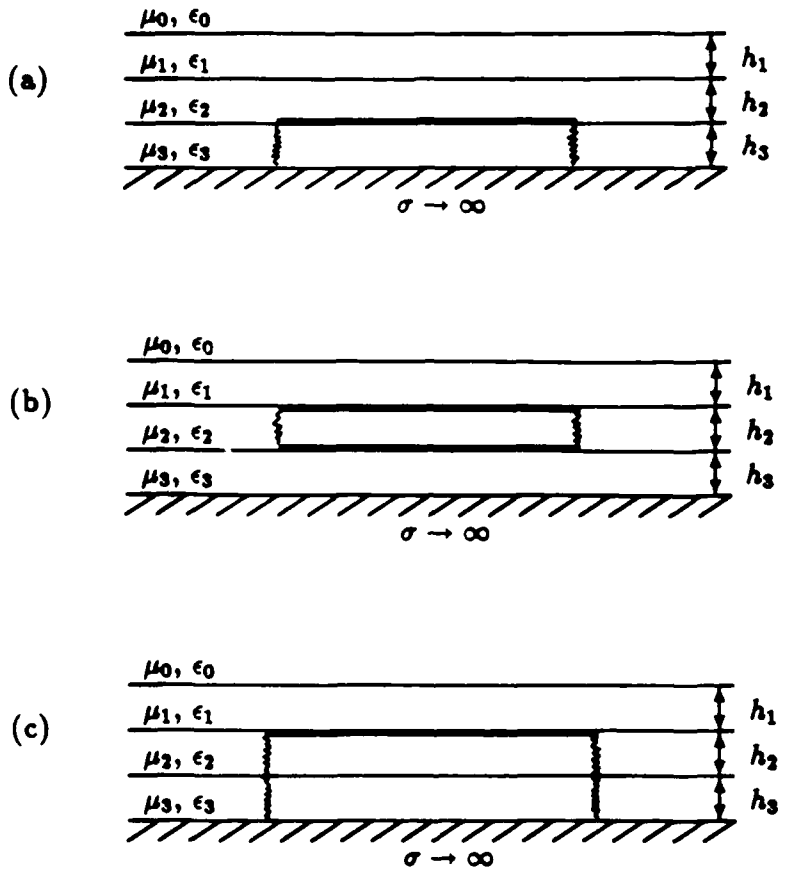
(a)
μ_0, ϵ_0
μ_1, ϵ_1
μ_2, ϵ_2
μ_3, ϵ_3
h_1
h_2
h_3
$\sigma \to \infty$
(b)
μ_0, ϵ_0
μ_1, ϵ_1
μ_2, ϵ_2
μ_3, ϵ_3
h_1
h_2
h_3
$\sigma \to \infty$
(c)
μ_0, ϵ_0
μ_1, ϵ_1
μ_2, ϵ_2
μ_3, ϵ_3
h_1
h_2
h_3
$\sigma \to \infty$

FIGURE 5

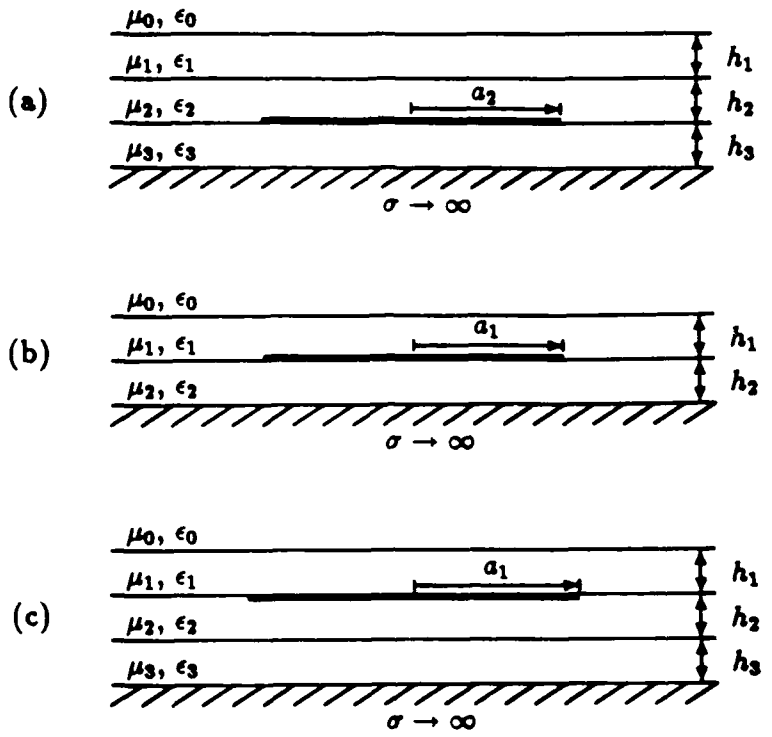
(a)
μ_0, ϵ_0
μ_1, ϵ_1
μ_2, ϵ_2
μ_3, ϵ_3
a_2
h_1
h_2
h_3
$\sigma \to \infty$
(b)
μ_0, ϵ_0
μ_1, ϵ_1
μ_2, ϵ_2
a_1
h_1
h_2
$\sigma \to \infty$
(c)
μ_0, ϵ_0
μ_1, ϵ_1
μ_2, ϵ_2
μ_3, ϵ_3
a_1
h_1
h_2
h_3
$\sigma \to \infty$

FIGURE 6

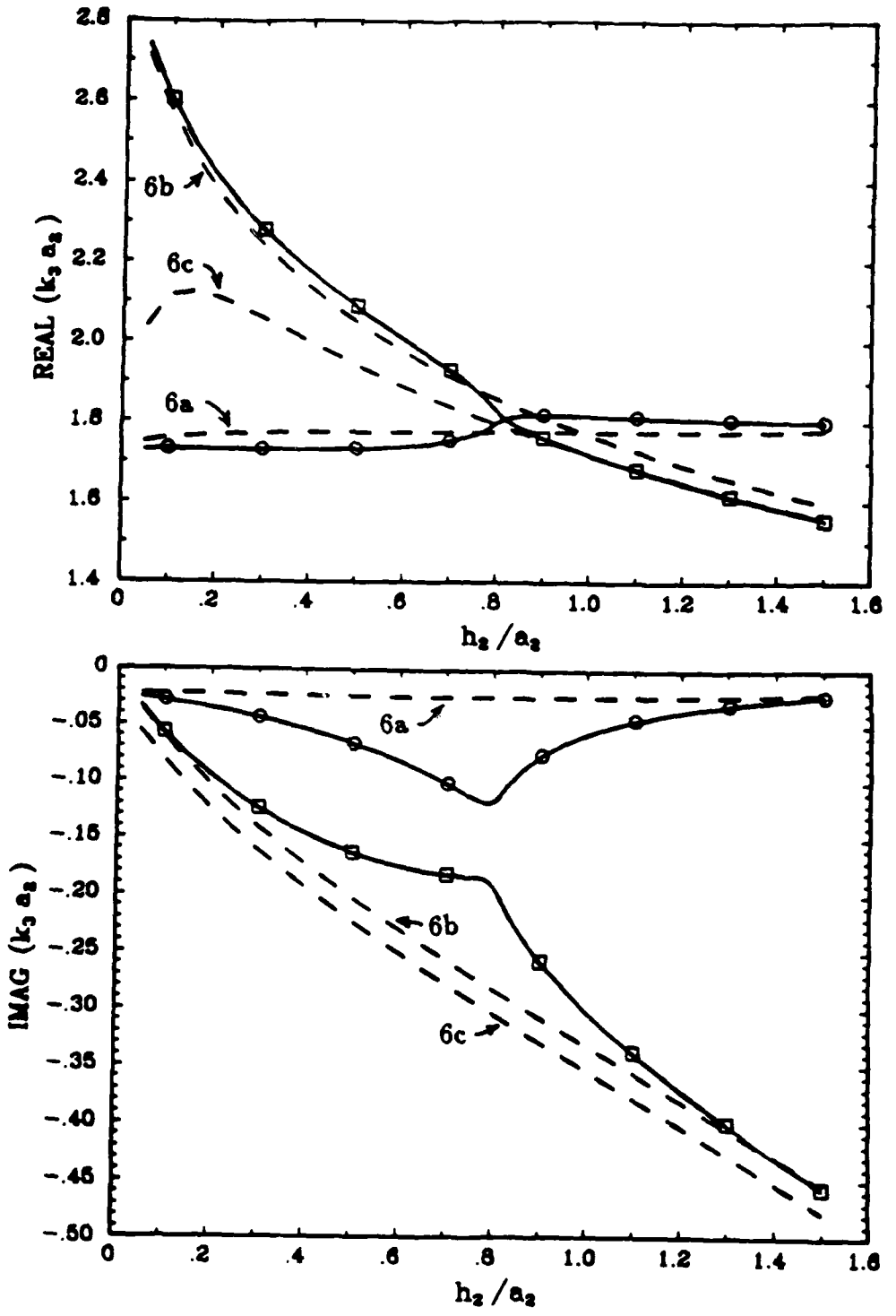
REAL ($k_2 a_2$)
2.8
2.6
2.4
2.2
2.0
1.8
1.6
1.4
6b
6c
6a
0
.2
.4
.6
.8
1.0
1.2
1.4
1.6
h_2 / a_2
IMAG ($k_2 a_2$)
0
-.05
-.10
-.15
-.20
-.25
-.30
-.35
-.40
-.45
-.50
6a
6b
6c
0
.2
.4
.6
.8
1.0
1.2
1.4
1.6
h_2 / a_2

FIGURE 7

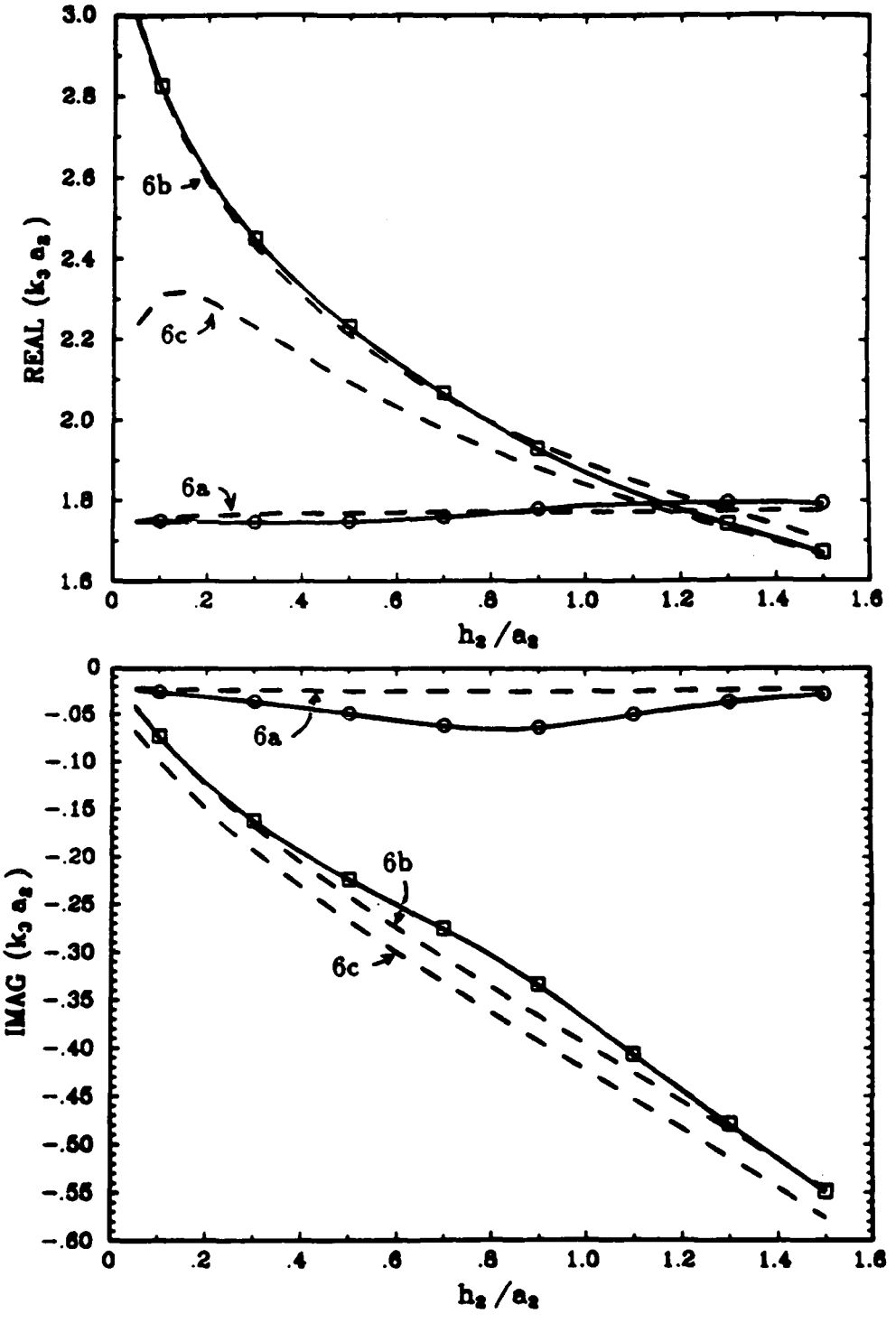
3.0
2.8
2.6
2.4
2.2
2.0
1.8
1.6
REAL (k_3 a_2)
6b
6c
6a
0
.2
.4
.6
.8
1.0
1.2
1.4
1.6
h_2 / a_2
0
-.05
-.10
-.15
-.20
-.25
-.30
-.35
-.40
-.45
-.50
-.55
-.60
IMAG (k_3 a_2)
6a
6b
6c
0
.2
.4
.6
.8
1.0
1.2
1.4
1.6
h_2 / a_2

FIGURE 8

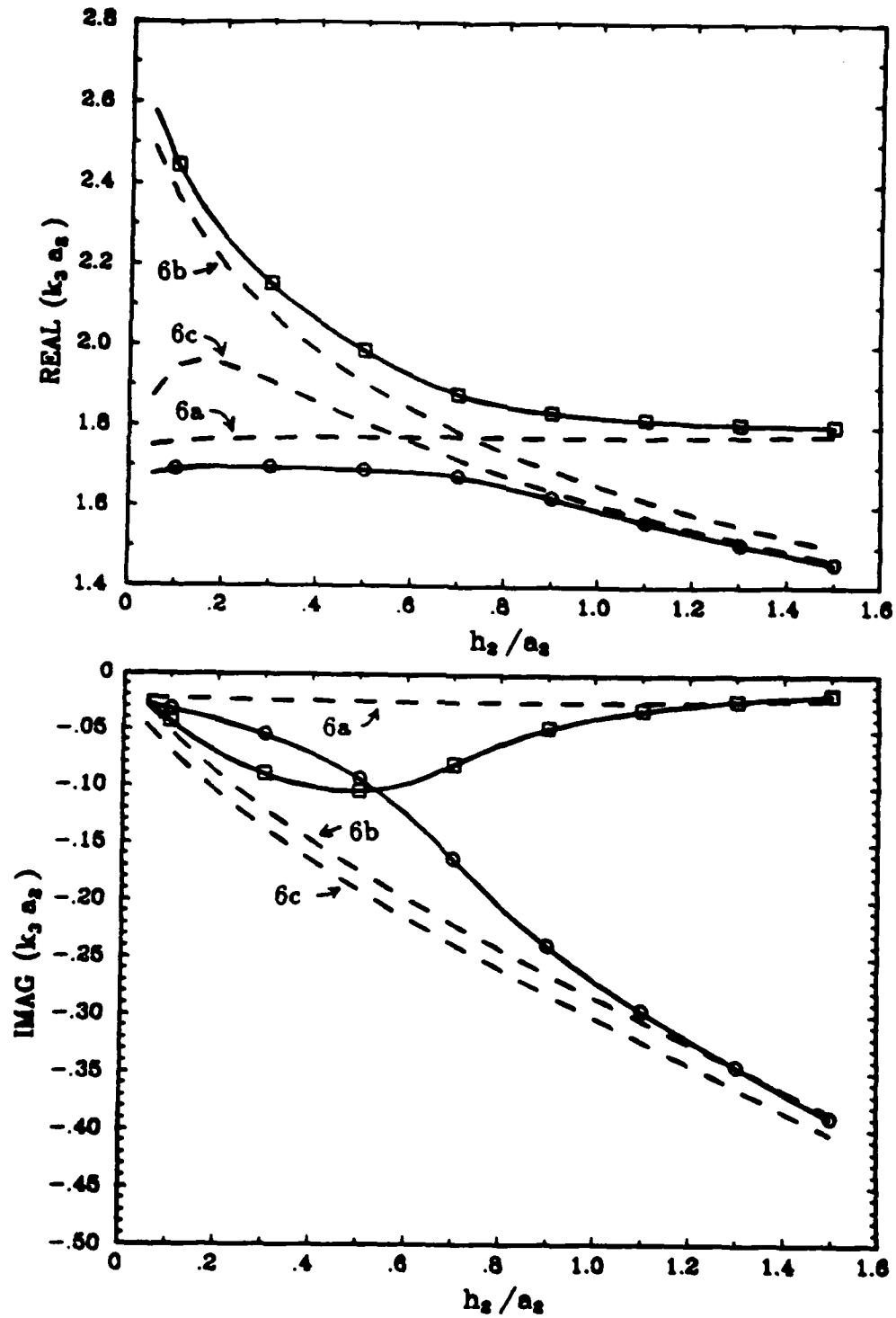
REAL ($k_3 a_3$)
2.8
2.6
2.4
2.2
2.0
1.8
1.6
1.4
6b
6c
6a
0
.2
.4
.6
.8
1.0
1.2
1.4
1.6
h_3 / a_3
IMAG ($k_3 a_3$)
0
-.05
-.10
-.15
-.20
-.25
-.30
-.35
-.40
-.45
-.50
6a
6b
6c
0
.2
.4
.6
.8
1.0
1.2
1.4
1.6
h_3 / a_3

FIGURE 9

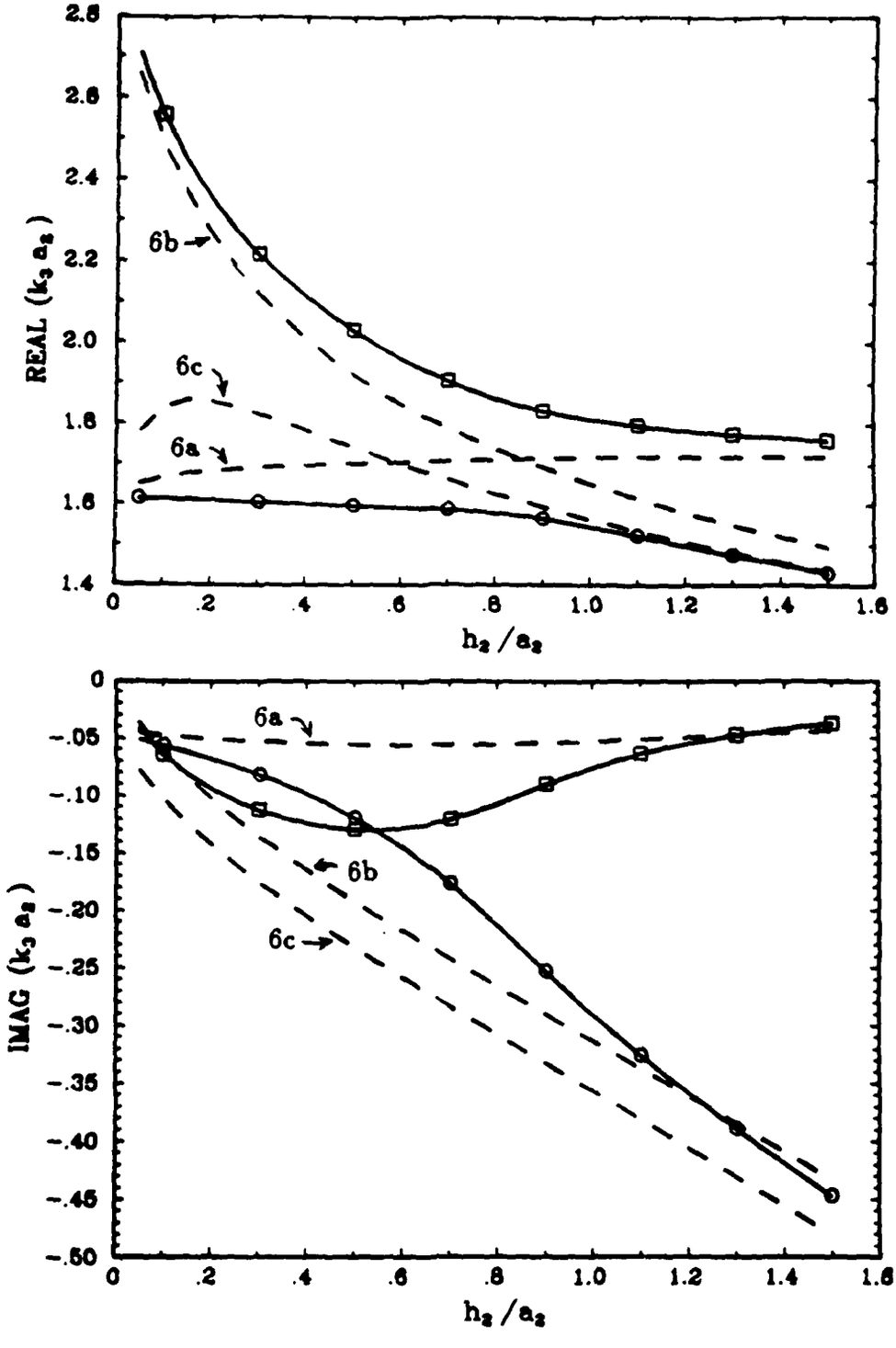
REAL ($k_3 a_2$)
2.8
2.6
2.4
2.2
2.0
1.8
1.6
1.4
6b
6c
6a
0
.2
.4
.6
.8
1.0
1.2
1.4
1.6
h_2 / a_2
IMAG ($k_3 a_2$)
0
-.05
-.10
-.15
-.20
-.25
-.30
-.35
-.40
-.45
-.50
6a
6b
6c
0
.2
.4
.6
.8
1.0
1.2
1.4
1.6
h_2 / a_2

FIGURE 10

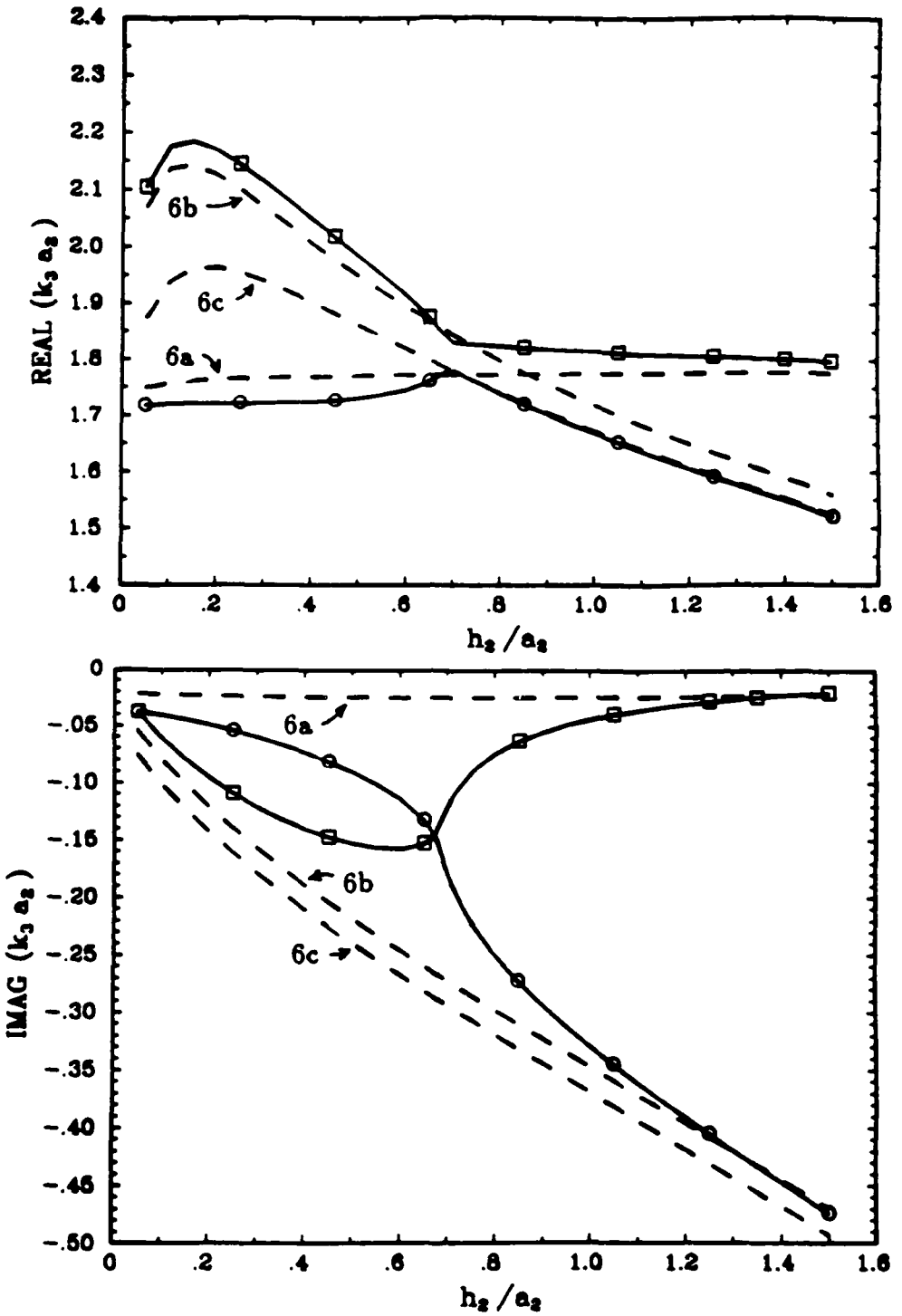
REAL ($k_3 a_2$)
2.4
2.3
2.2
2.1
2.0
1.9
1.8
1.7
1.6
1.5
1.4
6b
6c
6a
0
.2
.4
.6
.8
1.0
1.2
1.4
1.6
h_2 / a_2
IMAG ($k_3 a_2$)
0
-.05
-.10
-.15
-.20
-.25
-.30
-.35
-.40
-.45
-.50
6a
6b
6c
0
.2
.4
.6
.8
1.0
1.2
1.4
1.6
h_2 / a_2

FIGURE 11

PROPAGATION PROPERTIES OF STRIPLINES PERIODICALLY LOADED WITH CROSSING STRIPS

J. F. Kiang, S. M. Ali, and J. A. Kong

Department of Electrical Engineering and Computer Science
Massachusetts Institute of Technology Cambridge, MA02139

Abstract

A rigorous dyadic Green's function formulation in the spectral domain is used to study the dispersion characteristics of signal striplines in the presence of metallic crossing strips.

A set of coupled vector integral equations for the current distribution on the conductors is derived. Galerkin's method is then applied to derive the matrix eigenvalue equation for the propagation constant. The dispersion properties of the signal lines are studied for both cases of finite and infinite length crossing strips.

The effects of the structure dimensions on the passband and stopband characteristics are investigated. For crossing strips of finite length, the stopband is mainly affected by the period, the crossing strip length, and the separation between the signal and the crossing strips. For crossing strips of infinite length carrying travelling waves, attenuation along the signal line exists over the whole frequency range of operation.

I.Introduction

In microelectronic computer packaging, a problem of practical interest is the study of propagation characteristics of microstrip lines embedded in a layered medium in the presence of periodic crossing metallic strips.

The analysis of striplines and finlines with periodic stubs has been studied by Kitazawa and Mittra[1], where a technique based on the network-analytical formulation is used. A slow-wave coplanar waveguide on periodically doped semiconductor substrate has been carried out by Fukuoka and Itoh[2]. Gu and Kong[3] used a quasi-static approach to study single and coupled lines with capacitively loaded junctions. The propagation characteristics of signal lines in a mesh-plane environment has been presented by Rubin[4]. More recently, the propagation characteristics of signal lines in the presence of periodically perforated ground plane is studied by Chan and Mittra[5].

An analysis of a width-modulated microstrip periodic structure using quasi-static approach is presented in [6]. A hybrid spectral domain analysis for similar periodic structures have been carried out in [7].

In this paper, hybrid mode analysis is used to study the propagation characteristics of striplines periodically loaded with crossing metallic strips. The periodic crossing strips are assumed to have finite or infinite length. A dyadic Green's function formulation for the periodically loaded structure is derived. A coupled set of vector integral equations for the surface current distribution is formulated. Galerkin's method is then applied to transform the resulting set of integral equations for the current distribution into a determinantal equation from which the dispersion characteristics are obtained.

The propagation properties of one signal line and two coupled lines in the presence of periodic crossing strips are investigated. Numerical results for the passband and stopband characteristics are presented.

II. Dyadic Green's Function Formulation

The geometrical configuration of the problem is shown in Fig.1 where M signal striplines located at $z = z_m$, $m = 1, 2, \cdots, M$, are periodically loaded with crossing metallic strips having a period p. The crossing strips are of width w_c, length L_c, and are located in the plane $z = z_{M+1}$. Both the signal lines and the crossing strips are embedded in the same layer (l) having parameters (ϵ_l, μ_0).

In general, the electric field can be expressed in terms of the dyadic Green's function and the current distribution on the strip surfaces as[8]

$$\bar{E}_l(\bar{r}) = i\omega\mu_l \iiint_V \bar{\bar{G}}_{ll}(\bar{r}, \bar{r}') \cdot \bar{J}(\bar{r}')dV' \tag{1}$$

where $\bar{\bar{G}}_{ll}(\bar{r}, \bar{r}')$ is the dyadic Green's function when both the observation point $\bar{r}$ and the source point $\bar{r}'$ are located in the lth layer of the stratified medium. For $z > z'$,

$$\begin{aligned}
\bar{\bar{G}}_{ll}(\bar{r}, \bar{r}') = \frac{i}{8\pi^2} \iint_{-\infty}^{\infty} d\bar{k}_s e^{i\bar{k}_s \cdot (\bar{r}_s - \bar{r}'_s)} \frac{1}{k_{lz}} \\
\left\{ \frac{1}{(1 - R^{TE}_{\cup l} R^{TE}_{\cap l} e^{2ik_{lz}h_l})} \left[\hat{h}(k_{lz}) e^{ik_{lz}z_l} + R^{TE}_{\cup l} \hat{h}(-k_{lz}) e^{ik_{lz}(2h_l - z_l)} \right] \right. \\
\left[\hat{h}(k_{lz}) e^{-ik_{lz}z'_l} + R^{TE}_{\cap l} \hat{h}(-k_{lz}) e^{ik_{lz}z'_l} \right] \\
+ \frac{1}{(1 - R^{TM}_{\cup l} R^{TM}_{\cap l} e^{2ik_{lz}h_l})} \left[\hat{v}(k_{lz}) e^{ik_{lz}z_l} + R^{TM}_{\cup l} \hat{v}(-k_{lz}) e^{ik_{lz}(2h_l - z_l)} \right] \\
\left. \left[\hat{v}(k_{lz}) e^{-ik_{lz}z'_l} + R^{TM}_{\cap l} \hat{v}(-k_{lz}) e^{ik_{lz}z'_l} \right] \right\}.
\end{aligned} \tag{2a}$$

For $z < z'$,

$$\begin{aligned}
\bar{\bar{G}}_{ll}(\bar{r}, \bar{r}') = \frac{i}{8\pi^2} \iint_{-\infty}^{\infty} d\bar{k}_s e^{i\bar{k}_s \cdot (\bar{r}_s - \bar{r}'_s)} \frac{1}{k_{lz}} \\
\left\{ \frac{1}{(1 - R^{TE}_{\cup l} R^{TE}_{\cap l} e^{2ik_{lz}h_l})} \left[\hat{h}(-k_{lz}) e^{-ik_{lz}z_l} + R^{TE}_{\cap l} \hat{h}(k_{lz}) e^{ik_{lz}z_l} \right] \right. \\
\left[\hat{h}(-k_{lz}) e^{ik_{lz}z'_l} + R^{TE}_{\cup l} \hat{h}(k_{lz}) e^{ik_{lz}(2h_l - z'_l)} \right] \\
+ \frac{1}{(1 - R^{TM}_{\cup l} R^{TM}_{\cap l} e^{2ik_{lz}h_l})} \left[\hat{v}(-k_{lz}) e^{-ik_{lz}z_l} + R^{TM}_{\cap l} \hat{v}(k_{lz}) e^{ik_{lz}z_l} \right] \\
\left. \left[\hat{v}(-k_{lz}) e^{ik_{lz}z'_l} + R^{TM}_{\cup l} \hat{v}(k_{lz}) e^{ik_{lz}(2h_l - z'_l)} \right] \right\}
\end{aligned} \tag{2b}$$

where z_l and z_l' are the local coordinate defined as $z_l = z + d_l$, $z_l' = z' + d_l$, and

$$\begin{aligned}
\bar{k}_s &= \hat{x}k_x + \hat{y}k_y \\
k_l^2 &= k_s^2 + k_{lz}^2, \qquad k_s = |\bar{k}_s| \\
\hat{h}(\pm k_{lz}) &= \frac{\hat{x}k_y - \hat{y}k_x}{k_s} \\
\hat{v}(\pm k_{lz}) &= \mp\frac{k_{lz}\bar{k}_s}{k_l k_s} + \hat{z}\frac{k_s}{k_l} \\
\bar{r}_s &= \hat{x}x + \hat{y}y, \qquad \bar{r}_s' = \hat{x}x' + \hat{y}y'.
\end{aligned} \tag{3}$$

In (2), $R_{\cup l}^{TM}$ and $R_{\cup l}^{TE}$ are the reflection coefficients of TM mode and TE mode at the upper boundary of the lth layer, $R_{\cap l}^{TM}$ and $R_{\cap l}^{TE}$ are the reflection coefficients of TM mode and TE mode at the lower boundary of the lth layer. They can be obtained recursively as

$$R_{\cup l}^{\alpha} = \frac{R_{l(l-1)}^{\alpha} + R_{\cup(l-1)}^{\alpha} e^{2ik_{(l-1)z}h_{l-1}}}{1 + R_{l(l-1)}^{\alpha} R_{\cup(l-1)}^{\alpha} e^{2ik_{(l-1)z}h_{l-1}}} \qquad \alpha = (\text{ TE, TM }) \tag{4a}$$

$$R_{\cap l}^{\alpha} = \frac{R_{l(l+1)}^{\alpha} + R_{\cap(l+1)}^{\alpha} e^{2ik_{(l+1)z}h_{l+1}}}{1 + R_{l(l+1)}^{\alpha} R_{\cap(l+1)}^{\alpha} e^{2ik_{(l+1)z}h_{l+1}}} \qquad \alpha = (\text{ TE, TM }) \tag{4b}$$

where $R_{l(l-1)}^{\alpha}$ and $R_{l(l+1)}^{\alpha}$ are the Fresnel reflection coefficients of α mode across the interfaces at $z = -d_{l-1}$ and $z = -d_l$, respectively. The explicit forms are

$$R_{l(l\pm1)}^{TE} = \frac{k_{lz} - k_{(l\pm1)z}}{k_{lz} + k_{(l\pm1)z}}, \qquad R_{l(l\pm1)}^{TM} = \frac{\epsilon_{l\pm1}k_{lz} - \epsilon_l k_{(l\pm1)z}}{\epsilon_{l\pm1}k_{lz} + \epsilon_l k_{(l\pm1)z}}. \tag{5}$$

For our problem, only transverse currents $\bar{J}_s$ having no z component exist, the transverse electric field (to z) $\bar{E}_{ls}$ in layer (l) is thus given by

$$\bar{E}_{ls}(\bar{r}) = i\omega\mu_l \iint_S d\bar{r}_s' \bar{\bar{G}}_{ll}^T(\bar{r}, \bar{r}_s') \cdot \bar{J}_s(\bar{r}_s') dS' \tag{6}$$

where $\bar{\bar{G}}_{ll}^T(\bar{r}, \bar{r}')$ is the (2×2) transverse (to z) part of the dyadic Green's function, and can be expressed in the $\bar{k}_s$ domain as

$$\bar{\bar{G}}_{ll}^T(\bar{r}, \bar{r}') = \iint_{-\infty}^{\infty} d\bar{k}_s e^{i\bar{k}_s \cdot (\bar{r}_s - \bar{r}_s')} \bar{\bar{g}}_{ll}^T(\bar{k}_s, z, z') \tag{7}$$

where for $z > z'$,

$$\bar{\bar{g}}_{ll}^{T}(\bar{k}_s, z, z') = \frac{i}{8\pi^2 k_{lz}}$$
$$\left\{ \frac{(e^{ik_{lz}z_l} + R_{\cup l}^{TE} e^{ik_{lz}(2h_l - z_l)})(e^{-ik_{lz}z_l'} + R_{\cap l}^{TE} e^{ik_{lz}z_l'})}{(1 - R_{\cup l}^{TE} R_{\cap l}^{TE} e^{2ik_{lz}h_l})} \frac{1}{k_s^2} \begin{bmatrix} k_y^2 & -k_x k_y \\ -k_x k_y & k_x^2 \end{bmatrix} \right.$$
$$\left. + \frac{(e^{ik_{lz}z_l} - R_{\cup l}^{TM} e^{ik_{lz}(2h_l - z_l)})(e^{-ik_{lz}z_l'} - R_{\cap l}^{TM} e^{ik_{lz}z_l'})}{(1 - R_{\cup l}^{TM} R_{\cap l}^{TM} e^{2ik_{lz}h_l})} \frac{k_{lz}^2}{k_l^2 k_s^2} \begin{bmatrix} k_x^2 & k_x k_y \\ k_x k_y & k_y^2 \end{bmatrix} \right\} \quad (8a)$$

and for $z < z'$,

$$\bar{\bar{g}}_{ll}^{T}(\bar{k}_s, z, z') = \frac{i}{8\pi^2 k_{lz}}$$
$$\left\{ \frac{(e^{-ik_{lz}z_l} + R_{\cap l}^{TE} e^{ik_{lz}z_l})(e^{ik_{lz}z_l'} + R_{\cup l}^{TE} e^{ik_{lz}(2h_l - z_l')})}{(1 - R_{\cup l}^{TE} R_{\cap l}^{TE} e^{2ik_{lz}h_l})} \frac{1}{k_s^2} \begin{bmatrix} k_y^2 & -k_x k_y \\ -k_x k_y & k_x^2 \end{bmatrix} \right.$$
$$\left. + \frac{(e^{-ik_{lz}z_l} - R_{\cap l}^{TM} e^{ik_{lz}z_l})(e^{ik_{lz}z_l'} - R_{\cup l}^{TM} e^{ik_{lz}(2h_l - z_l')})}{(1 - R_{\cup l}^{TM} R_{\cap l}^{TM} e^{2ik_{lz}h_l})} \frac{k_{lz}^2}{k_l^2 k_s^2} \begin{bmatrix} k_x^2 & k_x k_y \\ k_x k_y & k_y^2 \end{bmatrix} \right\}. \quad (8b)$$

The transverse electric field can be expressed using Floquet harmonic representation in the y direction as

$$\bar{E}_{ls}(\bar{r}) = i\omega\mu_l \int_{-\infty}^{\infty} dx' \int_{-p/2}^{p/2} dy' \bar{\bar{G}}_{llp}^{T}(\bar{r}, \bar{r}_s') \cdot \bar{J}_s(\bar{r}_s') \quad (9)$$

where $\bar{\bar{G}}_{llp}^{T}(\bar{r}, \bar{r}')$ is given by

$$\bar{\bar{G}}_{llp}^{T}(\bar{r}, \bar{r}') = \frac{2\pi}{p} \sum_{n=-\infty}^{\infty} \int_{-\infty}^{\infty} dk_x e^{ik_x(x-x')} e^{ik_{yn}(y-y')} \bar{\bar{g}}_{ll}^{T}(k_x, k_{yn}, z, z') \quad (10)$$

where $k_{yn} = k_{y0} + 2n\pi/p$, k_{y0} is the propagation constant of the dominant harmonic in the Floquet representation. We assume that we have M signal striplines and one crossing strip within one period. Thus, $\bar{J}_s$ can be expressed as

$$\bar{J}_s(x, y) = \begin{cases} \bar{J}_m(x, y), & x_m - w_m/2 \le x \le x_m + w_m/2, z = z_m \\ 0, & \text{elsewhere.} \end{cases} \quad (11)$$

Substituting (11) into (9), we have

$$\bar{E}_{ls}(\bar{r}) = i\omega\mu_l(2\pi)^2 \sum_{m=1}^{M+1} \sum_{n=-\infty}^{\infty} e^{ik_{yn}y} \int_{-\infty}^{\infty} dk_x e^{ik_x x} \bar{\bar{g}}_{ll}^T(k_x, k_{yn}, z, z_m) \cdot \bar{\bar{J}}_m(k_x, k_{yn}) \quad (12)$$

where

$$\bar{\bar{J}}_m(k_x, k_{yn}) = \frac{1}{2\pi p} \int_{-\infty}^{\infty} dx' e^{-ik_x x'} \int_{-p/2}^{p/2} dy' e^{-ik_{yn} y'} \bar{J}_m(x', y'). \quad (13)$$

The electric field $\bar{E}_{ls}$ given by (12) satisfies the boundary conditions at the interfaces between the dielectric layers of the stratified medium. Imposing the final boundary condition that the tangential electric fields vanish on the metallic surfaces of the signal striplines and the crossing strips, we get a set of vector integral equations for the current distribution on all the metallic strips. Thus, we have

$$\sum_{m=1}^{M+1} \sum_{n=-\infty}^{\infty} e^{ik_{yn}y} \int_{-\infty}^{\infty} dk_x e^{ik_x x} \bar{\bar{g}}_{ll}^T(k_x, k_{yn}, z, z_m) \cdot \bar{\bar{J}}_m(k_x, k_{yn}) = 0,$$

$$x_q - w_q/2 \le x \le x_q + w_q/2, -p/2 \le y \le p/2, z = z_q,$$
$$q = 1, \cdots, M \quad (14a)$$

$$\sum_{m=1}^{M+1} \sum_{n=-\infty}^{\infty} e^{ik_{yn}y} \int_{-\infty}^{\infty} dk_x e^{ik_x x} \bar{\bar{g}}_{ll}^T(k_x, k_{yn}, z, z_m) \cdot \bar{\bar{J}}_m(k_x, k_{yn}) = 0,$$

$$-L_c/2 \le x \le L_c/2, -w_c/2 \le y \le w_c/2, z = z_{M+1} \quad (14b)$$

where (14a) satisfies the boundary condition on the M signal strips, and (14b) satisfies the boundary condition on the crossing strip. The task is to solve this set of vector integral equations using the moment method to get the dispersion relation.

III. Numerical Solution for the Dispersion Relation

A) One Signal Stripline Loaded with Crossing Metallic Strips

In this section, we study the case of one signal stripline in the presence of periodical crossing strips as shown in Fig.2. The signal stripline and the crossing strips are located in a dielectric layer bounded by two ground planes and placed, respectively, at $z = z_1$ and $z = z_2$.

To apply the moment method, we choose an appropriate set of basis functions to represent the surface current $\bar{J}_1(x,y)$ and $\bar{J}_2(x,y)$ as

$$\bar{J}_1(x,y) = \hat{x} \sum_{j=-N_1}^{N_2} a_j f_{1j}(x,y) + \hat{y} \sum_{j=-N_1}^{N_2} b_j f_{2j}(x,y) \tag{15a}$$

$$\bar{J}_2(x,y) = \hat{x} \sum_{j=1}^{N_3} c_j f_{3j}(x,y) + \hat{y} \sum_{j=0}^{N_4} d_j f_{4j}(x,y) \tag{15b}$$

where $\bar{J}_1(x,y)$ is the surface current on the signal stripline, $\bar{J}_2(x,y)$ is the surface current on the crossing strip, a_j, b_j, c_j, and d_j are the expansion coefficients, $f_{1j}(x,y)$, $f_{2j}(x,y)$, $f_{3j}(x,y)$ and $f_{4j}(x,y)$ are the basis functions. The explicit forms of the basis functions are as follows :

$$f_{1j}(x,y) = P_1(x,w_1)e^{ik_{yj}y} \tag{16a}$$

$$f_{2j}(x,y) = T_0(x,w_1)e^{ik_{yj}y} \tag{16b}$$

$$f_{3j}(x,y) = P_j(x,L_c)(p/2\pi)T_0(y,w_c) \tag{16c}$$

$$f_{4j}(x,y) = T_j(x,L_c)Q(y,w_c) \tag{16d}$$

where

$$P_j(\xi,\eta) = \begin{cases} (1/\eta)\sin(2j\pi\xi/\eta), & -\eta/2 \le \xi \le \eta/2 \\ 0, & \text{elsewhere} \end{cases} \tag{17a}$$

$$Q(\xi,\eta) = \begin{cases} (p/2\pi\eta)\cos(\pi\xi/\eta), & -\eta/2 \le \xi \le \eta/2 \\ 0, & \text{elsewhere} \end{cases} \tag{17b}$$

$$T_j(\xi,\eta) = \begin{cases} \cos(2j\pi\xi/\eta)/\sqrt{(\eta/2)^2 - \xi^2}, & -\eta/2 \le \xi \le \eta/2 \\ 0, & \text{elsewhere.} \end{cases} \tag{17c}$$

The surface current on the signal stripline is basically of travelling wave type. Due to the periodic loading, the basis functions on the signal stripline are chosen as a superposition of space harmonic modes. On the crossing strips, the surface current is basically of standing wave type, and the phase variation along the y direction on the crossing strips can be neglected.

Let $\tilde{P}_j(k_x,\eta)$, $\tilde{Q}(k_{yn},\eta)$, and $\tilde{T}_j(k_x,\eta)$ be the Fourier transforms of $P_j(x,\eta)$, $Q(y,\eta)$, and $T_j(x,\eta)$ respectively, we have

$$\tilde{P}_j(k_x,\eta)=\frac{1}{2\pi}\int_{-\eta/2}^{\eta/2}dxe^{-ik_xx}P_j(x,\eta)=i\frac{j(-1)^{j+1}\sin(k_x\eta/2)}{2\left[(k_x\eta/2)^2-(j\pi)^2\right]}=-\tilde{P}_j(-k_x,\eta) \tag{18a}$$

$$\tilde{Q}(k_{yn},\eta)=\frac{1}{p}\int_{-\eta/2}^{\eta/2}dye^{-ik_{yn}y}Q(y,\eta)=-\frac{\cos(k_{yn}\eta/2)}{(k_{yn}\eta)^2-\pi^2}=\tilde{Q}(-k_{yn},\eta) \tag{18b}$$

$$\tilde{T}_j(k_x,\eta)=\frac{1}{2\pi}\int_{-\eta/2}^{\eta/2}dxe^{-ik_xx}T_j(x,\eta)=\frac{1}{4}\left[J_0(k_x\eta/2-j\pi)+J_0(k_x\eta/2+j\pi)\right]=\tilde{T}_j(-k_x,\eta) \tag{18c}$$

where $J_0(\alpha)$ is the Bessel function of the zeroth order, $\tilde{P}_j(k_x,\eta)$ is an odd function of k_x, $\tilde{T}_j(k_x,\eta)$ is an even function of k_x, $\tilde{Q}(k_{yn},\eta)$ is an even function of k_{yn}. When $k_x\eta/2$ approaches $\pm j\pi$, $\tilde{P}_j(k_x,\eta)$ approaches $\pm 1/(4\pi i)$; when $k_{yn}\eta$ approaches $\pm\pi$, $\tilde{Q}(k_{yn},\eta)$ approaches $1/(4\pi)$.

With these basis functions, the Fourier transform of the surface current $\tilde{\bar{J}}_m(k_x,k_{yn})$ can be derived as

$$\tilde{\bar{J}}_1(k_x,k_{yn})=\hat{x}\sum_{j=-N_1}^{N_2}a_jF_{1j}(k_x,k_{yn})+\hat{y}\sum_{j=-N_1}^{N_2}b_jF_{2j}(k_x,k_{yn}) \tag{19a}$$

$$\tilde{\bar{J}}_2(k_x,k_{yn})=\hat{x}\sum_{j=1}^{N_3}c_jF_{3j}(k_x,k_{yn})+\hat{y}\sum_{j=0}^{N_4}d_jF_{4j}(k_x,k_{yn}) \tag{19b}$$

where $F_{ij}(k_x,k_{yn})$ is the Fourier transform of $f_{ij}(x,y)$, $i=1,2,3,4$. The explicit forms are

$$F_{1j}(k_x,k_{yn})=\delta_{jn}\tilde{P}_1(k_x,w_1) \tag{20a}$$

$$F_{2j}(k_x, k_{yn}) = \delta_{jn}\tilde{T}_0(k_x, w_1) \tag{20b}$$

$$F_{3j}(k_x, k_{yn}) = \tilde{T}_0(k_{yn}, w_c)\tilde{P}_j(k_x, L_c) \tag{20c}$$

$$F_{4j}(k_x, k_{yn}) = \tilde{Q}(k_{yn}, w_c)\tilde{T}_j(k_x, L_c) \tag{20d}$$

where δ_{jn} is the Kronecker delta function. Substituting (20) into (14), we have

$$\sum_{n=-\infty}^{\infty} e^{ik_{yn}y} \int_{-\infty}^{\infty} dk_x e^{ik_x x} \bar{\bar{g}}_{ll}^{T}(k_x, k_{yn}, z_1, z_1) \cdot \left[\hat{x} \sum_{j=-N_1}^{N_2} a_j F_{1j}(k_x, k_{yn}) + \hat{y} \sum_{j=-N_1}^{N_2} b_j F_{2j}(k_x, k_{yn})\right]$$
$$+\bar{\bar{g}}_{ll}^{T}(k_x, k_{yn}, z_1, z_2) \cdot \left[\hat{x} \sum_{j=1}^{N_3} c_j F_{3j}(k_x, k_{yn}) + \hat{y} \sum_{j=0}^{N_4} d_j F_{4j}(k_x, k_{yn})\right] = 0,$$

$$-w_1/2 \le x \le w_1/2, -p/2 \le y \le p/2, z = z_1 \tag{21a}$$

$$\sum_{n=-\infty}^{\infty} e^{ik_{yn}y} \int_{-\infty}^{\infty} dk_x e^{ik_x x} \bar{\bar{g}}_{ll}^{T}(k_x, k_{yn}, z_2, z_1) \cdot \left[\hat{x} \sum_{j=-N_1}^{N_2} a_j F_{1j}(k_x, k_{yn}) + \hat{y} \sum_{j=-N_1}^{N_2} b_j F_{2j}(k_x, k_{yn})\right]$$
$$+\bar{\bar{g}}_{ll}^{T}(k_x, k_{yn}, z_2, z_2) \cdot \left[\hat{x} \sum_{j=1}^{N_3} c_j F_{3j}(k_x, k_{yn}) + \hat{y} \sum_{j=0}^{N_4} d_j F_{4j}(k_x, k_{yn})\right] = 0,$$

$$-L_c/2 \le x \le L_c/2, -w_c/2 \le y \le w_c/2, z = z_2. \tag{21b}$$

Applying Galerkin's method, we choose $\hat{x}e^{-ik_{yk}y}P_i(x, w_1)$ $(k = -N_1, \cdots, N_2)$ and $\hat{y}e^{-ik_{yk}y}T_0(x, w_1)$ $(k = -N_1, \cdots, N_2)$ as testing functions for the signal stripline. Taking the inner product with (21a), we obtain $2(N_1 + N_2 + 1)$ equations. Similarly, taking the inner product of $\hat{x}f_{3i}(x, y)$ $(i = 1, \cdots, N_3)$ and $\hat{y}f_{4k}(x, y)$ $(k = 0, \cdots, N_4)$ with (21b), we obtain another $N_3 + N_4 + 1$ equations.

After arrangement, we get the following matrix equation :

$$\begin{bmatrix} Z_{i,j}^{(1,1)} & Z_{i,j}^{(1,2)} & Z_{i,j}^{(1,3)} & Z_{i,j}^{(1,4)} \\ Z_{i,j}^{(2,1)} & Z_{i,j}^{(2,2)} & Z_{i,j}^{(2,3)} & Z_{i,j}^{(2,4)} \\ Z_{i,j}^{(3,1)} & Z_{i,j}^{(3,2)} & Z_{i,j}^{(3,3)} & Z_{i,j}^{(3,4)} \\ Z_{i,j}^{(4,1)} & Z_{i,j}^{(4,2)} & Z_{i,j}^{(4,3)} & Z_{i,j}^{(4,4)} \end{bmatrix} \begin{bmatrix} a_j \\ b_j \\ c_j \\ d_j \end{bmatrix} = 0 \tag{22}$$

Each entity $Z_{i,j}^{(r,q)}$ in (22) is a submatrix, the explicit form of the elements is

$$Z_{i,j}^{(r,q)}(\omega, k_y) = \sum_{n=-\infty}^{\infty} \int_{-\infty}^{\infty} dk_x S_{i,j}^{(r,q)}(k_x, k_{yn}) \tag{23}$$

with

$$S_{i,j}^{(r,q)}(k_x, k_{yn}) = F_{ri}(-k_x, -k_{yn}) g_{ll}^{\alpha\beta}(k_x, k_{yn}, z_t, z_m) F_{qj}(k_x, k_{yn}) \tag{24}$$

where

$$z_t = \begin{cases} z_1, & \text{for } r = 1,2 \\ z_2, & \text{for } r = 3,4 \end{cases}, \qquad z_m = \begin{cases} z_1, & \text{for } q = 1,2 \\ z_2, & \text{for } q = 3,4 \end{cases} \tag{25a}$$

$$\alpha = \begin{cases} x, & \text{for } r = 1,3 \\ y, & \text{for } r = 2,4 \end{cases}, \qquad \beta = \begin{cases} x, & \text{for } q = 1,3 \\ y, & \text{for } q = 2,4 \end{cases}. \tag{25b}$$

The determinantal equation for the propagation constant k_{y0} can be solved by setting the determinant of the coefficient matrix of (22) equal to zero :

$$\det\left[Z(\omega, k_{y0})\right] = 0 \tag{26}$$

B)Two Symmetrical Signal Striplines Loaded with Crossing Strips

In this section, we consider the case where two identical signal striplines of width w_1 are located symmetrically at $(\pm x_c, z_1)$ as shown in Fig.3.

For the even modes, $J_{mx}(x,y)$ is an odd function of x, and $J_{my}(x,y)$ is an even function of x. Therefore, the surface currents can be expanded as

$$\bar{J}_1(x,y) = \hat{x} \sum_{j=-N_1}^{N_2} a_j f_{1j}^{(e)}(x,y) + \hat{y} \sum_{j=-N_1}^{N_2} b_j f_{2j}^{(e)}(x,y) \tag{27a}$$

$$\bar{J}_2(x,y) = \hat{x} \sum_{j=1}^{N_3} c_j f_{3j}^{(e)}(x,y) + \hat{y} \sum_{j=0}^{N_4} d_j f_{4j}^{(e)}(x,y) \tag{27b}$$

where the basis functions are

$$f_{1j}^{(e)}(x,y) = \Big[P_1(x-x_c,w_1) + P_1(x+x_c,w_1)\Big] e^{ik_{yj}y} \tag{28a}$$

$$f_{2j}^{(e)}(x,y) = \Big[T_0(x-x_c,w_1) + T_0(x+x_c,w_1)\Big] e^{ik_{yj}y} \tag{28b}$$

$$f_{3j}^{(e)}(x,y) = P_j(x,L_c)(p/2\pi)T_0(y,w_c) \tag{28c}$$

$$f_{4j}^{(e)}(x,y) = T_j(x,L_c)Q(y,w_c). \tag{28d}$$

Following the same procedure as for the case of one signal stripline by applying the Galerkin's method, a determinantal equation similar to (26) is obtained.

For the odd modes, $J_{mx}(x,y)$ is an even function of x, and $J_{my}(x,y)$ is an odd function of x. Therefore, the surface currents are expanded as

$$\bar{J}_1(x,y) = \hat{x} \sum_{j=-N_1}^{N_2} a_j f_{1j}^{(o)}(x,y) + \hat{y} \sum_{j=-N_1}^{N_2} b_j f_{2j}^{(o)}(x,y) \tag{29a}$$

$$\bar{J}_2(x,y) = \hat{x} \sum_{j=1}^{N_3} c_j f_{3j}^{(o)}(x,y) + \hat{y} \sum_{j=0}^{N_4} d_j f_{4j}^{(o)}(x,y) \tag{29b}$$

where the basis functions are

$$f_{1j}^{(o)}(x,y) = \Big[P_1(x-x_c,w_1) - P_1(x+x_c,w_1)\Big] e^{ik_{yj}y} \tag{30a}$$

$$f_{2j}^{(o)}(x,y) = \Big[T_0(x-x_c,w_1) - T_0(x+x_c,w_1)\Big]e^{ik_{yj}y} \tag{30b}$$

$$f_{3j}^{(o)}(x,y) = U_j(x,L_c)(p/2\pi)T_0(y,w_c) \tag{30c}$$

$$f_{4j}^{(o)}(x,y) = V_j(x,L_c)Q(y,w_c) \tag{30d}$$

where

$$U_j(\xi,\eta) = \begin{cases} (1/\eta)\cos[(2j-1)\pi\xi/\eta], & -\eta/2 \le \xi \le \eta/2 \\ 0, & \text{elsewhere} \end{cases} \tag{31a}$$

$$V_j(\xi,\eta) = \begin{cases} \sin[(2j-1)\pi\xi/\eta]/\sqrt{(\eta/2)^2-\xi^2}, & -\eta/2 \le \xi \le \eta/2 \\ 0, & \text{elsewhere.} \end{cases} \tag{31b}$$

Let $\tilde{U}_j(k_x,\eta)$ and $\tilde{V}_j(k_x,\eta)$ be the Fourier transform of $U_j(x,\eta)$ and $V_j(x,\eta)$, then

$$\tilde{U}_j(k_x,\eta) = \frac{(2j-1)(-1)^j\cos(k_x\eta/2)}{(k_x\eta)^2-[(2j-1)\pi]^2} = \tilde{U}_j(-k_x,\eta) \tag{32a}$$

$$\tilde{V}_j(k_x,\eta) = \frac{1}{4i}\Big[J_0(k_x\eta/2-(j-1/2)\pi) - J_0(k_x\eta/2+(j-1/2)\pi)\Big] = -\tilde{V}_j(-k_x,\eta). \tag{32b}$$

When $k_x\eta/2$ approaches $\pm(j-1/2)\pi$, $\tilde{U}_j(k_x,\eta)$ approaches $1/(4\pi)$.

C)One Signal Stripline Loaded with Crossing Strips of Infinite Length

In this section, we consider the case where one signal line is loaded by infinitely long crossing strips as shown in Fig.2 with $L_c \to \infty$. When the crossing strips are very long such that the reflections from ends can be neglected, we can assume travelling waves along it. So, we investigate the possibility of the existence of such a mode of operation, and its effect on the propagation characteristics of the signal line.

The surface current on the signal strip is of the same form as in the case (A) of finite crossing strips. For the crossing strips, we choose travelling wave basis functions[9], [10] and some local basis functions on the center to account for the effect of the presence of the signal line. Hence, the surface currents are expanded as

$$\bar{J}_1(x,y) = \hat{x} \sum_{j=-N_1}^{N_2} a_j f_{1j}^{(t)}(x,y) + \hat{y} \sum_{j=-N_1}^{N_2} b_j f_{2j}^{(t)}(x,y) \tag{33a}$$

$$\bar{J}_2(x,y) = \hat{x} \sum_{j=1}^{N_3} c_j f_{3j}^{(t)}(x,y) + \hat{y} \sum_{j=0}^{N_4} d_j f_{4j}^{(t)}(x,y) \tag{33b}$$

where the basis functions $f_{1j}^{(t)}(x,y)$ and $f_{2j}^{(t)}(x,y)$ are the same as $f_{1j}(x,y)$ and $f_{2j}(x,y)$ respectively. The functional forms of $f_{3j}^{(t)}(x,y)$ and $f_{4j}^{(t)}(x,y)$ are

$$f_{3j}^{(t)}(x,y) = \begin{cases} \Big[R_j(x,h) - R_j(-x,h)\Big](p/2\pi)T_0(y,w_c), & 1 \le j \le N_3 - 1 \\ \Big[-S_m(k_e x - \pi/2) + iS_m(k_e x) & \\ +S_m(-k_e x - \pi/2) - iS_m(-k_e x)\Big](p/2\pi)T_0(y,w_c), & j = N_3 \end{cases} \tag{34a}$$

$$f_{4j}^{(t)}(x,y) = \begin{cases} R_0(x,h)Q(y,w_c), & j = 0 \\ \Big[R_j(x,h) + R_j(-x,h)\Big]Q(y,w_c), & 1 \le j \le N_4 - 1 \\ \Big[-S_m(k_e x - \pi/2) + iS_m(k_e x) & \\ -S_m(-k_e x - \pi/2) + iS_m(-k_e x)\Big]Q(y,w_c), & j = N_4 \end{cases} \tag{34b}$$

where k_e is assumed to be the propagation constant of a single crossing strip of infinite length in the absence of the signal line, $R_j(x,h)$ is the local basis function with width

$2h$, $S_m(\xi)$ is the travelling wave basis function with $m/2$ periods as shown in Fig.4. The explicit forms are

$$R_j(x,h) = \begin{cases} \sin k_e(h - |x - jh|)/\sin k_e h, & (j-1)h \le x \le (j+1)h \\ 0, & \text{elsewhere} \end{cases} \tag{35a}$$

$$S_m(\xi) = \begin{cases} \sin\xi, & 0 \le \xi \le m\pi \\ 0, & \text{elsewhere.} \end{cases} \tag{35b}$$

It will be shown that only finite number of periods of the travelling wave basis functions are sufficient for the convergence of the solution. Any increase in the number of periods of these basis functions will have a negligible effect on the numerical results.

Let $\tilde{R}_j(k_x, w)$ and $\tilde{S}_m(k_x)$ be the Fourier transform of $R_j(x,h)$ and $S_m(\xi)$, then

$$\tilde{R}_j(k_x,h) = -\frac{k_e e^{-ik_x jh}(\cos k_x h - \cos k_e h)}{\pi \sin k_e h(k_x^2 - k_e^2)} \tag{36a}$$

$$\tilde{S}_m(k_x) = \frac{k_e}{2\pi(k_x^2 - k_e^2)}\left[(-1)^m e^{-i(m\pi/k_e)k_x} - 1\right]. \tag{36b}$$

When k_x approaches $\pm k_e$, $\tilde{R}_j(k_x,h)$ and $\tilde{S}_m(k_x)$ approach $(h/2\pi)e^{\mp ik_e jh}$ and $\mp im/4k_e$, respectively.

With these basis functions, the Fourier transform of the surface current $\tilde{\bar{J}}_m(k_x, k_{yn})$ can be derived as

$$\tilde{\bar{J}}_1(k_x,k_{yn}) = \hat{x}\sum_{j=-N_1}^{N_2} a_j F_{1j}^{(t)}(k_x,k_{yn}) + \hat{y}\sum_{j=-N_1}^{N_2} b_j F_{2j}^{(t)}(k_x,k_{yn}) \tag{37a}$$

$$\tilde{\bar{J}}_2(k_x,k_{yn}) = \hat{x}\sum_{j=1}^{N_3} c_j F_{3j}^{(t)}(k_x,k_{yn}) + \hat{y}\sum_{j=0}^{N_4} d_j F_{4j}^{(t)}(k_x,k_{yn}) \tag{37b}$$

where $F_{ij}^{(t)}(k_x,k_{yn})$ is the Fourier transform of $f_{ij}^{(t)}(x,y)$, $i = 1,2,3,4$. The explicit forms are

$$F_{1j}^{(t)}(k_x,k_{yn}) = \delta_{jn}\tilde{P}_1(k_x,w_1) \tag{38a}$$

$$F_{2j}^{(t)}(k_x,k_{yn}) = \delta_{jn}\tilde{T}_0(k_x,w_1) \tag{38b}$$

$$F_{3j}^{(t)}(k_x,k_{yn}) = \tilde{T}_0(k_{yn},w_c)\tilde{A}_{3j}(k_x) \tag{38c}$$

$$F_{4j}^{(t)}(k_x,k_{yn}) = \tilde{Q}(k_{yn},w_c)\tilde{A}_{4j}(k_x) \tag{38d}$$

where

$$\tilde{A}_{3j}(k_x) = \begin{cases} 2\tilde{R}_j^{(o)}(k_x,h), & 1 \le j \le N_3 - 1 \\ k_e[\pi(k_x^2 - k_e^2)]^{-1}\Big[(-1)^m i \sin[k_x\pi(m+1/2)/k_e] & \\ \quad +(-1)^m \sin(m\pi k_x/k_e) - i\sin(k_x\pi/2k_e)\Big], & j = N_3 \end{cases} \tag{39a}$$

$$\tilde{A}_{4j}(k_x) = \begin{cases} \tilde{R}_0^{(e)}(k_x,h), & j = 0 \\ 2\tilde{R}_j^{(e)}(k_x,h), & 1 \le j \le N_4 - 1 \\ k_e[\pi(k_x^2 - k_e^2)]^{-1}\Big[-(-1)^m \cos[k_x\pi(m+1/2)/k_e] & \\ \quad +i(-1)^m \cos(m\pi k_x/k_e) + \cos(k_x\pi/2k_e) - i\Big], & j = N_4 \end{cases} \tag{39b}$$

where $\tilde{R}_j^{(e)}(k_x,h)$ and $\tilde{R}_j^{(o)}(k_x,h)$ are the even and the odd parts of $\tilde{R}_j(k_x,h)$ respectively. It is observed that $\tilde{A}_{3j}(-k_x) = -\tilde{A}_{3j}(k_x)$, and $\tilde{A}_{4j}(-k_x) = \tilde{A}_{4j}(k_x)$.

Applying the Galerkin's procedure with the following testing functions :

$$w_{1j}(x,y) = P_1(x,w_1)e^{-ik_{yj}y} \tag{40a}$$

$$w_{2j}(x,y) = T_0(x,w_1)e^{-ik_{yj}y} \tag{40b}$$

$$w_{3j}(x,y) = R_j(x,h)(p/2\pi)T_0(y,w_c) \tag{40c}$$

$$w_{4j}(x,y) = R_j(x,h)Q(y,w_c) \tag{40d}$$

the matrix eigenvalue equation is obtained.

IV. Numerical Results and Discussions

By utilizing the symmetry properties of the dyadic Green's function, the basis functions, and the testing functions, each matrix element in (22) can be reduced to an integral over $0 \leq k_x < \infty$. In computing the integrals (23) numerically, the path of integration in the complex k_x-plane is deformed below the real axis to avoid the poles corresponding to the waveguide modes[11].

Fig.5 shows the dispersion relation for a single signal line with crossing strips. Numerical computations were performed with two different numbers of basis functions, and the results were found to be the same up to three decimal points. The basis functions used are given by (15). For $L_c = 2.3$ mm, the first stopband occurs in the frequency range when $0.3162 < k_0 p/\pi < 0.3203$.

Fig.6 shows the interaction of $n = -1$ Floquet mode with TE_1 (TM_1) parallel-plate waveguide mode. For frequencies above f_*, k_y starts to have large imaginary part, giving rise to a higher order stopband. However, we are interested in operating frequencies where k_y is real within the passbands below f_*, and thus the region above f_* is of no practical importance.

Next, the effects of crossing strip length L_c on the lower and upper ferquency bounds of the stopband are investigated. The normalized frequency for the two bounds of the stopband is presented as a function of L_c. The result for $p = 0.5$ mm is plotted in Fig.7(a). It is observed that both bounds of the stopband are very sensitive to the crossing strip length L_c. This behavior is repeated when L_c is changed by approximately an integral number of wavelengths. This can be explained in the following way : The crossing strips behave like open-circuited stubs periodically loading the signal line. The crossing strips will have a capacitive or inductive behavior depending on its length. At a certain length of crossing strips, the behavior switches from being inductive (or capacitive) to capacitive (or inductive). This switching occurs at $L_c \approx n\lambda_1$, where λ_1 is the wavelength in the dielectric medium calculated at the center frequency. At these lengths, the stopbands

become very wide.

In Fig.7(b), the normalized frequency of the bounds of the stopband are plotted as function of L_c with the period $p = 1.0$ mm. Behavior similar to that in Fig.7(a) is observed, but the values of L_c at which the switching of frequency occurs are doubled.

In Fig.8, the effects of the crossing strip width w_c on the stopband frequency bounds are investigated. The normalized frequency at the bounds of the stopband is presented for $L_c = 2.7$ mm. As the crossing strip width becomes smaller, the stopband becomes narrower.

In Fig.9, we investigate the effect of the separations t_1 and t_3 on the stopband while keeping t_2 constant. It is observed that the stopband becomes smaller when the separation is decreased, and when the separation is larger than 0.2 mm, the upper frequency bound of the stopband reaches a constant.

In Fig.10, the bounds of the first stopband is plotted as a function of the distance t_2 while fixing the separation $t_1 = t_3 =$ constant. It is observed that for $L_c = 1.0$ mm, the separation t_2 affects the upper bound of the first stopband significantly.

Fig.11 shows the case of two coupled signal striplines in the presence of periodic crossing strips of finite length. The frequency bounds of stopband are presented in Fig.11(a) and Fig.11(b) for the even mode and the odd mode, respectively, with $p = 0.5$ mm and $L_c = 1.7$ mm. The basis functions used are given by (27) and (29) for the even and the odd modes, respectively. When the separation becomes larger than L_c, the stopband width of the even mode approaches zero, but the stopband width of the odd mode is still finite. This is because the odd mode has stronger coupling between two signal lines than the even mode.

Fig.12 shows the dispersion relation of a single stripline in the presence of crossing strips of infinite length. The basis functions used are given by (33). We choose the travelling wave basis functions to have three periods. The results using seven periods are also shown for comparison, and it is found that the travelling wave basis function of three

periods is sufficient. The imaginary part of the propagation constant is approximately a linear function of frequency, and the magnitude can be as high as one percent of the real part. This is due to the assumption that the surface current along the crossing strips is a travelling wave. Part of the power along the signal line couples to the crossing strips, exciting travelling wave surface current flowing away from the signal stripline. These travelling wave surface current guides some power away from the signal line, hence reduce the guided power along the signal line.

In this case, the passband stopband behavior which is characteristic of periodic structures does not appear. The wave number k_{y0} has nonzero imaginary part over all frequencies. This is due to the power guided by the travelling wave along the crossing strips. Around $k_{y0} = n\pi/p$, the separation between two neighboring crossing strips is $n\lambda/2$ where λ is the wavelength of the guided mode. The power carried by the crossing strips at these frequencies is very small because the current on the signal line have opposite phase on both sides of the crossing strip. Also, in this case, the higher order waveguide mode is not excited.

Conclusions

A rigorous dyadic Green's function formulation for the periodic structure is derived to study the dispersion properties of single and coupled signal lines periodically loaded with crossing strips. The passband and stopband characteristics are investigated when crossing strips are of finite or infinite length.

For crossing strips of finite length, the stopband properties are mainly affected by the period, the length of crossing strips, and the separation between the signal and crossing strips. Also, at higher frequencies, higher order stopbands occur. For crossing strips of infinite length, attenuation along the signal line exists over the whole frequency range due to the power guided by the travelling wave along crossing strips.

Acknowledgments

This work was supported by the RADC Contract F19628-88-K-0013, the ARO Contract DAAL03-88-K-0057, the ONR Contract N00014-89-J-1019, the Joint Services Electronics Program under the Contract DAAL03-86-K-0002, and the NSF Grant 8620029-ECS.

References

[1] T. Kitasawa and R. Mittra,"An investigation of striplines and fin lines with periodic stubs," *IEEE Trans. Microwave Theory Tech.*, vol.MTT-32, no.7, pp.684-688, July 1984.

[2] Y. Fukuoka and T. Itoh,"Slow-wave coplanar waveguide on periodically doped semiconductor substrate," *IEEE Trans. Microwave Theory Tech.*, vol.MTT-31, no.12, pp.1013-1017, December 1983.

[3] Q. Gu and J. A. Kong, "Transient analysis of single and coupled lines with capacitively loaded junctions," *IEEE Trans. Microwave Theory Tech.*, vol.MTT-34, no.9, pp.952-964, September 1986.

[4] B. J. Rubin,"The propagation characteristics of signal lines in a mesh-plane environment," *IEEE Trans. Microwave Theory Tech.*, vol.MTT-32, no.5, pp.522-531, May 1984.

[5] C. H. Chan and R. Mittra, "The propagation characteristics of signal lines embedded in a multilayered structure in the presence of a periodically perforated ground plane," *IEEE Trans. Microwave Theory Tech.*, vol.MTT-36, no.6, pp.968-975, June 1988.

[6] N. V. Nair and A. K. Mallick, "An analysis of a width-modulated microstrip periodic structure," *IEEE Trans. Microwave Theory Tech.*, vol.MTT-32, no.2, pp.200-204, February 1984.

[7] F. J. Glandorf and I. Wolff, "A spectral-domain analysis of periodically nonuniform microstrip lines," *IEEE Trans. Microwave Theory Tech.*, vol.MTT-35, no.3, pp.336-343, March 1987.

[8] J. A. Kong,"*Electromagnetic Wave Theory*," New York : Wiley, 1986.

[9] R. W. Jackson and D. M. Pozar, "Full-wave analysis of microstrip open-end and gap discontinuities," *IEEE Trans. Microwave Theory Tech.*, vol.MTT-33, no.10, pp.1036-1042, October 1985.

[10] H. Y. Yang and N. G. Alexopoulos, "A dynamic model for microstrip-slotline transition and related structures," *IEEE Trans. Microwave Theory Tech.*, vol.MTT-36, no.2, pp.286-293, February 1988.

[11] E. H. Newman and D. Forrai, "Scattering from a microstrip patch," *IEEE Trans. Antennas Propagat.*, vol.AP-35, no.3, pp.245-251, March 1987.

Fig.1 Geometrical configuration of signal strip lines periodically loaded with crossing metallic strips embedded in layer (l) of a stratified medium.

Fig.2 Geometrical configuration of one signal strip line periodically loaded with crossing strips embedded in a one-layer medium.

Fig.3 Geometrical configuration of two signal strip lines periodically loaded with crossing strips embedded in a one-layer medium.

Fig.4 The basis functions used for infinitely long crossing strips, $m = 4$, $N_3 = N_4 = 6$.

Fig.5 Dispersion relation of one signal strip line periodically loaded with crossing strips of finite length,
$\epsilon_r = 10$, $t_1 = t_2 = t_3 = 0.2$ mm, $p = 0.5$ mm,
$w_1 = w_c = 0.125$ mm, $L_c = 2.3$ mm,
$N_1 = 1$, $N_2 = 0$, $N_3 = 4$, $N_4 = 3$,
$\times$: $N_1 = 1$, $N_2 = 0$, $N_3 = 6$, $N_4 = 5$,
ω_U : upper bound of the first stopband,
ω_L : lower bound of the first stopband.

Fig.6 Interaction of Floquet modes with TE_1 (TM_1) parallel-plate waveguide mode,
$k = \omega\sqrt{\mu_0\epsilon_0\epsilon_r}$, $d = t_1 + t_2 + t_3$.

Fig.7(a) The effects of L_c on the upper and lower bounds of the stopband,
$\epsilon_r = 10$, $t_1 = t_2 = t_3 = 0.2$ mm,
$p = 0.5$ mm, $w_1 = w_c = 0.125$ mm,
$N_1 = 1$, $N_2 = 0$, $N_3 = 5$, $N_4 = 4$.

Fig.7(b) The effects of L_c on the upper and lower bounds of the stopband,
$\epsilon_r = 10$, $t_1 = t_2 = t_3 = 0.2$ mm,
$p = 1.0$ mm, $w_1 = w_c = 0.125$ mm,
$N_1 = 1$, $N_2 = 0$, $N_3 = 5$, $N_4 = 4$.

Fig.8 The effects of w_c on the upper and
lower bounds of the stopband,
$\epsilon_r = 10$, $t_1 = t_2 = t_3 = 0.2$ mm,
$p = 0.5$ mm, $w_1 = 0.125$ mm, $L_c = 2.7$ mm,
$N_1 = 1$, $N_2 = 0$, $N_3 = 4$, $N_4 = 3$.

Fig.9 The effects of t_1 and t_3 on the upper and
lower bounds of the stopband,
$\epsilon_r = 10$, $t_2 = 0.2$ mm, $p = 0.5$ mm,
$w_1 = w_c = 0.125$ mm, $L_c = 1.0$ mm,
$N_1 = 1$, $N_2 = 0$, $N_3 = 2$, $N_4 = 1$.

Fig.10 The effects of t_2 on the upper and
lower bounds of the stopband,
$\epsilon_r = 10$, $t_1 = t_3 = 0.2$ mm, $p = 0.5$ mm,
$w_1 = w_c = 0.125$ mm, $L_c = 1.0$ mm,
$N_1 = 1$, $N_2 = 0$, $N_3 = 2$, $N_4 = 1$.

Fig.11(a) The effects of x_c on the upper and
lower bounds of the stopband,
for two signal strip lines,
$\epsilon_r = 10$, $t_1 = t_2 = t_3 = 0.2$ mm, $p = 0.5$ mm,
$w_1 = w_c = 0.125$ mm, $L_c = 1.7$ mm,
$N_1 = 1$, $N_2 = 0$, $N_3 = 3$, $N_4 = 2$.

Fig.11(b) The effects of x_c on the upper and
lower bounds of the stopband,
for two signal strip lines,
$\epsilon_r = 10$, $t_1 = t_2 = t_3 = 0.2$ mm, $p = 0.5$ mm,
$w_1 = w_c = 0.125$ mm, $L_c = 1.7$ mm,
$N_1 = 1$, $N_2 = 0$, $N_3 = 3$, $N_4 = 2$.

Fig.12 The dispersion relation for one signal strip line
periodically loaded with crossing strips of infinite length,
$\epsilon_r = 10$, $t_1 = t_2 = t_3 = 0.2$ mm, $p = 2.5$ mm,
$w_1 = w_c = 0.125$ mm, $h = \lambda_e/8$, $m = 6$,
$\times : m = 14$.

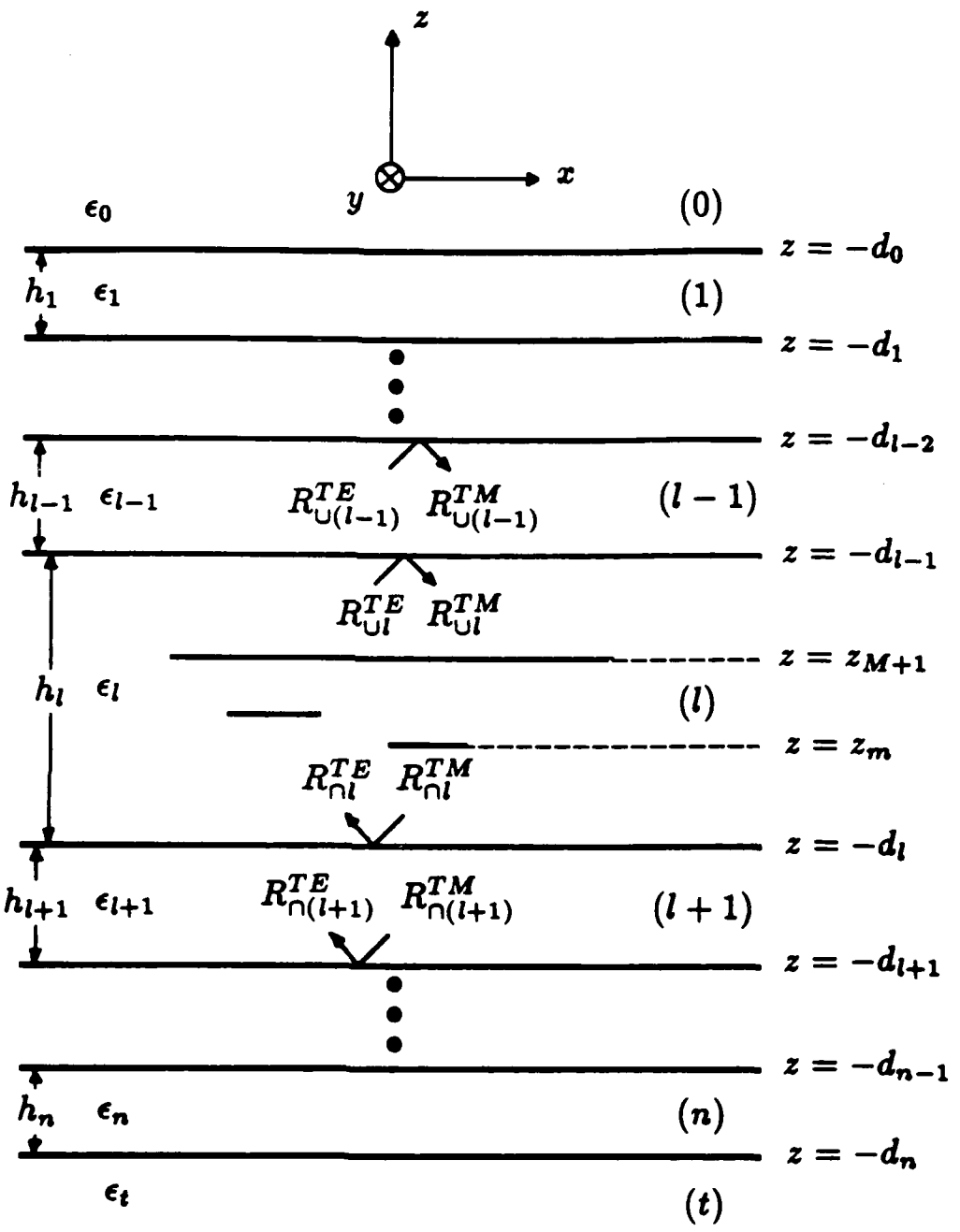
z
x
y
ϵ_0
(0)
$z = -d_0$
h_1 ϵ_1
(1)
$z = -d_1$
$z = -d_{l-2}$
h_{l-1} ϵ_{l-1}
$R^{TE}_{\cup(l-1)}$ $R^{TM}_{\cup(l-1)}$
$(l-1)$
$z = -d_{l-1}$
$R^{TE}_{\cup l}$ $R^{TM}_{\cup l}$
$z = z_{M+1}$
h_l ϵ_l
(l)
$z = z_m$
$R^{TE}_{\cap l}$ $R^{TM}_{\cap l}$
$z = -d_l$
h_{l+1} ϵ_{l+1}
$R^{TE}_{\cap(l+1)}$ $R^{TM}_{\cap(l+1)}$
$(l+1)$
$z = -d_{l+1}$
$z = -d_{n-1}$
h_n ϵ_n
(n)
$z = -d_n$
ϵ_t
(t)

Fig. 1

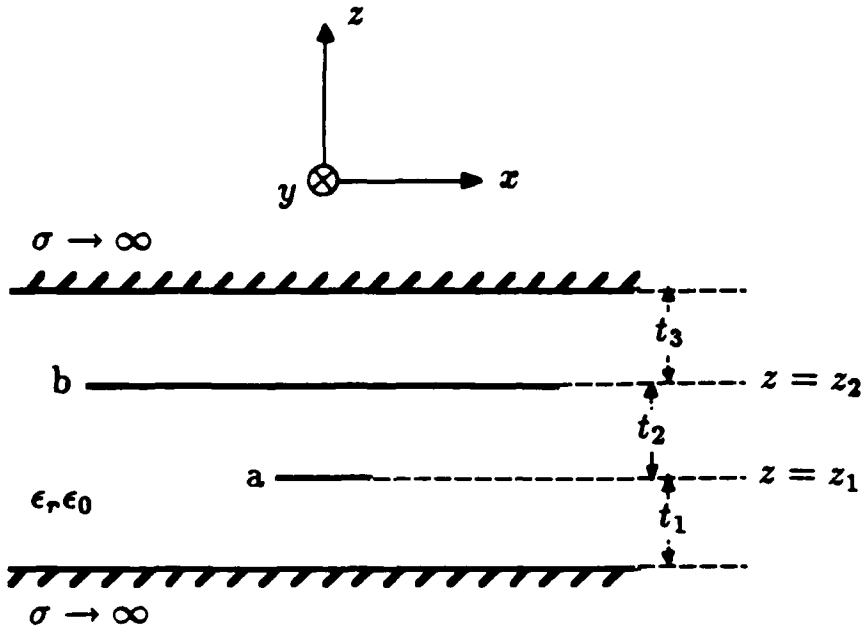

a : signal strip b : crossing strip

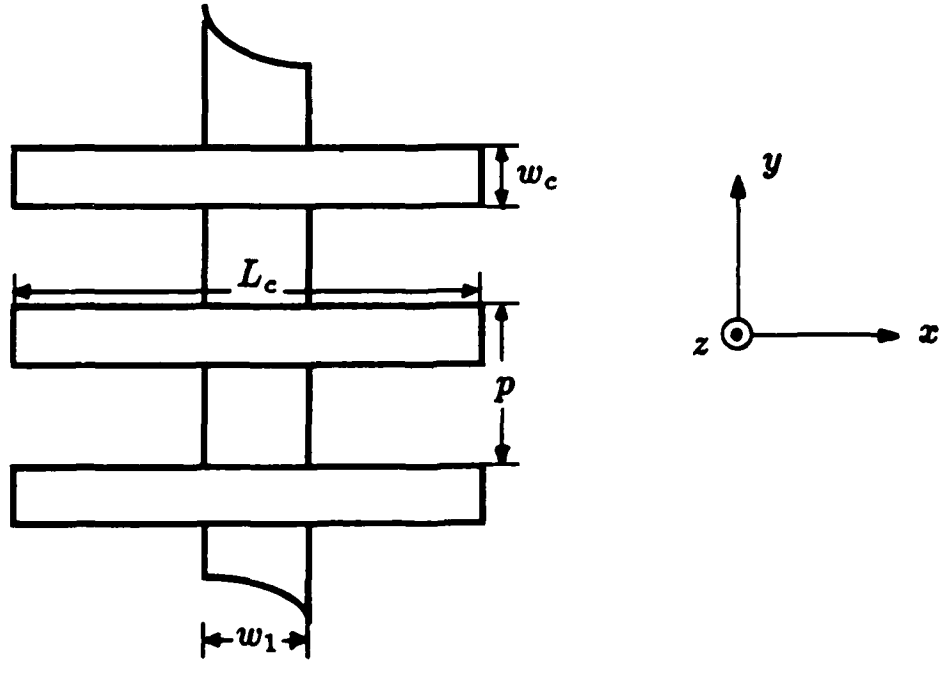

Fig. 2

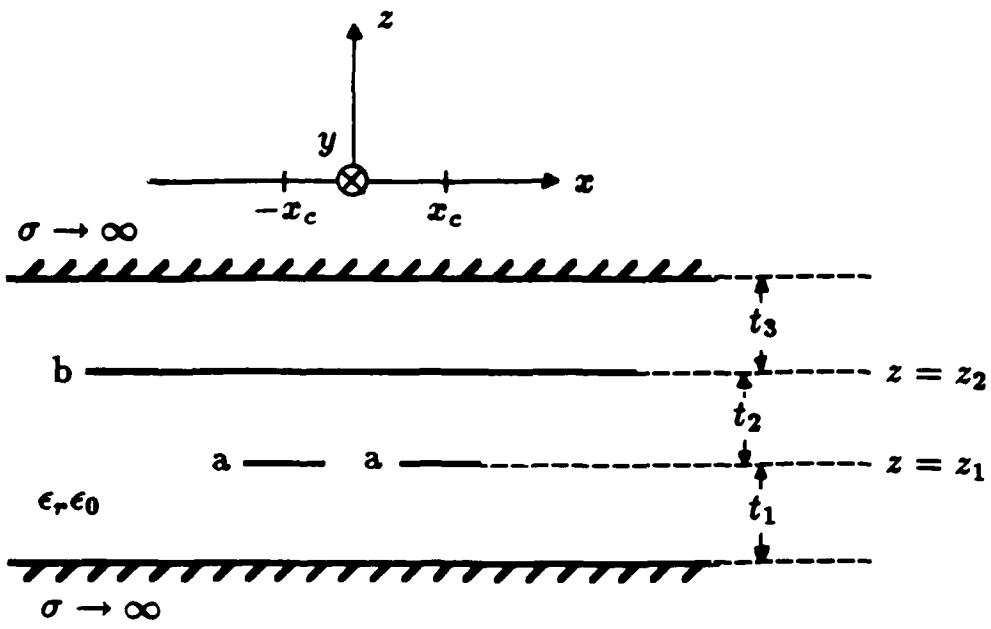

a : signal strip b : crossing strip

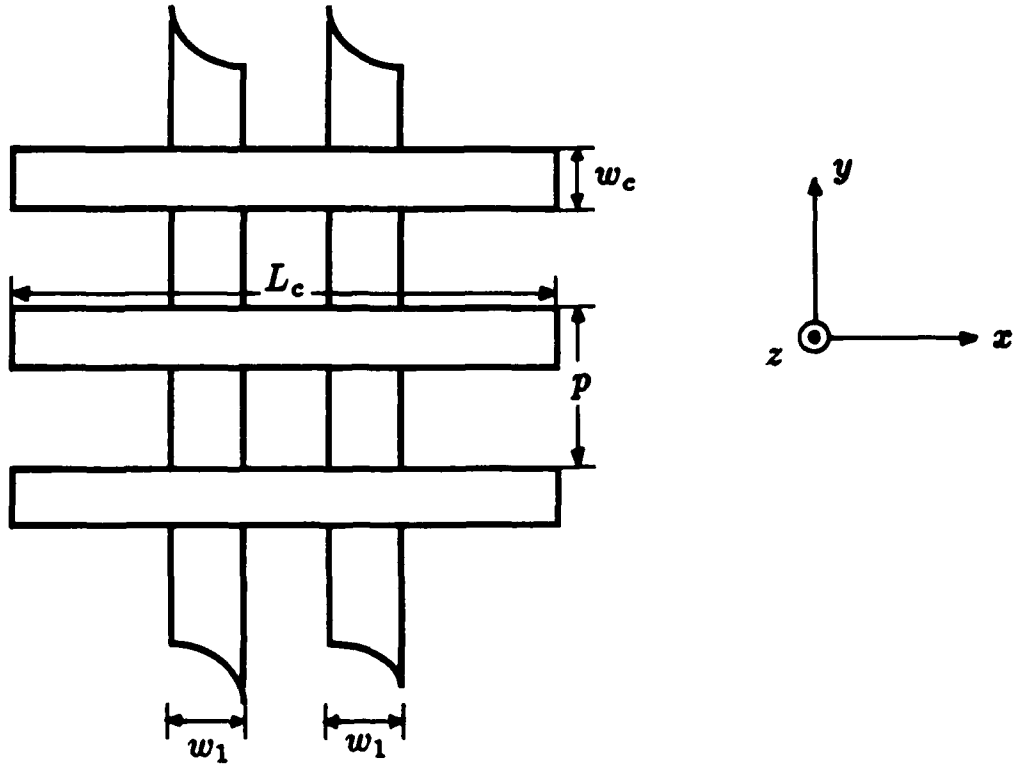

Fig. 3

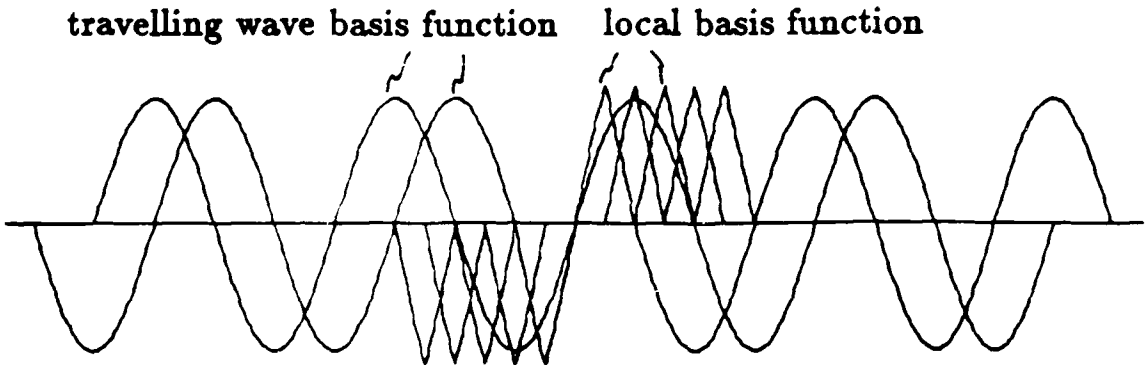
travelling wave basis function
local basis function

J_{2x}

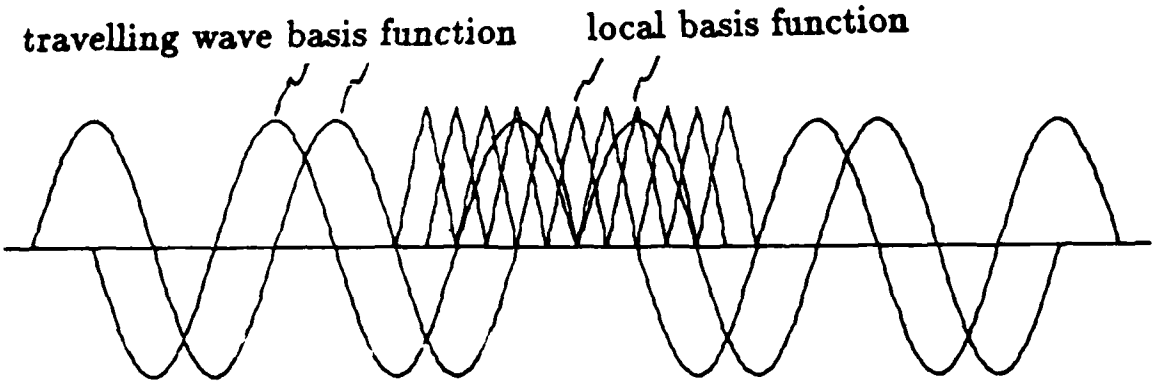
travelling wave basis function
local basis function

J_{2y}

Fig. 4

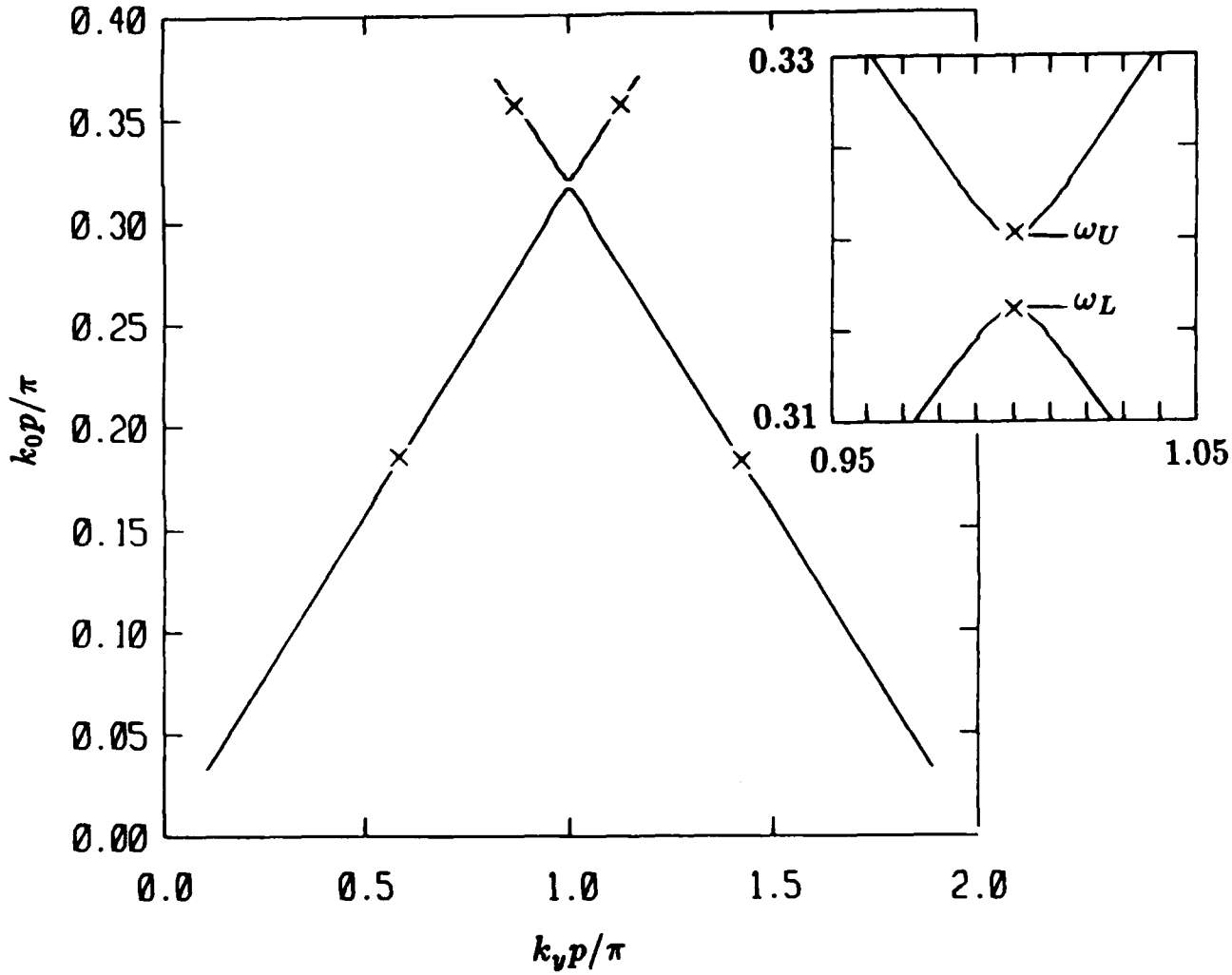
0.40
0.35
0.30
0.25
0.20
0.15
0.10
0.05
0.00
$k_0 p/\pi$
0.0
0.5
1.0
1.5
2.0
$k_v p/\pi$
0.33
0.31
0.95
1.05
ω_U
ω_L

Fig. 5

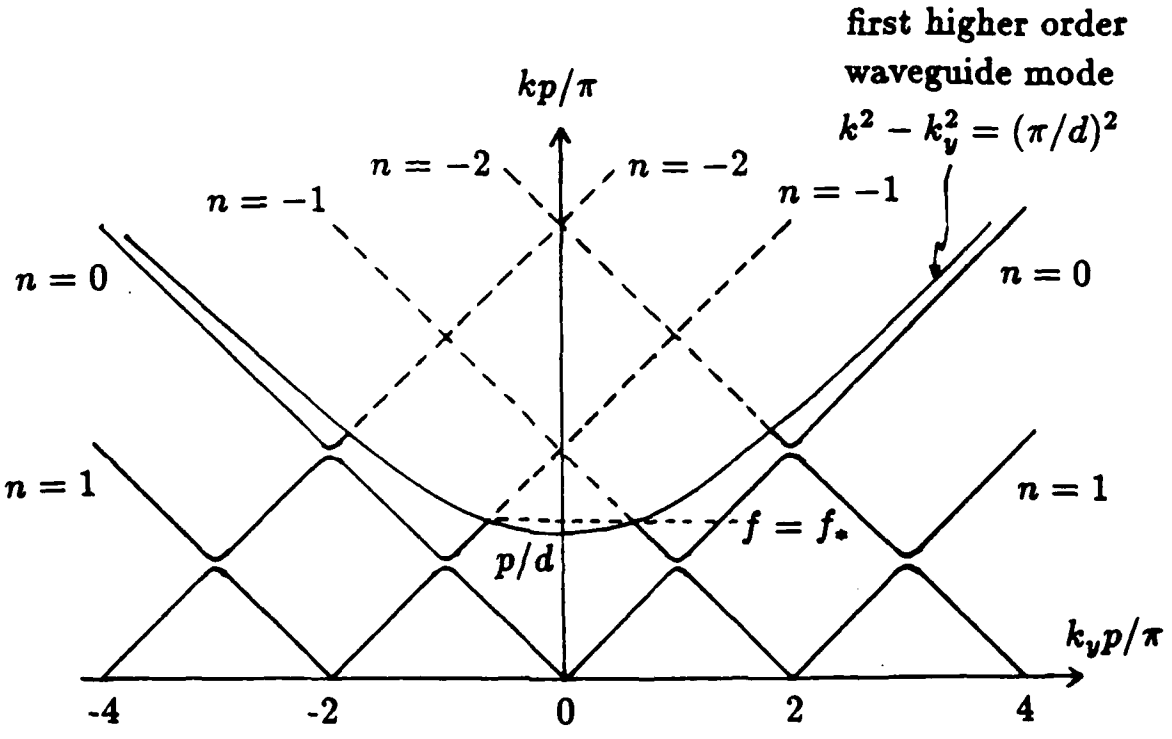
first higher order
waveguide mode
$k^2 - k_y^2 = (\pi/d)^2$
kp/π
$n = -2$
$n = -2$
$n = -1$
$n = -1$
$n = 0$
$n = 0$
$n = 1$
$n = 1$
$f = f_*$
p/d
$k_y p/\pi$
-4
-2
0
2
4

Fig. 6

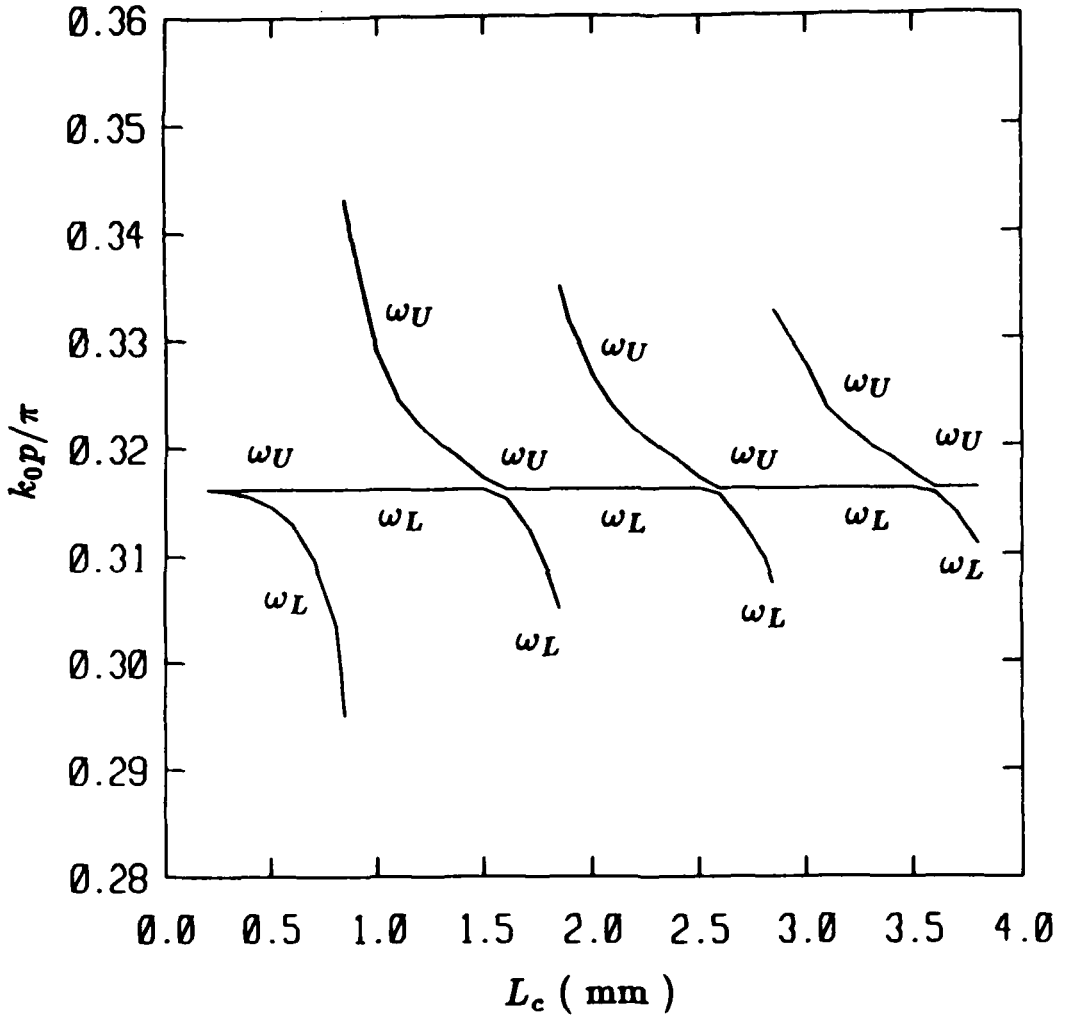
0.36
0.35
0.34
0.33
0.32
0.31
0.30
0.29
0.28
k_0p/π
ω_U
ω_L
0.0
0.5
1.0
1.5
2.0
2.5
3.0
3.5
4.0
L_c (mm)

Fig. 7(a)

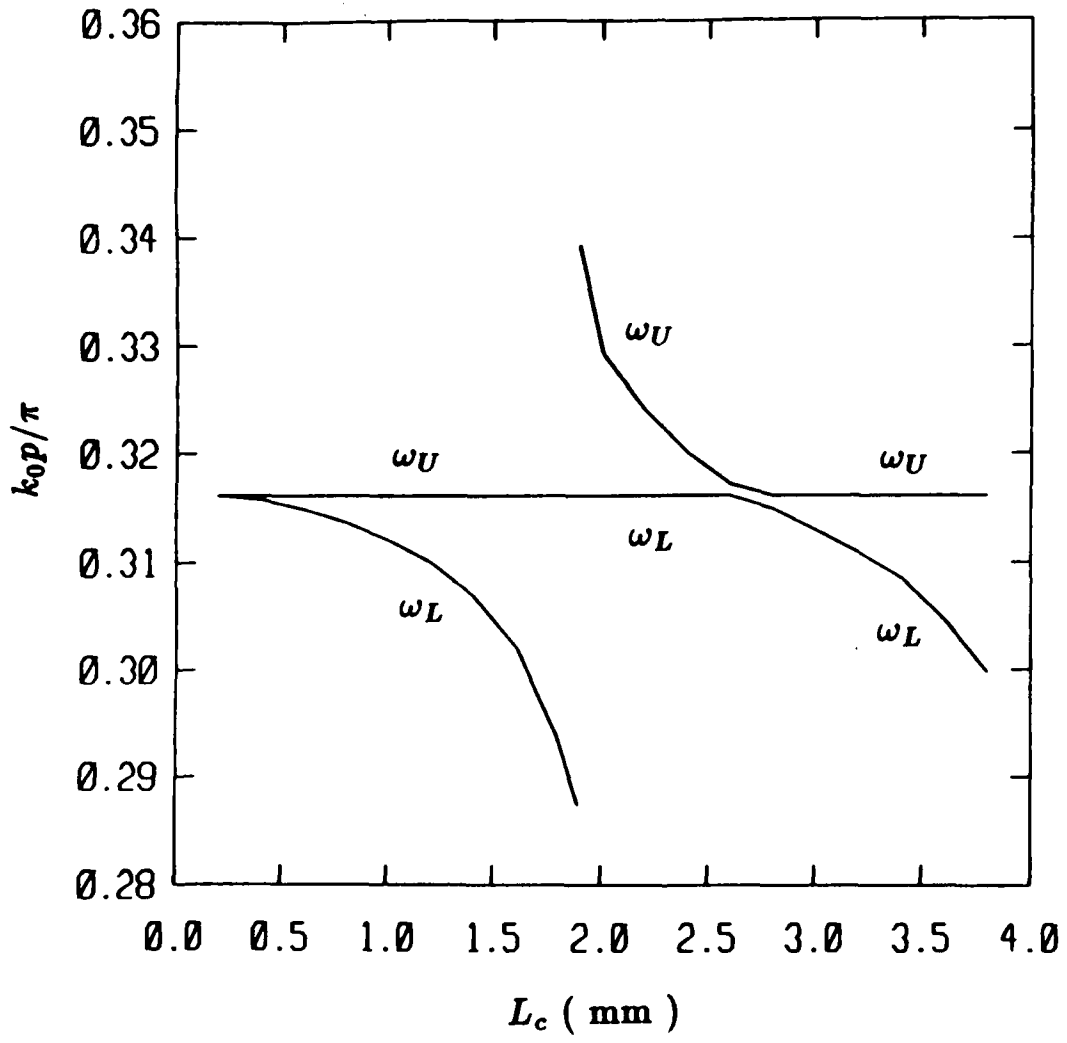
0.36
0.35
0.34
0.33
0.32
0.31
0.30
0.29
0.28
k_0p/π
ω_U
ω_U
ω_U
ω_L
ω_L
ω_L
0.0
0.5
1.0
1.5
2.0
2.5
3.0
3.5
4.0
L_c (mm)

Fig. 7(b)

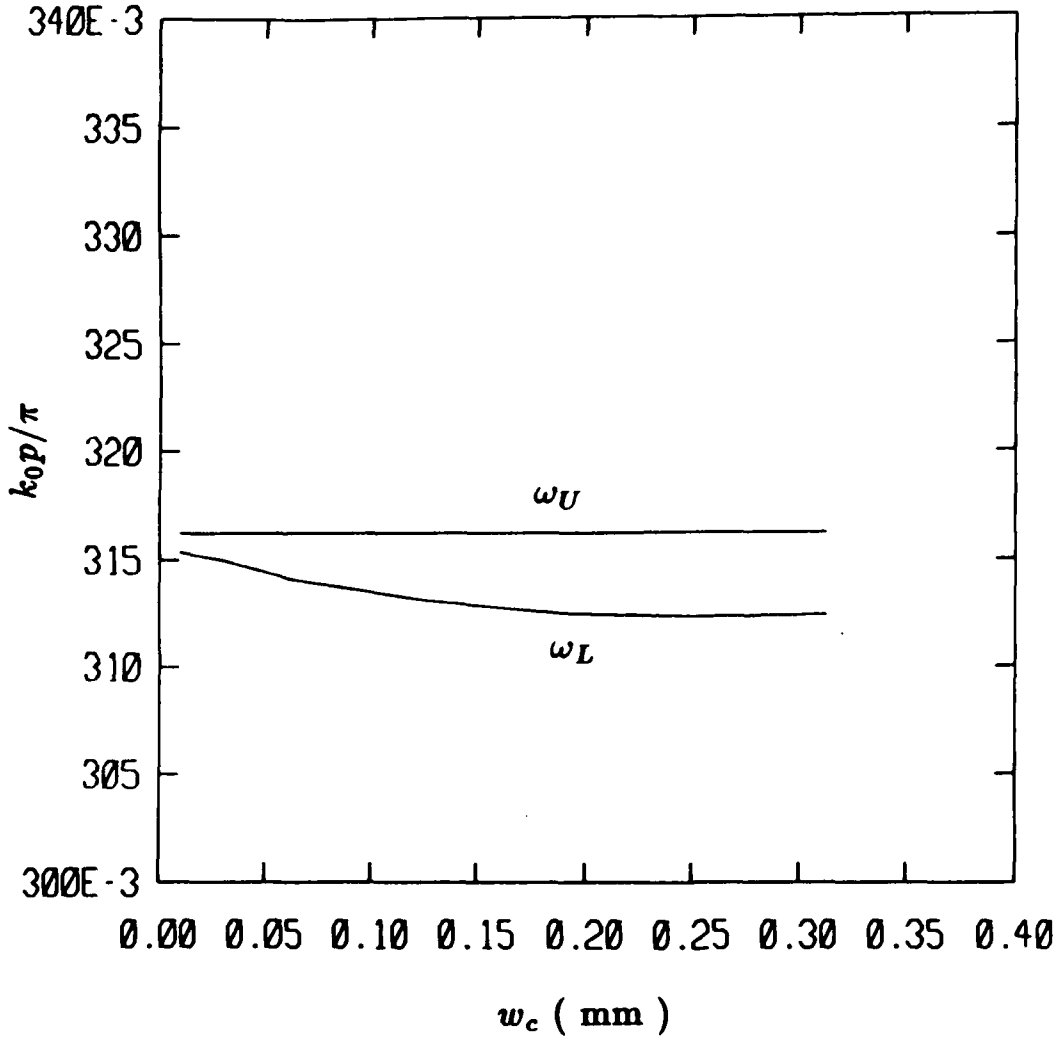
340E-3
335
330
325
320
315
310
305
300E-3
k_0p/π
ω_U
ω_L
0.00 0.05 0.10 0.15 0.20 0.25 0.30 0.35 0.40
w_c (mm)

Fig. 8

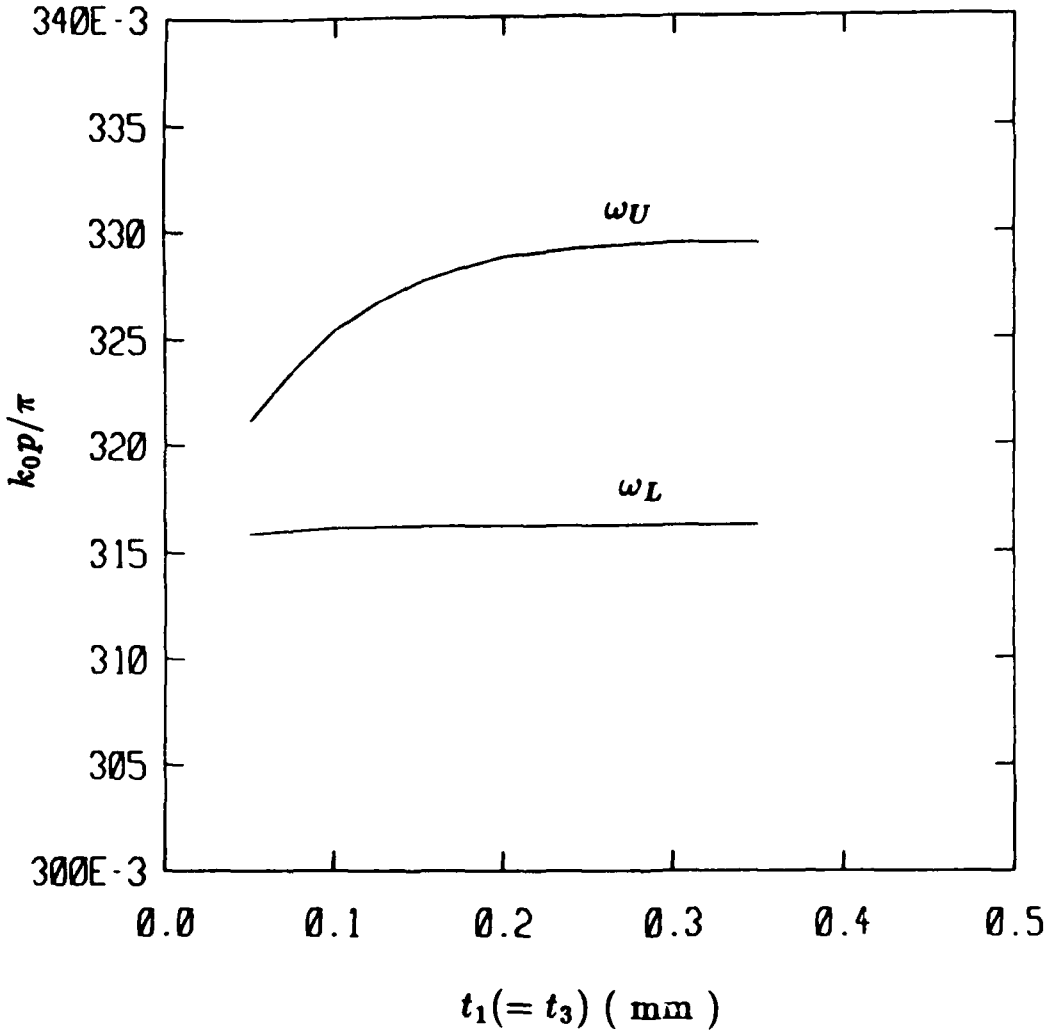
340E-3
335
330
325
320
315
310
305
300E-3
k_0p/π
ω_U
ω_L
0.0
0.1
0.2
0.3
0.4
0.5
$t_1(=t_3)$ (mm)

Fig. 9

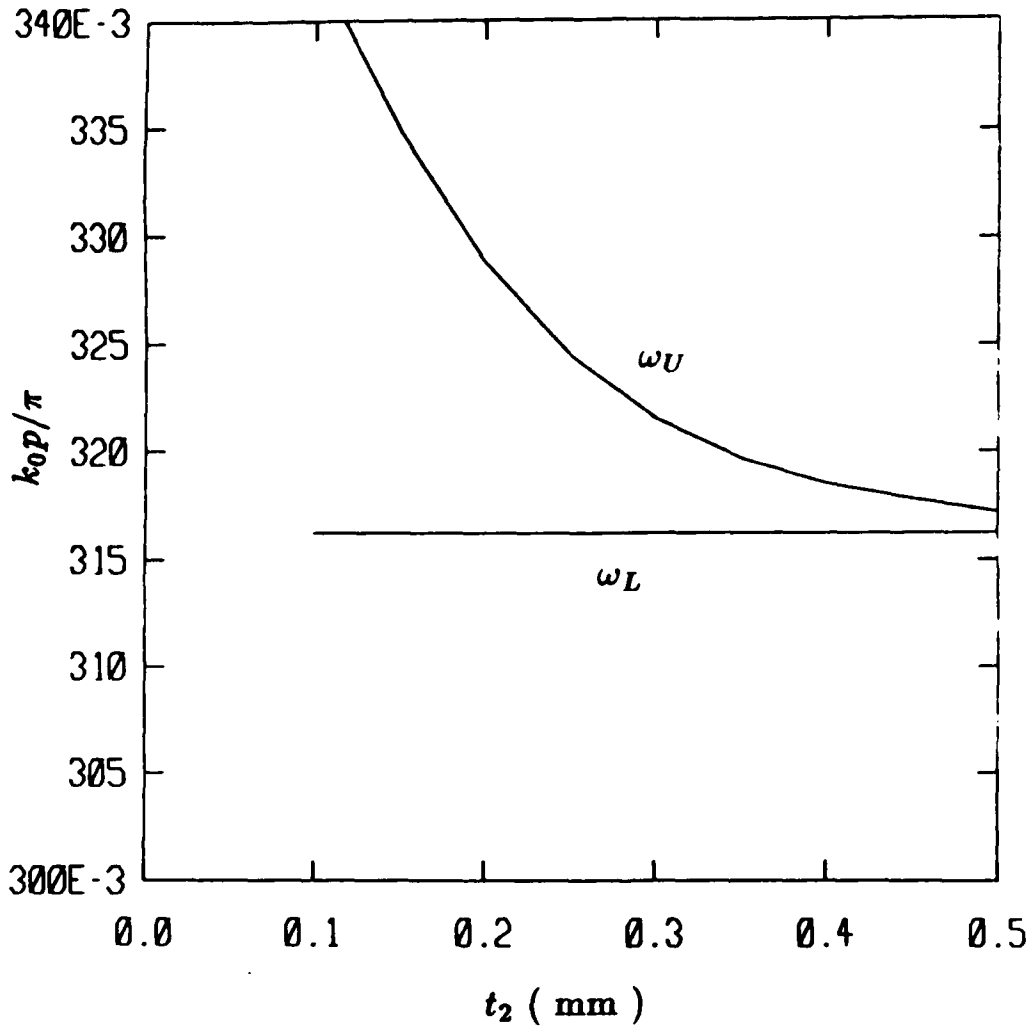
340E-3
335
330
325
320
315
310
305
300E-3
k_0p/π
ω_U
ω_L
0.0
0.1
0.2
0.3
0.4
0.5
t_2 (mm)

Fig. 10

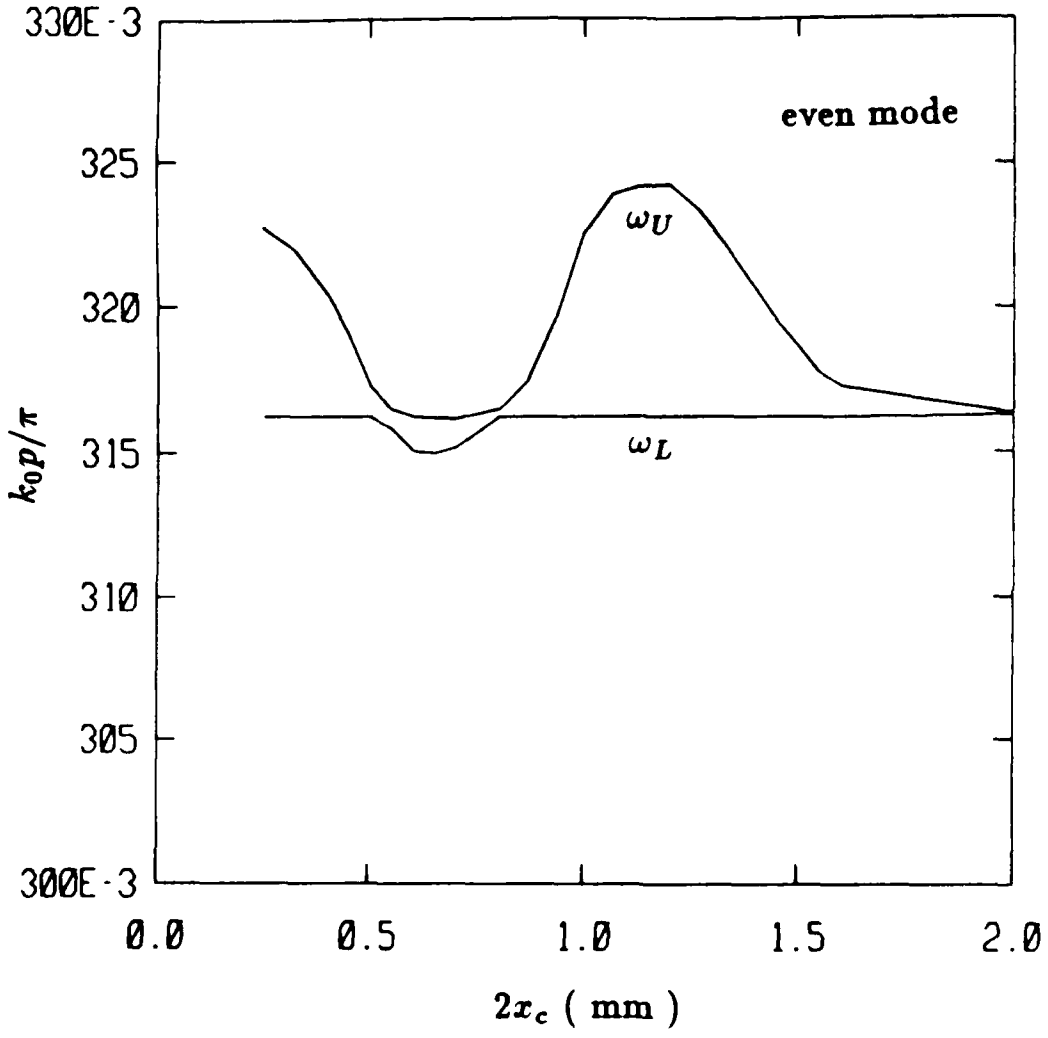
330E-3
325
320
315
310
305
300E-3
even mode
ω_U
ω_L
$k_0 p/\pi$
0.0
0.5
1.0
1.5
2.0
$2x_c$ (mm)

Fig 11(a)

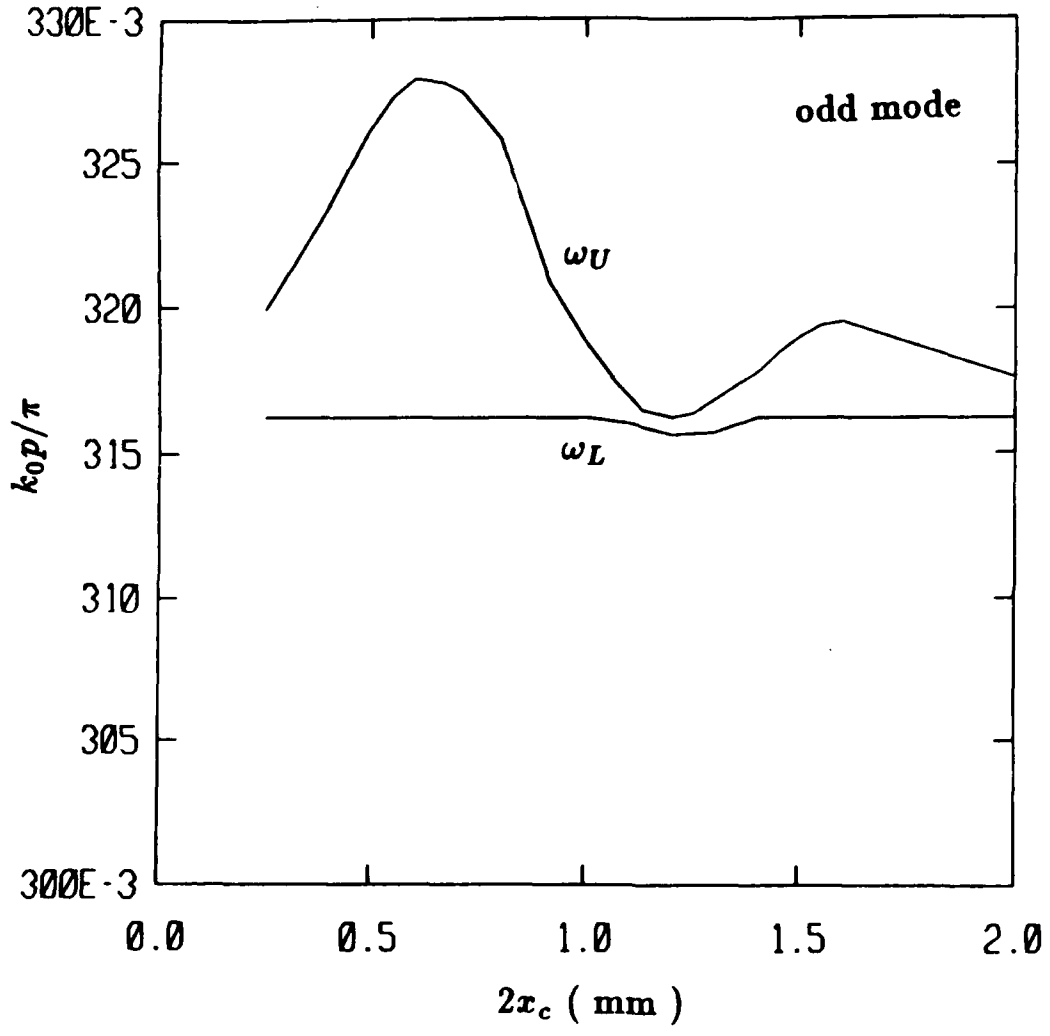
330E-3
325
320
315
310
305
300E-3
odd mode
ω_U
ω_L
k_0p/π
0.0
0.5
1.0
1.5
2.0
$2x_c$ (mm)

Fig. 11(b)

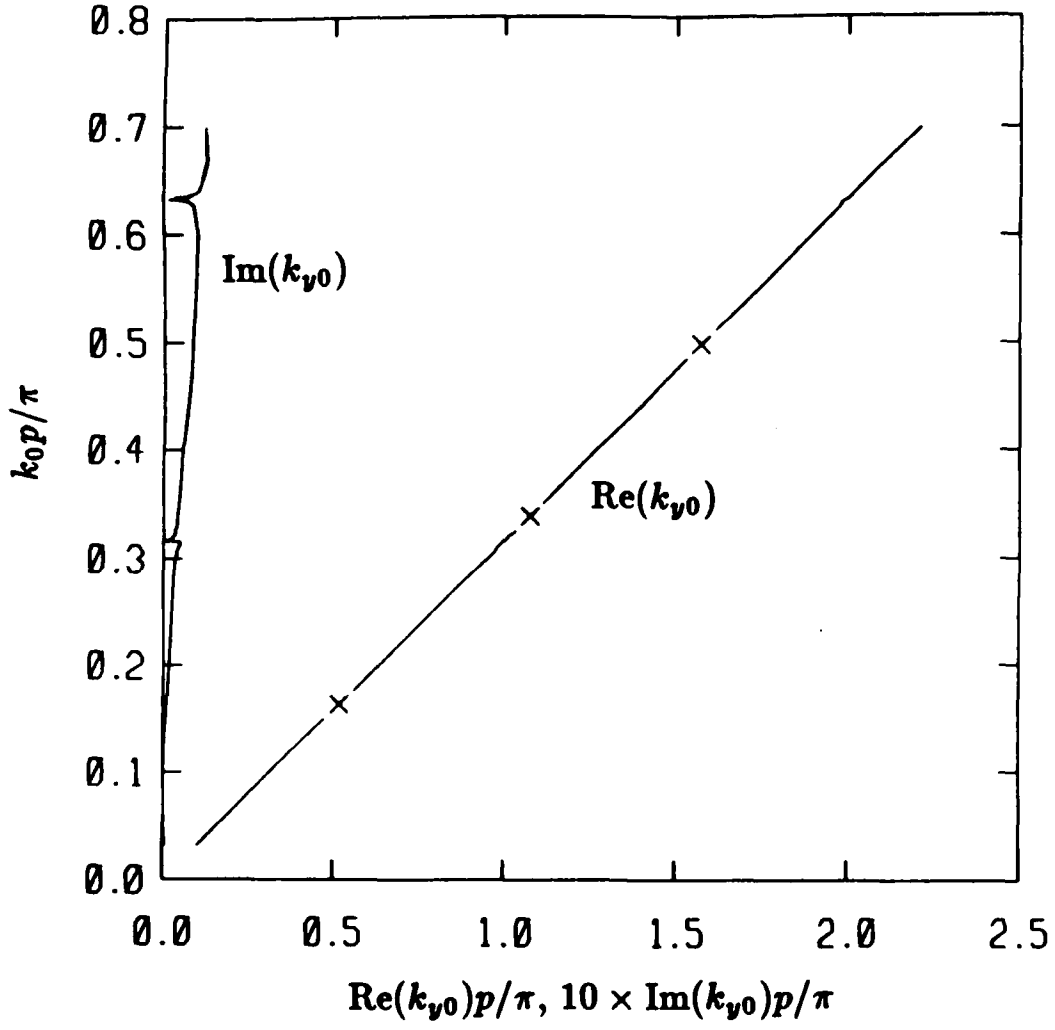
0.8
0.7
0.6
0.5
0.4
0.3
0.2
0.1
0.0
k_0p/π
$\mathrm{Im}(k_{y0})$
$\mathrm{Re}(k_{y0})$
0.0
0.5
1.0
1.5
2.0
2.5
$\mathrm{Re}(k_{y0})p/\pi$, $10 \times \mathrm{Im}(k_{y0})p/\pi$

Fig. 12

Journal of Electromagnetic Waves and Applications, Vol. 3, No. 3, 183-197, 1989

Transient Analysis of Frequency-Dependent Transmission Line Systems Terminated with Nonlinear Loads

Q. Gu

Shanghai Xinhua Radio Factory
Shanghai, PRC

Y. E. Yang and J. A. Kong

Department of Electrical Engineering and Computer Science
and Research Laboratory of Electronics
Massachusetts Institute of Technology
Cambridge, MA 02139, USA

Abstract– A new method for analyzing frequency-dependent transmission line systems with nonlinear terminations is presented. The generalized scattering matrix formulation is used as the foundation for the time domain iteration scheme. Compared to the admittance matrix approach proposed in a previous paper, it has the advantage of shorter impulse response which leads to smaller computer memory requirement and faster computation time. Examples of a microstrip line loaded with nonlinear elements are given to illustrate the efficiency of this method.

I. INTRODUCTION

In recent years, the effect of the interconnection lines on high-speed integrated circuits has become more and more important. As the speeds of integrated circuits increase, the propagation delay as well as the dispersion and loss of interconnection lines can no longer be neglected. Traditional lumped element circuit models must be supplemented by dispersive transmission line models in order to account for these effects. This has created the need for new numerical procedures that can be easily incorporated into current CAD tools. To make matters more complicated, the interconnection lines are terminated with not only linear elements but also nonlinear semiconductor devices, such as diodes and transistors.

Several techniques are now commonly used to deal with nonlinear circuit problems, for example, the direct time domain approaches [1,2], and the semi-frequency domain approaches, such as the harmonic balance [3,4] and the modified harmonic balance techniques [5,6]. Semi-frequency domain approaches are useful for microwave and millimeter wave integrated circuits but become impractical for digital integrated circuits because of their wide-band nature. On the other hand, frequency-dependent parameters often make it awkward to apply the direct time domain approach to interconnection line systems. The time-domain finite-difference method [7] and the time-domain method of moments [8] have been proposed to deal directly with electromagnetic scattering from nonlinear loads.

However, dispersion problems are absent from the discussions.

Liu and Tesche [1] developed a combined time-domain frequency-domain treatment of antennas and scatterers with nonlinear loads. In their work, the transfer function (impulse response) of the linear portion of the investigated system is first obtained through the frequency-domain analysis, and it is then used to solve the entire nonlinear problem in the time domain. Subsequent improvements to this method have been suggested by Djordjevic, Sarkar and Harrington [9] through artificially introducing pairs of quasi-matched passive networks, and by Caniggia [10] and Schutt-Aine and Mittra [11], through macromodel and scattering parameter analysis based on a fixed reference impedance.

In this paper we shall present an extended and more natural method that will completely eliminate the need for any artificial networks or fixed reference impedances. Its close ties to the physics of transmitted and reflected waves on transmission lines also help in achieving the purpose of reducing computation time. The algorithm is explained in the next section. In Section III the details of applying our formulations to frequency-dependent transmission lines with nonlinear loads are illustrated in the analyses of a nonlinearly-loaded dispersive transmission line.

II. ANALYSIS BASED ON WAVE TRANSMISSION AND REFLECTION

An arbitrary system of n dispersive transmission lines can be represented by the following coupled linear ordinary differential equations in the frequency domain:

$$\begin{aligned} -\frac{d}{dx}[V] &= j\omega[L]\cdot[I] + [R]\cdot[I] \\ -\frac{d}{dx}[I] &= j\omega[C]\cdot[V] + [G]\cdot[V] \end{aligned} \tag{1}$$

Treating the n transmission lines as a $2n$-port system, we can derive from (1) the admittance matrix $[Y]$, which relates terminal voltages to terminal currents:

$$I_j = \sum_{k=1}^{2n} Y_{jk} V_k \tag{2}$$

The time domain counterparts become convolution relations:

$$i_j(t) = \sum_{k=1}^{2n} \int_0^t d\tau\, y_{jk}(t-\tau)\, v_k(\tau) \tag{3}$$

where y_{jk} is the inverse Fourier transform of $Y_{jk}(\omega)$. The terminal voltages and currents for any particular system can then be uniquely determined once the terminal conditions

$$[i(t)] = [f(v(t))] \tag{4}$$

are given. If all the terminations contain only linear elements, we can solve the problem in the frequency domain. Otherwise, iteration procedures are usually required for obtaining the solutions. The analyses presented in [1] and [9] are based on equations (3) and (4). Although their approaches are straightforward, there

exist problems that could possibly affect the efficiency of numerical computation. First of all, the parameter $y_{jk}(t)$ is equivalent to the current measured at port j with a voltage impulse excitation of unit amplitude at port k while ports other than k are short-circuited. Owing to strong reflections at the terminations, the duration of $y_{jk}(t)$ is usually long for slightly lossy transmission line systems, and even infinite for a lossless system. The long duration puts great demands on computer memory and execution time as required to perform convolution integrals of $[v(t)]$ and $[y(t)]$ during the iterative solution of nonlinear equations.

In order to overcome the disadvantage of using the parameters $\{y_{jk}\}$, the authors in [9] artificially insert a pair of complementary passive networks between the end of the transmission lines and the actual terminations. The purpose of that is to make the augmented linear network, which consists of the transmission line portion and the artificial network directly connected to the end of the transmission lines, a quasi-matched linear system so that the duration of the impulse responses for the augmented linear system can be effectively shortened. However, the other artificial network which is directly attached to the original load will contain negative resistors and hence may render the numerical solution unstable, especially when the transmission lines are lossless.

Instead of dealing with terminal voltage and current, we will analyze the transmission line system from the viewpoint of voltage waves. We choose the input and output waves at the terminal ports of the transmission lines as the variables of the problem as shown in Fig. 1. The parameters $\{B_j\}$ and $\{C_j\}$ are defined as follows:

$$B_j(\omega) = \frac{1}{2}\left[V_j(\omega) - Z_{0j}(\omega) \cdot I_j(\omega)\right] \tag{5}$$

$$C_j(\omega) = \frac{1}{2}\left[V_j(\omega) + Z_{0j}(\omega) \cdot I_j(\omega)\right] \tag{6}$$

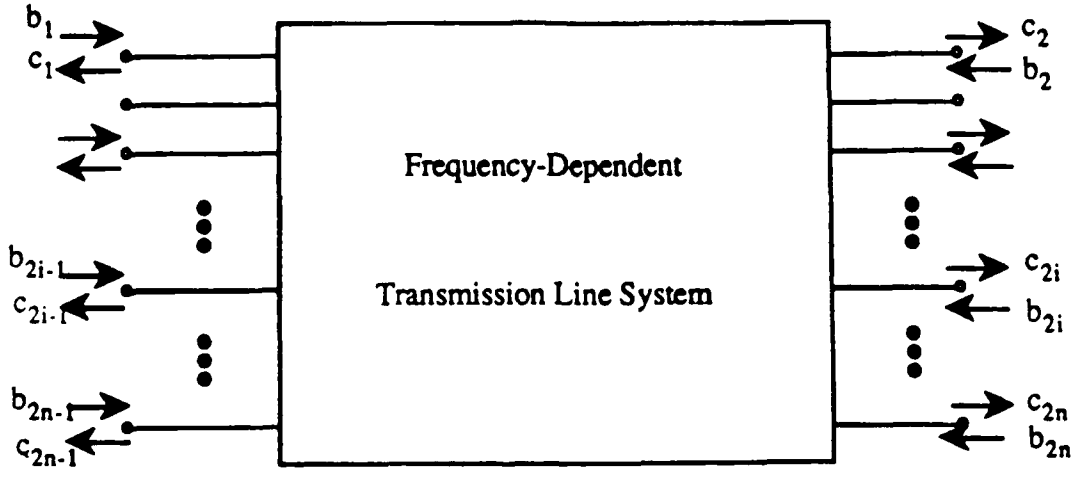

Figure 1. Linear multi-port network consisting of transmission lines.

where $Z_{0j}(\omega) = \sqrt{L_{jj}(\omega)/C_{jj}(\omega)}$ is the frequency-dependent characteristic impedance on line connected to port j. The linear dispersive transmission line system is thus characterized by a *scattering matrix* $[S_{ij}]$, i.e.,

$$\begin{bmatrix} C_1 \\ C_2 \\ C_3 \\ \vdots \\ C_{2n} \end{bmatrix} = \begin{bmatrix} S_{11} & S_{12} & S_{13} & \cdots & S_{1,2n} \\ S_{21} & S_{22} & S_{23} & \cdots & S_{2,2n} \\ S_{31} & S_{32} & S_{33} & \cdots & S_{3,2n} \\ \vdots & \vdots & \vdots & \ddots & \vdots \\ S_{2n,1} & S_{2n,2} & S_{2n,3} & \cdots & S_{2n,2n} \end{bmatrix} \begin{bmatrix} B_1 \\ B_2 \\ B_3 \\ \vdots \\ B_{2n} \end{bmatrix} \tag{7}$$

or

$$C_j(\omega) = \sum_{k=1}^{2n} S_{jk}(\omega) B_k(\omega) \qquad (k = 1, 2, \ldots, 2n) \tag{8}$$

It is easy to realize from the above equations that for all $j \neq k$, $S_{jk}(\omega)$ is equal to $2V_j(\omega)$ if all ports are loaded with their transmission line characteristic impedances and only a voltage source of amplitude 1 is applied at port k. This corresponds to impulse response or transfer functions in the time domain. If the coupling between individual transmission lines is weak, the system will be close to being perfectly matched. In this case we can conclude that the inverse Fourier transform of S_{jk}, denoted as $h_{jk}(t)$, will be of much shorter duration than $y_{ik}(t)$. Therefore we can effectively reduce the memory required to store the past values of h_{jk} and the time to compute the convolution integrals in

$$c_j(t) = \sum_{k=1}^{2n} \int_0^t d\tau \, h_{jk}(t-\tau) \, b_k(\tau) \tag{9}$$

without inserting any artificial networks.

We now have to solve $[b(t)]$ and $[c(t)]$ by incorporating the nonlinear boundary conditions of the problem. Specifically at port j, equations (5) and (6) lead to [8]

$$V_j(\omega) = B_j(\omega) + C_j(\omega) \tag{10}$$

and

$$2C_j(\omega) = V_j(\omega) + Z_{0j}(\omega) \, I_j(\omega) \tag{11}$$

By taking inverse Fourier transform on both sides of (10) and (11), we obtain their time domain counterparts:

$$v_j(t) = b_j(t) + c_j(t) \tag{12}$$

$$v_j(t) = 2c_j(t) - \int_0^t d\tau \, z_{0j}(t-\tau) \, f_j(v_j(\tau)) \tag{13}$$

where

$$z_{0j}(t) = \mathcal{F}^{-1}\left[Z_{0j}(\omega)\right]$$

Our problem will be solved in a time-marching fashion. At any instant t, the iteration procedure is as follows:

(i) Set up initial guess of $[b(t)]$. A reasonable choice is to take values from the previous time step.

(ii) Compute individual $\{c_j(t)\}$ using (9).

(iii) Apply standard nonlinear equation techniques such as Newton-Raphson method to (13) to solve for individual $\{v_j(t)\}$.

(iv) Obtain the next guess of $[b(t)]$ from the relation $b_j(t) = v_j(t) - c_j(t)$, and compare the guess with the previous one. If the error is above a pre-set tolerance, repeat steps (ii) to (iv) with the new guess.

For all practical purposes, we further divide these variables into two sets. The first corresponds to the source side of the transmission line system (Fig. 2), identified by odd-numbered subscripts, and the other corresponds to the load side (sourceless) with even-numbered subscripts (Fig. 3). The reason for doing so is based the following observations. The transfer functions linking $\{b_{2j}\}$ to $\{c_{2j+1}\}$ and $\{b_{2j+1}\}$ to $\{c_{2j}\}$ include time delay operators in order to account for the finite speed of propagation. In other words, $\{c_{2j+1}\}$ depend not on the present but the past values of $\{b_{2j}\}$ and the like for $\{c_{2j}\}$ on $\{b_{2j+1}\}$. As we carry out the iteration procedure step by step, the present values in one set will not interfere with those in the other. Therefore, the update of variables can be done simultaneously for any given time if parallel processing facilities are available.

In the next section we shall present the application of this method to a single dispersive line loaded by nonlinear impedance.

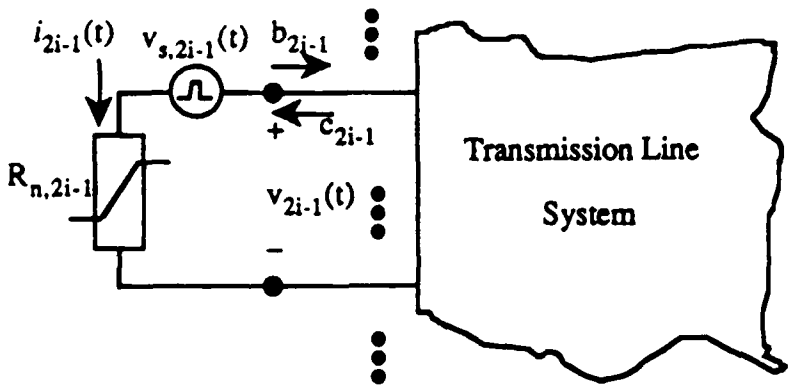

Figure 2. Odd-numbered ports (source side).

III. NONLINEARLY-LOADED DISPERSIVE TRANSMISSION LINE

Shown in Fig. 4 is a uniform dispersive transmission line of length l driven by a source $e_0(t)$ with a linear source resistance R_s at one end, and terminated by a nonlinear resistor R_n at the other end. The transmission line portion of this problem can be described in terms of the frequency dependent characteristic impedance $Z_0(\omega)$ and effective propagation constant $\beta(\omega)$. It can be shown that the frequency-domain *scattering matrix* is given as follows

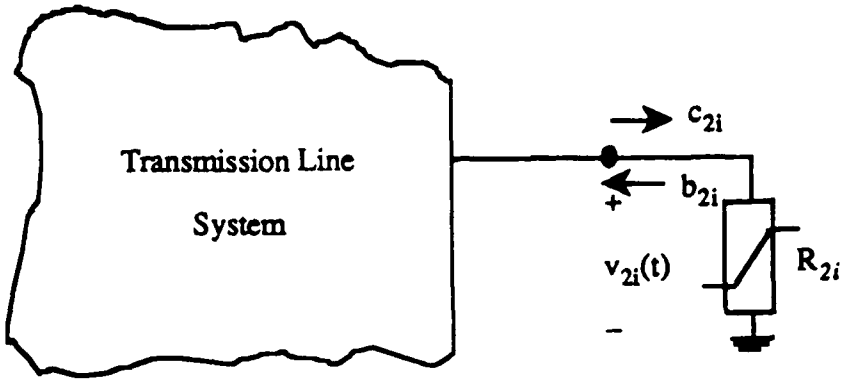

Figure 3. Even-numbered ports (load side).

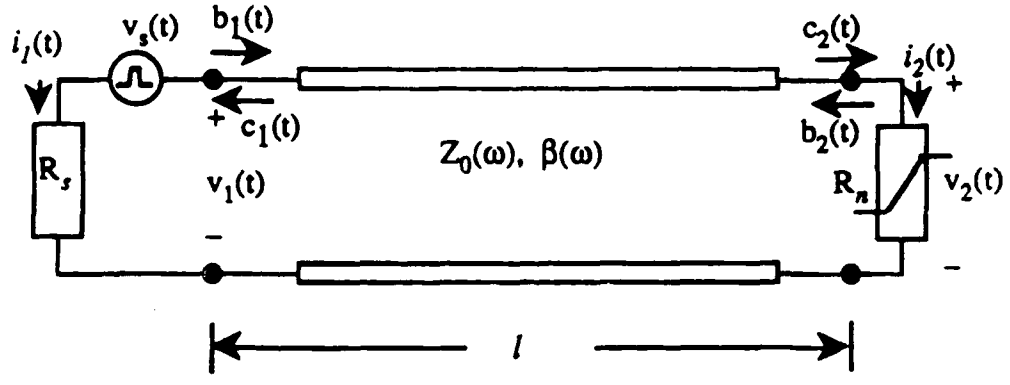

Figure 4. Nonlinearly loaded dispersive transmission line.

$$\begin{bmatrix} S_{11}(\omega) & S_{12}(\omega) \\ S_{21}(\omega) & S_{22}(\omega) \end{bmatrix} = \begin{bmatrix} 0 & e^{-j\beta(\omega)l} \\ e^{-j\beta(\omega)l} & 0 \end{bmatrix} \tag{14}$$

Noting that both S_{11} and S_{22} are zero for all time; therefore, we only need to consider S_{12} and S_{21}, which involve time delays. The simplicity of (14)

can be attributed to our definition of scattering matrix. As an example, we consider a microstrip line of width W. The substrate is of thickness h and has a dielectric constant ϵ_r. Numerous empirical formulas are available from the literature (see for example [13-15]). In this paper, we will use the following expressions to calculate the frequency dependence of microstrip line characteristic impedance and effective dielectric constant $\epsilon_e(\omega)$, which is defined from $\beta(\omega) = \omega\sqrt{\mu_0\epsilon_e\epsilon_0}$:

$$\epsilon_e(\omega) = \epsilon_r - \frac{\epsilon_r - \epsilon_e(0)}{1 + \frac{\epsilon_e(0)}{\epsilon_r}\left(\frac{\omega}{\omega_t}\right)^2} \tag{15}$$

$$Z_0(\omega) = \frac{\eta h}{W_e(\omega)\sqrt{\epsilon_e(\omega)}} \tag{16}$$

and the effective width $W_e(\omega)$ is governed by the equation

$$W_e(\omega) = W + \frac{W_e(0) - W}{1 + \omega/\omega_g} \tag{17}$$

where

$$\omega_t = \frac{\pi Z_0(0)}{\mu_0 h} \tag{18}$$

$$\omega_g = \frac{\pi c}{W\sqrt{\epsilon_r}} \tag{19}$$

and the low-frequency limits of ϵ_e and Z_0 are respectively

$$\epsilon_e(0) = \frac{\epsilon_r + 1}{2} + \frac{\epsilon_r - 1}{2} F(W/h) \tag{20}$$

with

$$F(W/h) \approx \begin{cases} (1 + 12h/W)^{-1/2} + 0.04(1 - W/h)^2, & \text{if } W/h \le 1 \\ (1 + 12h/W)^{-1/2}, & \text{if } W/h > 1 \end{cases} \tag{21}$$

and

$$Z_0(0) = \begin{cases} \dfrac{\eta}{2\pi\sqrt{\epsilon_e(0)}} \ln\left(\dfrac{8h}{W} + 0.25\dfrac{W}{h}\right), & \text{if } W/h \le 1 \\ \dfrac{\eta}{\sqrt{\epsilon_e(0)}} \left\{\dfrac{W}{h} + 1.393 + 0.667 \ln\left(\dfrac{W}{h} + 1.444\right)\right\}^{-1}, & \text{if } W/h > 1 \end{cases} \tag{22}$$

Note that $W_e(0)$ in (17) is derived from (16) by substituting in $Z_0(0)$ and $\epsilon_e(0)$.

In this paper, we assume that the width W is equal to 0.508 mm and the depth and the dielectric constant of the substrate are equal to 0.216 mm and 10.2 respectively. It can be readily derived from the formulas that the effective permittivity in the low-frequency limit is equal to 7.46, and the high-frequency characteristic impedance is $Z_0(\infty) = 50.2\,\Omega$. The calculation of the impulse response function $h_{12}(t)(= h_{21})$, the inverse Fourier transform of $S_{12}(\omega)$, however, is not trivial. Because $\lim_{\omega\to\infty} S_{12}(\omega)$ does not approach 0, the inverse Fourier transform is singular. If numerical computations are not carried out with great care, the accuracy

would be questionable. In [16] a similar Fourier integral was calculated. The only difference is that the input is not an impulse function, and hence it is numerically integrable. The authors proposed using Taylor expansion method and the method of stationary phase for narrow-band input signals. But for other input waveforms a brute force numerical integration method was applied which proved to be very time-consuming. To overcome the difficulty of numerical integration once and for all, our approach is to separate the transfer function S_{12} into two parts, one that can be analytically inverted to an impulse function, and one that is well-behaved and integrable. The latter requires that the integrand approaches 0 as ω goes to infinity. This leads to a natural way of separation:

$$\begin{aligned} e^{-j\beta(\omega)l} &= \left(e^{-j\beta(\omega)l} - e^{-j\beta_\infty l}\right) + e^{-j\beta_\infty l} \\ &= e^{-j\beta_\infty l}\left\{\left[e^{-j(\beta(\omega)-\beta_\infty)l} - 1\right] + 1\right\} \end{aligned} \tag{23}$$

where $\beta_\infty = \omega\sqrt{\mu\epsilon_0\epsilon_r}$.

In (23), the factor $e^{-j\beta_\infty l}$ corresponds to a time delay of $\tau_r = l/(c\sqrt{\epsilon_r})$ and the inverse Fourier transform of 1 is an impulse function. Therefore, defining $h(t) = \mathcal{F}^{-1}\{e^{-j(\beta(\omega)-\beta_\infty)l} - 1\}$, we then have

$$h_{12}(t) = \delta(t - \tau_r) + h(t - \tau_r) \tag{24}$$

Now only $h(t)$ needs to be evaluated numerically. Because the kernel of this Fourier inversion has essentially a finite range of integration, the calculation becomes easier. The impulse response function for a 10 mm long microstrip line is shown in Fig. 5. Only a limited portion of $h_{12}(t)$ surrounds the impulse function. This is consistent with our claim that the impulse response has a very limited duration.

Because the scattering parameters h_{11} and h_{22} are zero, the input-output wave variable pair $\{b_j(t), c_j(t)\}$ are only linked through (12). The iterative solution to a single transmission line problem is therefore relatively simple. Once we finish calculating $v_j(t)$, iteration step (iv) will readily return the correct values for $b_j(t)$. There is no need to go back to step (i).

We first examine the response from a Gaussian pulse with an amplitude of 1.0 volts and a width of 10 ps measured at its half amplitude is used as the source. The source resistance R_s is 50 Ω. The load characteristics is fully described by the following equation:

$$i_2 = I_0\left[\exp\left(\frac{v_2}{0.025}\right) - 1\right] \text{ nA} \tag{25}$$

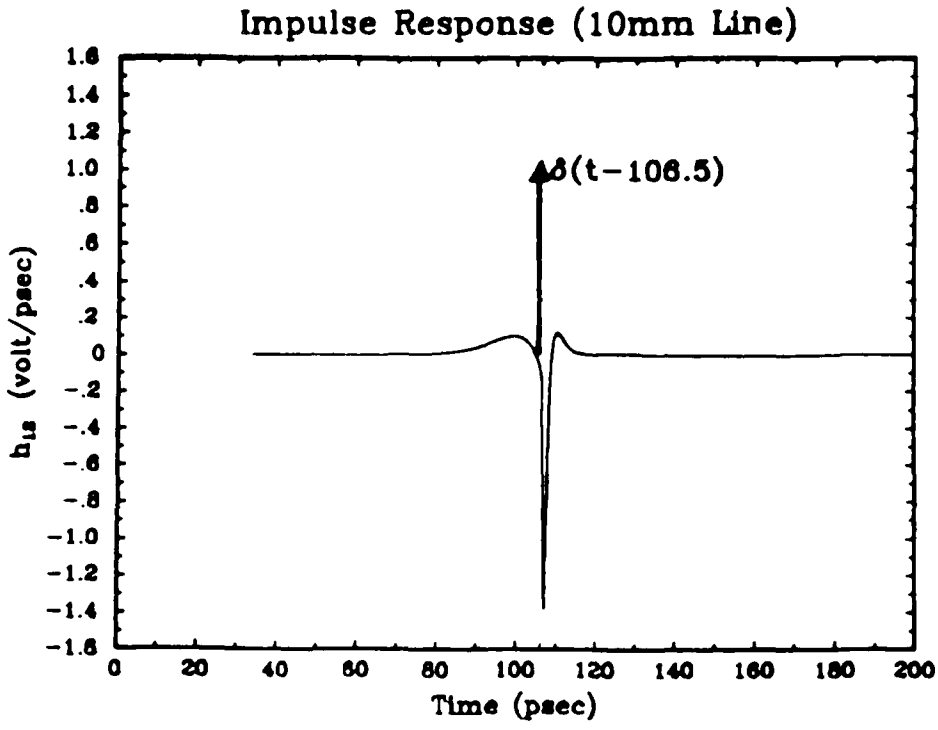

Figure 5. Impulse response $h_{12}(t)$.

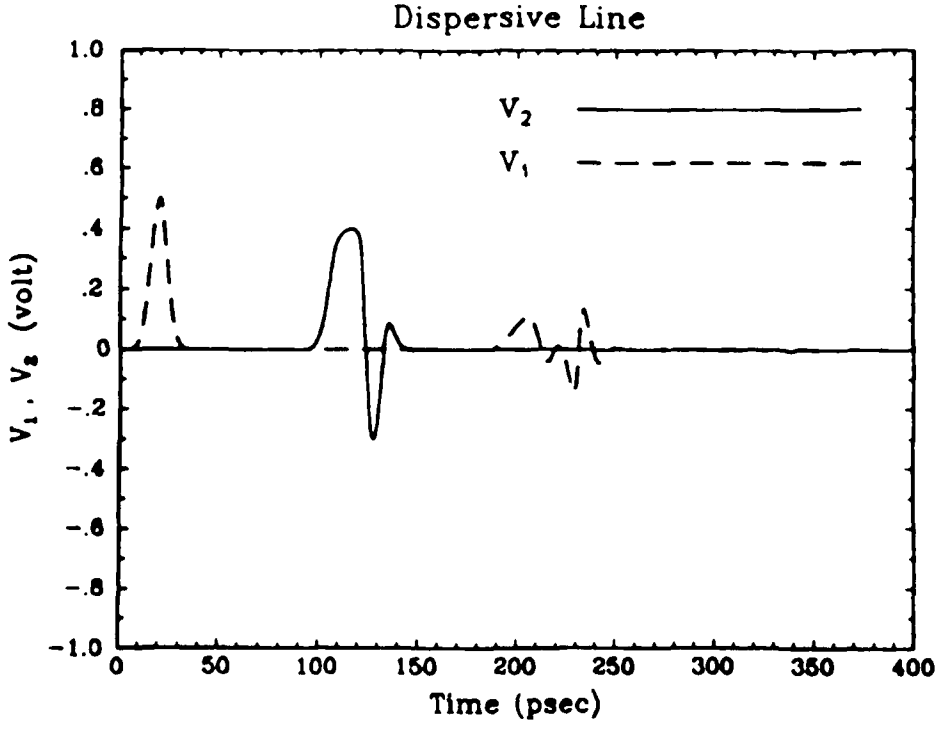

Figure 6. Terminal voltages vs. time at both the source end and the load end.

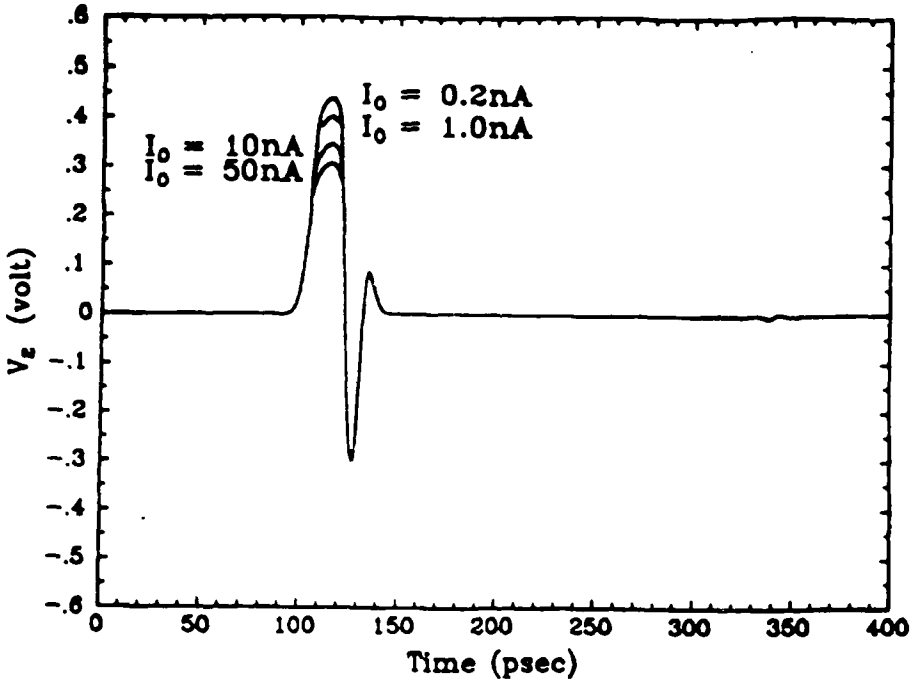

Figure 7. Load voltages as I_0 varies.

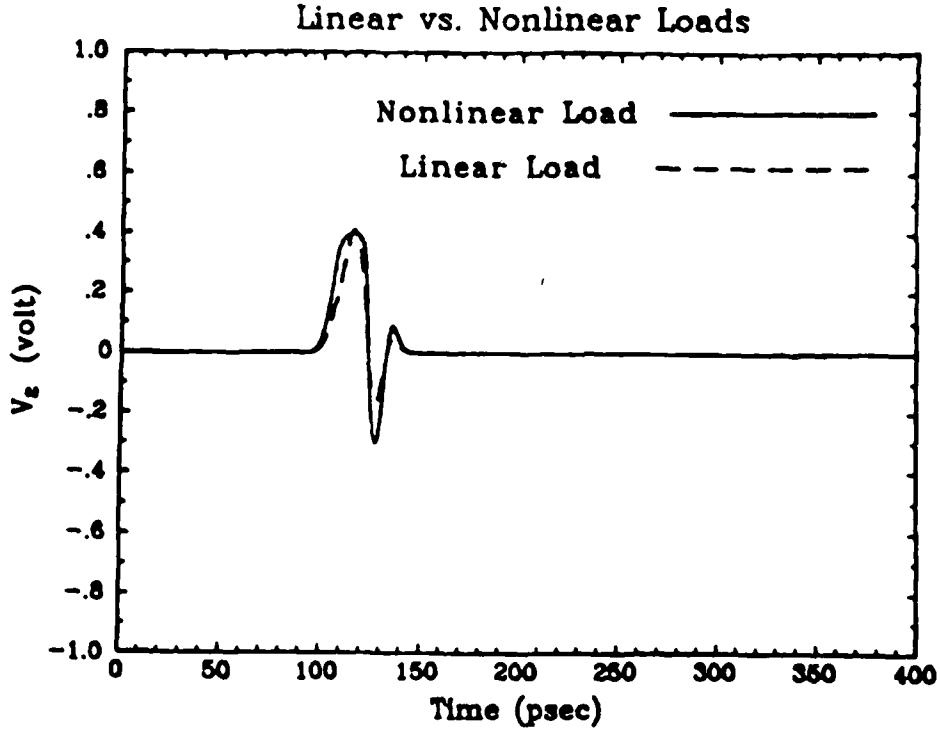

Figure 8. Load voltages for linear and nonlinear terminations.

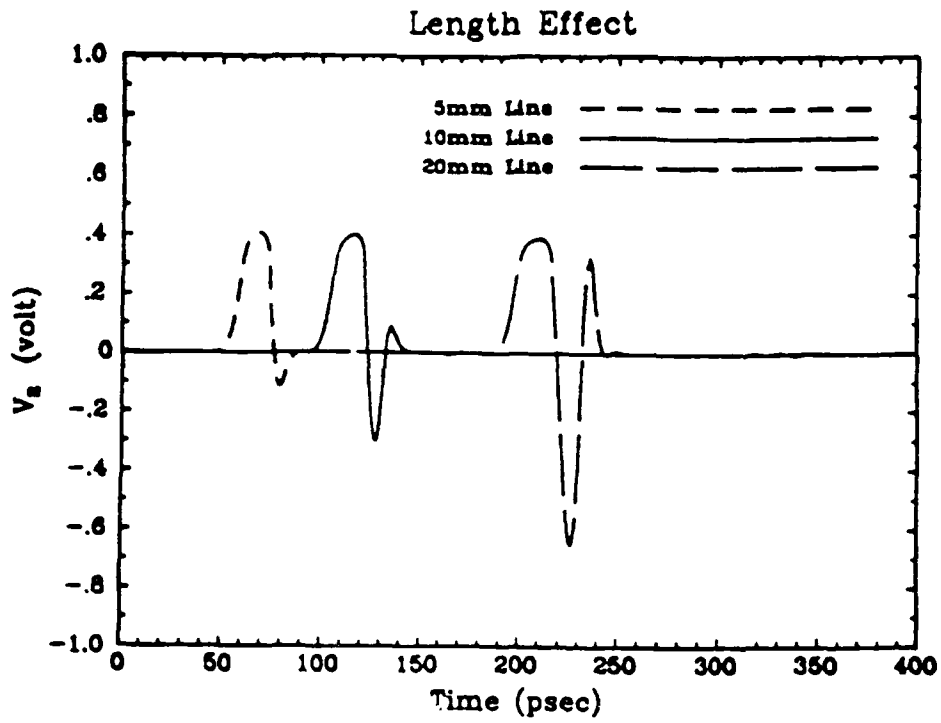

Figure 9. Load voltages for different line lengths.

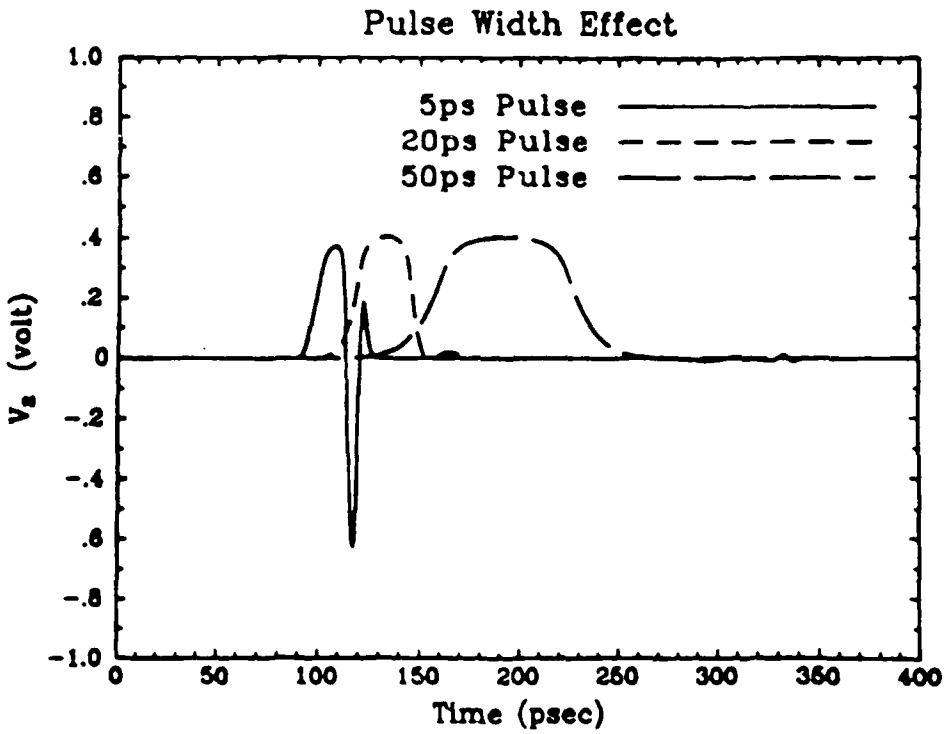

Figure 10. Load voltages for different pulse widths.

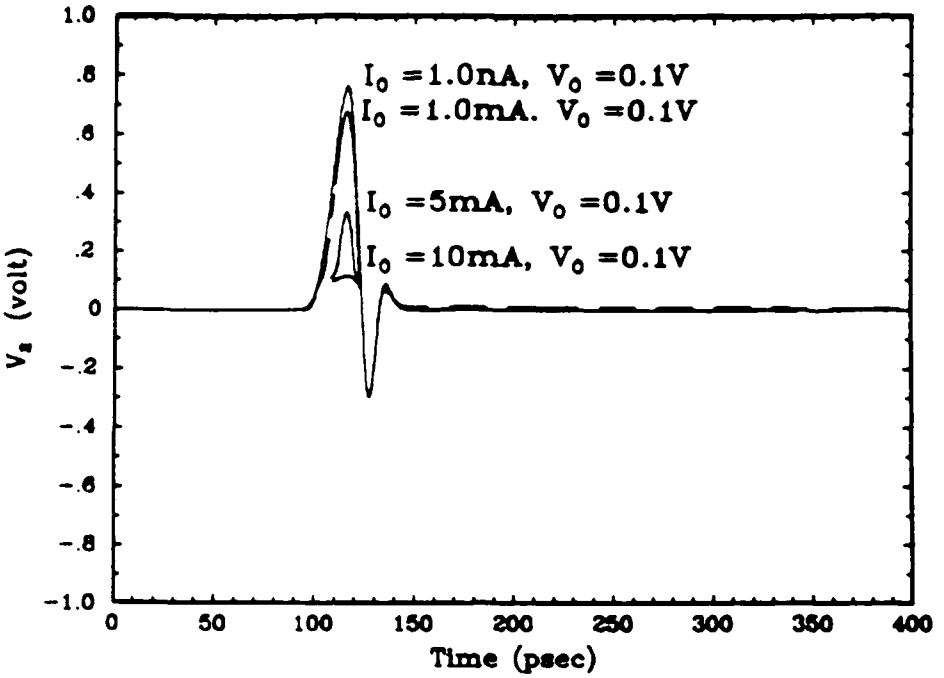

Figure 11. Load voltages for another type of nonlinear termination.

For the case $I_0 = 1.0$, the time responses at both ends are plotted in Fig. 6. The pulse has been broadened and the negative trailing edge is rather significant. In order to analyze what comes from dispersion of the transmission line and what comes from the load nonlinearity, we compared the plots of the load responses when I_0 is varied from 0.2 to 50.0 in (25), and when the load is a 50 Ω linear resistor. The results are depicted in Figs. 7 and 8. Apparently the nonlinearity contributes most to the broadening effect. The negative trailing edge originates from dispersion, but is enhanced by the nonlinear load. Since the load characteristics is similar to that of a typical diode, it behaves like an open circuit with respect to an incoming negative voltage wave. This gives rise to roughly twice the response compared to the one at the 50 Ω load, which is nearly matched to the transmission line. The large negative trailing edge also accounts for the extended ringing after it is reflected back to the source end.

In Fig. 9, the load end voltages for 5 mm and 20 mm lines are compared against the 10 mm line case. The number of zero crossings increases with length, as expected from the transmission line dispersion. Similar phenomenon is observed when shorter pulses are injected, as in Fig. 10. The centers of these pulses are intentionally separated to allow clearer comparison. It is interesting to note the similarity of the 5 ps pulse output and the 20 mm line output in Fig. 9.

We have also tested our iteration algorithm on another class of nonlinear loads

with i-v characteristics described as

$$i_2 = I_0\left[\tanh\left(\frac{v_2 - v_0}{0.025}\right) + 1.0\right] \tag{26}$$

Unlike the one described in (25), there is cap on the positive current. The result is that positive voltage has a larger amplitude, which is controlled by I_0, as shown in Fig. 11.

The time resolution used in all but the 5 psec pulse input case is 0.4 psec with a total of 1000 points. For the latter, the resolution is 0.2 psec and there are 2000 points. Because very limited portion of the impulse response $h_{12}(t)$ is significant, the actual number of points involved in the convolution integral is far lower. We used the Newton-Raphson iteration procedure for the nonlinear equation (13). On a VAX Station 3500, the testing cases take about 4 to 27 seconds of CPU time to generate the solutions with 1000 points. The large variation in computation times is due to different convergent rates for different types of nonlinearity.

IV. CONCLUSIONS

A new method for the transient analysis of a frequency-dependent transmission line system terminated with nonlinear loads has been presented. This method is not only effective for saving the CPU time required for solving nonlinear transient problems, but is also compact and natural in form. Our generalized scattering matrix approach is closely tied to the concept of waves. Therefore, no extended reflection arises as a result of artificial boundary conditions as can occur with the admittance matrix method, and duration of the impulse responses for the waves in the transmission line system is very limited. This is the key to reducing the amount of computation time and memory.

The detailed procedure for solving this kind of nonlinear transient problem is given through an analysis of a nonlinearly-loaded microstrip transmission line with linear source resistance. Extension of this approach to multiple transmission line systems with nonlinear source and terminations is being studied and will be reported in future work.

ACKNOWLEDGMENTS

This paper was supported by the ARO Contract DAAL03-88-5-0057, NSF Grant 8620029-ECS, the Joint Service Electronics Programs under the Contract DAAL03-86-K-0002, and the Digital Equipment Corporation.

The Editor thanks S. Ali and two anonymous Reviewers for reviewing the paper.

REFERENCES

1. Liu, T. K., and F. M. Tesche, "Analysis of antennas and scatterers with nonlinear loads," *IEEE Trans. Antennas Propagat.*, Vol. AP-2?, 131–139, 1976.
2. Gu, Q., J. A. Kong, and Y. E. Yang, "Time domain analysis of nonuniformly coupled line systems," *J. Electro. Waves Applic.*, Vol. 1, 109–1?2, 1987.
3. Nakhla, M. S., and J. Vlach, "A piecewise harmonic balance technique for determi-

nation of periodic response of nonlinear systems," *IEEE Trans. Circuits & Systems*, Vol. CAS–23, 85–91, 1976.
4. Rizzoli, V., V. Lipparini, and E. Marazzi, "A general purpose program for nonlinear microwave circuit design," *IEEE Trans. Microwave Theory Tech.*, Vol. MTT–31, 762–770, Sept. 1983.
5. Gilmore, R. J., and F. J. Rosenbaum, "Modelling of nonlinear distortion in GaAs MESFETS," *IEEE 1984 Int. Microwave Symp. Dig.*, 430–431, June 1984.
6. Gilmore, R., "Nonlinear circuit design using the modified harmonic balance algorithm," *IEEE Trans. Microwave Theory Tech.*, Vol. MTT–34, No. 12, 1294–1307, Dec. 1986.
7. Merewether, D. E., and T. F. Ezell,"The interaction of cylindrical posts and radiation-induced electric field pulses in ionized media," *IEEE Trans. Nuclear Sci.*, Vol. NS–21, 4–13, 1974.
8. Schuman, H., "Time-domain scattering from a nonlinearly loaded wire," *IEEE Trans. Antennas Propag.*, Vol. AP–22, 611–613, 1974.
9. Djordjevic, A. R., T. K. Sarkar, and R. F. Harrington, "Analysis of transmission lines with arbitrary nonlinear terminal networks," *IEEE Trans. Microwave Theory Tech.*, Vol. MTT–34, No. 6, 660– 666, June 1986.
10. Caniggia, S., "EMC design of digital systems using macromodelling procedures for integrated circuits and their interconnections," *Proc. EMC Symp.*, 465–470, 1983.
11. Schutt-Aine, J. E., and R. Mittra, "Scattering parameter transient analysis of transmission lines loaded with nonlinear terminations," *IEEE Trans. Microwave Theory Tech.*, Vol. MTT–36, 529–536, 1988.
12. Collin, R. E., *Field Theory of Guided Waves*, McGraw-Hill Book Company Inc., 1960.
13. Pramanick, P., and P. Bhartia, "An accurate description of dispersion in microstrip," *Microwave J.*, 89–93, Dec. 1983.
14. Gupta, K. C., *Microstrip Lines and Slotlines*, Artech House, Dedham, Massachusetts, 1979.
15. Kirchning, M., and R. H. Jansen, "Accurate wide-range design equations for the frequency-dependent characteristic of parallel coupled microstrip lines," *IEEE Trans. Microwave Theory Tech.*, Vol. MTT–32, 83–90, Jan. 1984.
16. Veghte, R., and C. A. Balanis, "Dispersion of transient signals in microstrip transmission lines," *IEEE Trans. Microwave Theory Tech.*, Vol. MTT–34, No. 12, 1427–1436, Dec. 1986.

Qisheng Gu was born in Jiangsu, China. He graduated from Fudan University, Shanghai China in 1960. From 1960 to 1962, he worked on automatic control systems at Shanghai Designing Institute of Machinery and Electrical Engineering, China. In 1962, he joined the Department for Research and Development at Shanghai Xinhua Radio Factory, where he was engaged in research of microwave systems and circuits. Since October 1982, he has been a senior engineer and the Deputy Director of the Department. Between 1983 and 1987, he was a visiting scientist in the Research Laboratory of Electronics, Massachusetts Institute of Technology. He is a member of the Shaghai Electronics Association Council and the Microwave Committee of the Chinese Institute of Electronics.

Ying-Ching Eric Yang was born in Taiwan in 1959. He received his B.S.E.E. degree from National Taiwan University in 1981 and the M.S. and E.E. degrees from the Massachusetts Institute of Technology in 1985 and 1986, and is currently working toward his Ph.D. degree. From 1981 to 1983 he served in the R.O.C. Navy as an instructor. Since 1983 he has been with the department of electrical engineering and computer science and the Research Laboratory of Electronics of the Massachusetts Institute of Technology, where he worked as a Research Assistant and a Teaching Assistant. He was an IBM Graduate Fellow during the academic year 1986–87. His reseach interest is in the time-domain

electromagnetic wave propagation within microelectronic integrated circuits. Mr. Yang is a member of the IEEE and Sigma Xi.

Jin Au Kong is Professor of Electrical Engineering and Chairman of Area IV on Energy and Electromagnetic Systems in the Department of Electrical Engineering and Computer Science at the Massachusetts Institute of Technology, Cambridge, Massachusetts. His research interest is in the field of electromagnetic wave theory and applications. He is the author of *Electromagnetic Wave Theory* (Wiley, 1975, 1986), coauthor of of *Applied Electromagnetism* (Brook/Cole, 1983 PWS, 1987) and *Theory of Microwave Remote Sensing* (Wiley, 1985), and Editor of *Research Topics in Electromagnetic Wave Theory* (Wiley, 1981), Chief Editor of the Elsevier book series on Progress in Electromagnetics Research (PIER) and the Wiley Series in Remote Sensing.

END

6-89

DTIC